

# **The extracellular matrix in bronchopulmonary dysplasia: the role of the lysyl oxidase family**

Inaugural Dissertation

submitted to the  
Faculty of Medicine  
in partial fulfillment of the requirements  
for the PhD Degree  
of the Faculties of Veterinary Medicine and Medicine  
of the Justus Liebig University Giessen

by  
**Mižíková Ivana**

of  
Košice, Slovakia

Giessen, 2017

Director / Chairman: Prof. Dr. Klaus-Dieter Schlüter

Department of Physiology

Faculty of Medicine of the Justus Liebig University Giessen

First Supervisor and Committee Member: Prof. Dr. Werner Seeger

Second Supervisor and Committee Member: Prof. Dr. Dr. Thomas Braun

Committee Members: Prof. Dr. Werner Seeger  
Prof. Dr. Dr. Thomas Braun  
Prof. Dr. Anja Sterner-Kock

Date of Doctoral Defense: 19. 1. 2018

*If you eliminate the impossible, whatever remains, however  
Improbable, must be the truth.*

Mr. Spock

# I Table of contents

I	Table of contents .....	3
II.	List of figures.....	6
III.	List of tables .....	8
IV.	List of abbreviations.....	9
V.	Summary .....	13
VI.	Zusammenfassung .....	14
1	INTRODUCTION.....	16
1.1	Development and structure of the lung .....	16
1.1.1	Early (prenatal) lung development.....	16
1.1.2	Late (postnatal) lung development.....	19
1.2	Bronchopulmonary dysplasia.....	20
1.3	The extracellular matrix in context of normal and aberrant lung development .....	22
1.3.1	Key components of extracellular matrix in the context of lung development .....	24
1.4	The lysyl oxidase family .....	27
2	AIMS OF THE STUDY .....	31
3	MATERIALS AND METHODS .....	32
3.1	Materials.....	32
3.1.1	Equipment .....	32
3.1.2	Reagents .....	35
3.1.3	Purchased primary cells and cell-lines .....	39
3.2	Methods.....	40
3.2.1	Animal experiments .....	40
3.2.2	Design-based stereology .....	45

3.2.3	Cell culture and cell treatments .....	47
3.2.4	Gene expression analysis .....	51
3.2.5	Analysis of protein expression, activity and deposition.....	56
3.2.6	Cloning and lentiviral production .....	59
3.2.7	Statistical analysis .....	63
4	RESULTS .....	64
4.1	Exposure of immature mouse lungs to 85% O <sub>2</sub> dysregulates lysyl oxidase expression.....	64
4.2	Inhibition of lysyl oxidase activity in the lungs of developing mice exposed to 85% O <sub>2</sub> .....	66
4.3	Cross-linking of collagen and elastin in the lungs of developing mouse pups upon hyperoxia exposure and treatment with β-aminopropionitrile .....	68
4.4	The impact of hyperoxia exposure and β-aminopropionitrile administration on elastin fibers formation in the parenchyma of the developing mouse lung.....	72
4.5	Treatment of hyperoxia-exposed mouse pups did not preserve normal lung architecture .....	75
4.6	Expression profile of lysyl oxidase family members in various cell-types present in the lung.....	81
4.7	Knockdown of <i>Lox</i> , <i>Loxl1</i> and <i>Loxl2</i> expression impacts the transcriptome of primary mouse lung fibroblasts.....	82
4.8	Lentiviral overexpression of lysyl oxidase family members impacts the gene expression in murine fibroblasts .....	88
4.9	Role of lysyl oxidase enzymatic activity in lysyl oxidase-mediated gene regulation.....	91
4.10	The expression of LOX, LOXL1 and LOXL2 target-genes in a murine model of aberrant lung development .....	94
5	DISCUSSION .....	98

5.1	The expression of lysyl oxidases is dysregulated in animal models of bronchopulmonary dysplasia.....	98
5.2	Lysyl oxidase activity is essential for early postnatal development .....	99
5.3	Normalization of lysyl oxidase activity improves the formation of elastin and collagen cross-links and elastin foci structure in mouse model of bronchopulmonary dysplasia.....	100
5.4	Normalization of lysyl oxidase activity does not improve alveolarization and septal formation in mouse model of bronchopulmonary dysplasia.....	101
5.5	Lysyl oxidase family members have gene regulatory roles in lung fibroblasts.....	102
5.6	Gene regulatory functions for lysyl oxidases in the context of <i>in vivo</i> animal model of bronchopulmonary dysplasia .....	104
6	CONCLUSIONS .....	106
7	REFERENCES .....	107
8	DECLARATION.....	113
9	ACKNOWLEDGEMENTS .....	114
10	<i>CURRICULUM VITAE</i> .....	115
11	APPENDIX .....	117

## II. List of figures

Figure 1. Progression of prenatal and postnatal lung development. ....	17
Figure 2. Histological structure of the lung of a patient with bronchopulmonary dysplasia and a healthy age-matched control lung. ....	21
Figure 3. Elastin deposition during lung formation in bronchopulmonary dysplasia and in the hyperoxia-based mouse model of bronchopulmonary dysplasia. ....	23
Figure 4. Chemical reaction catalyzed by lysyl oxidase. ....	28
Figure 5. Visiopharm NewCast counting tools used in the stereological analysis of lung structure. ....	46
Figure 6. The expression of lysyl oxidase family members is dysregulated during aberrant late lung development. ....	65
Figure 7. Effect of $\beta$ -aminopropionitrile administration on mouse viability. ....	67
Figure 8. Lysyl oxidase enzymatic activity was normalized by the administration of $\beta$ -aminopropionitrile. ....	68
Figure 9. Effect of hyperoxia exposure and $\beta$ -aminopropionitrile administration on the levels of collagen and formation of collagen cross-links in the lungs of developing mouse pups at postnatal day 19.5. ....	70
Figure 10. Effect of hyperoxia-exposure and $\beta$ -aminopropionitrile administration on the levels of elastin and elastin cross-links in the lungs of developing mouse pups at postnatal day 19.5. ....	72
Figure 11. Hyperoxia-exposure and $\beta$ -aminopropionitrile administration alter the formation of elastin foci in developing alveolar septa. ....	74
Figure 12. Impact of the hyperoxia-exposure and $\beta$ -aminopropionitrile administration on the lung architecture at postnatal day 9.5. ....	77
Figure 13. Impact of the hyperoxia-exposure and $\beta$ -aminopropionitrile administration on the lung architecture at postnatal day 19.5. ....	80
Figure 14. Relative expression of lysyl oxidase family members in various mouse lung cell-types cultured <i>in vitro</i> . ....	81
Figure 15. Short interfering RNA-mediated knockdown of lysyl oxidases in primary mouse lung fibroblast cultures. ....	83

Figure 16. Microarray analysis validation following the short interfering RNA-mediated knockdown of lysyl oxidases in primary mouse lung fibroblasts. ....	85
Figure 17. Lentivirus-mediated overexpression of lysyl oxidases in the mouse NIH/3T3 fibroblast cell-line.....	90
Figure 18. Inhibition of lysyl oxidase enzymatic activity in primary mouse lung fibroblasts. ....	92
Figure 19. Microarray analysis validation following the $\beta$ -aminopropionitrile administration in primary mouse lung fibroblasts.....	94
Figure 20. Gene expression of <i>Lox</i> and selected LOX target-genes in a mouse model of an arrested lung development.....	96
Figure 21. Gene expression of <i>Loxl1</i> and <i>Loxl2</i> , as well as selected LOXL1 and LOXL2 target-genes in a mouse model of an arrested lung development.....	97

### III. List of tables

Table 1. Buffers required for treatment of lungs and embedding in Technovit 7100. ....	43
Table 2. Antibodies used for alveolar epithelial type II cells isolation. ....	49
Table 3. Media used for alveolar epithelial type II cells isolation and culture. ....	49
Table 4. List of siRNA oligonucleotides used in knockdown experiments. ....	51
Table 5. Primers employed for sex determination. ....	53
Table 6. Primers employed for a real-time RT-PCR analysis. ....	55
Table 7. Primary and secondary antibodies used for western blot analysis. ....	58
Table 8. Primers used for amplification of <i>Lox</i> , <i>Lox11</i> and <i>Lox12</i> sequences. ....	60
Table 9. Effect of hyperoxia exposure and $\beta$ -aminopropionitrile administration on deposition of collagen in the developing mouse lungs at postnatal day 19.5. ....	69
Table 10. Effect of hyperoxia exposure and $\beta$ -aminopropionitrile administration on deposition of elastin in developing mouse lungs at postnatal day 19.5. ....	71
Table 11. Stereo-morphometric parameters of developing mouse lungs after hyperoxia exposure and $\beta$ -aminopropionitrile administration assessed at postnatal day 9.5. ....	76
Table 12. Stereo-morphometric parameters of developing mouse lungs after hyperoxia exposure and $\beta$ -aminopropionitrile administration assessed at postnatal day 19.5. ....	78
Table 13. List of differentially up- and down-regulated genes after a <i>Lox</i> knockdown as assessed by microarray analysis. ....	84
Table 14. List of differentially up- and down-regulated genes after a <i>Lox11</i> knockdown as assessed by microarray analysis. ....	86
Table 15. List of differentially up- and down-regulated genes after a <i>Lox12</i> knockdown as assessed by microarray analysis. ....	87
Table 16. List of differentially up- and down-regulated genes after $\beta$ -aminopropionitrile administration in primary mouse lung fibroblasts as assessed by microarray analysis. ....	93

#### IV. List of abbreviations

AECII	Alveolar epithelial type II cell
BAPN	$\beta$ -aminopropionitrile
bp	Base pair
BPD	Bronchopulmonary dysplasia
cDNA	Complementary DNA
CE	Coefficient of error
CLD	Chronic lung disease
Ct	Threshold cycle
CV	Coefficient of variation
ddH <sub>2</sub> O	Double distilled water
Des	Desmosine
DHLNL	Dihydroxylysino-norleucine
DMEM	Dulbecco's modified Eagle medium
DNA	Deoxyribonucleic acid
E	Embryonic day
EC	Epithelial cell
ECM	Extracellular matrix
EDTA	Ethylenediaminetetraacetic acid
EGTA	Ethylene glycol-bis ( $\beta$ -aminoethyl ether)- <i>N,N,N',N'</i> -tetraacetic acid
EMT	Epithelial-to-mesenchymal transition
EtOH	Ethanol
FC	Fold change
FBS	Fetal bovine serum

FiO <sub>2</sub>	Fraction of oxygen in the inspired air
<i>g</i>	Gravitational acceleration
HBSS	Hank's balanced salt solution
HEK	Human embryonic kidney
HEPES	4-(2-hydroxyethyl)-1-piperazineethanesulfonic acid
HHL	Histidinohydroxylysineonorleucine
HLNL	Hydroxylysineonorleucine
HP	Hydroxylysylpyridinoline
IgG	immunoglobulin G
Isodes	Isodesmosine
i.p.	Intraperitoneally
kg	Kilogram
LTBP	Latent TGF-β binding protein
mg	Milligram
ml	Milliliter
MLI	Mean linear intercept
mM	Millimolar
MMP	Matrix metalloproteinase
MuLV	Murine leukemia virus
MΦ	Macrophage
μg	Microgram
μl	Microliter
μM	Micromolar
n	Number
N	Normality, equivalent concentration
NP-40	Nonyl phenoxypolyethoxylethanol, Tergitol-type NP-40

n.s.	Not significant
P	Postnatal day
PASMC	Pulmonary arterial smooth muscle cell
PBS	Phosphate buffered saline
PCR	Polymerase chain reaction
PDGF	Platelet-derived growth factor
PF	Pulmonary fibroblast
PFA	Paraformaldehyde
PLOD	Procollagen-lysine, 2-oxoglutarate 5-dioxygenase (Lysyl hydroxylase)
PVDF	Polyvinylidene difluoride
P (corr)	Corrected <i>P</i> value
P/S	Penicillin/streptomycin
RDS	Respiratory distress syndrome
RFU	Relative fluorescence units
RNA	Ribonucleic acid
rpm	Rotations per minute
RT	Room temperature
RT-PCR	Reverse transcription-PCR
scr. siRNA	Scrambled siRNA
SD	Standard deviation
SE	Standard error
siRNA	Short interfering RNA
$\alpha$ SMA	$\alpha$ -smooth muscle actin
SMC	Smooth muscle cell
TAE	Tris-acetate-EDTA
TE	Tris-EDTA

TEMED	Tetramethylethylenediamine
TGF- $\beta$	Transforming growth factor- $\beta$
TGM	Transglutaminase
TIMP	Tissue inhibitors of matrix metalloproteinase
T <sub>m</sub>	Melting temperature
Tris	Trisaminomethane
tRNA	Total RNA
UrAc	Uranyl acetate
UV	Ultraviolet
WFI	Water for injection
WT	Wild-type

## V. Summary

Extracellular matrix (ECM) formation and remodeling play a central role in the processes of lung alveolarization and secondary septation. A key component of ECM structure is a complex collagen and elastin network of fibers. Formation and maintenance of this crucial structure is perturbed in aberrant lung development in patients with bronchopulmonary dysplasia (BPD) as well as in experimental animal models of BPD. Lysyl oxidases comprise a family of five members, which facilitate the covalent cross-linking of collagen and elastin molecules, thus controlling ECM structural homeostasis. Moreover, alternative non-matrix gene regulatory roles for these enzymes have been proposed. Recently, lysyl oxidases have been implicated in the pathogenesis of various lung diseases, including cancer, fibrosis, pulmonary hypertension and BPD. Although several studies report perturbations to lysyl oxidase expression, and elastin and collagen deposition associated with the arrest of alveolarization in BPD, a causal role for lysyl oxidases in this processes has not yet been fully addressed.

In the study presented here, lysyl oxidase activity was neutralized *in vivo* in a murine hyperoxia-based model of BPD. In addition, non-matrix roles for three of the five family members, *Lox*, *Loxl1* and *Loxl2* were explored on the primary mouse fibroblasts background.

In the first part of the study, an arrest in alveolarization in developing mouse lungs was induced by hyperoxia exposure. Damage to alveolar formation was accompanied by an increase in lysyl oxidase activity, and an increase in the abundance of collagen and collagen cross-links. In contrast, the abundance of the insoluble elastin and elastin cross-links desmosine and isodesmosine was decreased, resulting in a substantial shift in collagen-to-elastin ratio. Normalization of lysyl oxidase catalytic activity partially restored normal levels of collagen. The abundance of elastin cross-links and the formation of elastin foci was also improved. However, no significant improvement in lung alveolarization was observed. In the second part of the study, a microarray analysis after small interfering (si)RNA knockdown in primary mouse lung fibroblasts revealed a dysregulation of expression of a large group of genes, including several ECM-relevant players, such as *Mmp3*, *Mmp9*, *Rarres1* or *Eln*. Moreover, the expression patterns of these genes in an *in vivo* animal model of BPD correlated with observations made *in vitro*. Importantly, the gene regulatory roles of lysyl oxidases were independent of lysyl oxidase catalytic activity.

## VI. Zusammenfassung

Die Entstehung und Umwandlung von extrazellulärer Matrix (EZM) spielt eine zentrale Rolle bei der Lungenalveolarisierung und der sekundären Septierung. Die Schlüsselkomponente der EZM Struktur ist ein komplexes Netzwerk aus Kollagen- und Elastinfibrillen. Die Entstehung und Aufrechterhaltung dieser wichtigen Strukturen ist bei Patienten, die an bronchopulmonaler Dysplasie (BPD) leiden, genauso wie in tierexperimentellen Modellen von BPD, im Sinne einer gestörten Lungenentwicklung, verändert. Lysyloxidasen sind eine Enzymfamilie, die aus fünf Mitgliedern besteht und für die Kontrolle der strukturellen Homöostase der EZM zuständig sind, indem sie die kovalente Quervernetzung von Kollagen- und Elastinmolekülen übernehmen. Zudem wurden weitere nicht-EZM bezogene genregulatorische Funktionen dieser Enzyme vermutet. Kürzlich konnte gezeigt werden, dass Lysyloxidasen eine Rolle in der Pathogenese verschiedener Lungenerkrankungen, einschließlich Tumorerkrankungen, Fibrose, pulmonale Hypertonie und BPD, spielen. Obwohl verschiedene Studien von der Veränderung der Lysyloxidasenexpression und der veränderten Einlagerung von Kollagen und Elastin im Zusammenhang mit dem Alveolarisierungsstopp bei BPD berichten, wurde die kausale Rolle der Lysyloxidasen in diesen Prozessen bisher nicht untersucht.

In der hier vorgestellten Studie, wurde die Aktivität der Lysyloxidase *in vivo* in einem Hyperoxie basierten Mausmodell der BPD ausgeschaltet. Außerdem wurde die nicht Matrix bezogene Rolle von drei der fünf Familienmitglieder Lox, Lox11 und Lox12 in primären Mausfibroblasten untersucht.

Im ersten Teil der Studie wurde der Alveolarisierungsstopp in sich entwickelnden Mauslungen durch Hyperoxie Exposition ausgelöst. Der Schaden an der alveolären Formation wurde von einer gesteigerten Lysyloxidasenaktivität begleitet, genauso wie von einer erhöhten Kollagenmenge und vermehrten Kollagenquervernetzungen. Im Gegensatz dazu, waren der Überschuss von unlöslichem Elastin und die Anzahl der Elastinquervernetzungen mit Desmosin und Isodesmosin verringert, was in einer deutlichen Veränderung des Kollagen/Elastin-Verhältnisses resultierte. Die Ausschaltung der enzymatischen Aktivität der Lysyloxidase konnte die Kollagenmenge immerhin teilweise normalisieren. Ebenso verbesserten sich die Zahl der Elastinquervernetzungen und die Entstehung der Elastinfoci. Dennoch konnte kein förderlicher Effekt auf die

Lungenalveolarisierung beobachtet werden. Im zweiten Teil der Studie zeigte eine Microarray Analyse nach Ausschaltung der Enzyme durch small interfering (si)RNAs in primären murinen Lungenfibroblasten die Dysregulation einer großen Gruppe von Genen, inklusive einiger EZM-relevanter Gene, wie *Mmp3*, *Mmp9*, *Rarres1* oder *Eln*. Zudem korrelierten die Expressionsmuster dieser Gene *in vitro* mit Daten aus einem *in vivo* Modell der BPD. Interessanterweise waren diese genregulatorischen Eigenschaften der Lysyloxidasen unabhängig von ihrer katalytischen Aktivität.

# **1 INTRODUCTION**

## **1.1 Development and structure of the lung**

The primary function of the lung of all air-breathing mammals is the transport of inspired oxygen from the atmosphere into the bloodstream and simultaneous clearance of accumulated carbon dioxide from the blood. This process, which occurs in smallest respiratory units of the lung, the alveoli, takes place across a double alveolo-capillary barrier, composed of the alveolar epithelium, capillary endothelium and adjacent structures of the extracellular matrix (ECM). In order to achieve maximal efficiency of gas exchange, this barrier must be as thin as possible and the alveolar surface area must be as large as possible. Therefore, the main objectives of lung development, namely late lung development, are the formation of a complex structure comprising a large number of alveoli and the formation of thin alveolo-capillary barrier facilitating an effective gas exchange [1-6].

The process of lung development consists of five developmental stages, which are traditionally divided into two phases - early (mainly prenatal) and late (mainly postnatal) lung development (Figure 1) [7, 8].

### **1.1.1 Early (prenatal) lung development**

In order to produce a fully-functional organ, enabling breathing and gas exchange in postnatal environment, the fetal lung must undergo rapid anatomical changes within a relatively short period of time. Based on their morphological and histological characteristics, four developmental stages are usually distinguished within early lung development in humans (three stages in mice) [6].

#### **Embryonic stage**

The core lung structure is derived from the endoderm of the primitive foregut at approximately three to seven weeks post-conception in humans (embryonic day [E]9–E12 in the mouse) and undergo main conducting airway branching during the embryonic stage of the early lung development. First, epithelial cells migrating into the surrounding mesenchyme form a primitive trachea, which further branches into two main, epithelium-lined, bronchial

buds. This early left and right main bronchus subsequently divides into further lobar and segmental bronchi [1, 6, 9, 10].

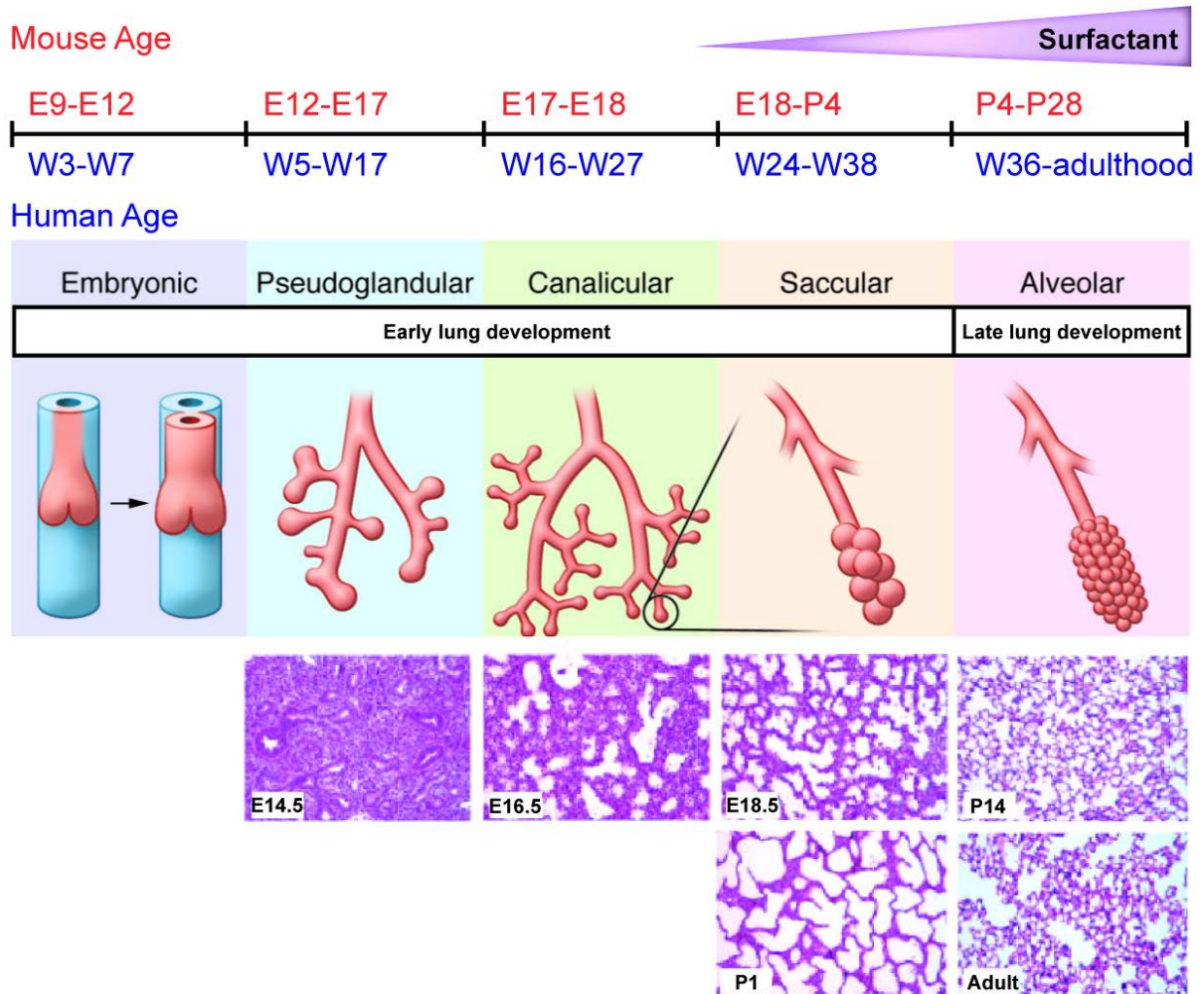


**Figure 1. Progression of prenatal and postnatal lung development.**

Schematic illustration of major stages of early and late lung development and their timing in human and in mouse. *E*, embryonic day; *P*, postnatal day; *W*, week. In addition, representative lung sections from mouse lungs at E14.5, E16.5, E18.5, P1, P14 and adult mice are illustrated. Synthesized from several sources [5-7, 9, 11-13].

### **Pseudoglandular stage**

Airway branching continues during the pseudoglandular stage, which occurs between the 5<sup>th</sup> and 17<sup>th</sup> week post-conception in humans (E12–E17 in mice) and the formation of the conducting airways and terminal bronchioles is fully completed. Pulmonary arteries and veins are developed during this period, and the cartilage begins to form around the large airways. The first ciliated epithelial cells and immature, cuboidal type II cells appear [3, 6, 9, 14].

### **Canalicular stage**

The canalicular stage, which occurs between the 16<sup>th</sup> and 27<sup>th</sup> week post-conception in humans, is mainly characterized by the thinning of the interstitial tissue and formation of acinar units, marking the beginning of the alveolarization process. The thinning of the interstitial mesenchyme leads to closer contact between the forming capillaries and the differentiating epithelium and the formation of the thin air-blood barrier. The primitive cuboidal epithelium is now visibly differentiated into flattened type I alveolar epithelial cells, and the lamellar bodies-containing type II alveolar epithelial cells. The presence of surfactant protein can be detected by week 24 [6, 9, 13]. Due to advances in perinatal medicine, the canalicular stage became the earliest possible period for a successful preterm birth in humans [9, 15]. Canalicular stage is also the last period of prenatal lung development in mice, spanning E17 and E18 [5].

### **Saccular stage**

The last fully prenatal stage of lung development in humans and the first stage of postnatal lung development in mice (24–38 weeks post-conception in humans, and E18-postnatal day [P]4 in mice) is characterized by the enlargement of the peripheral airways, formation of saccular units, further thinning of air-blood barrier and the start of secondary septation.

## 1.1.2 Late (postnatal) lung development

### Alveolar stage

This stage of alveolar formation is the last stage of lung development in both humans and mice. Although the alveolar stage in humans starts prenatally (36 weeks post-conception), it is largely a postnatal process, taking place during the first 36 months of postnatal life (and possibly beyond). Unlike in humans, alveolarization in mice is entirely postnatal process, taking place between P4-P28 [6, 7, 9, 16]. Alveolar stage is characterized by two, largely interconnected events: secondary septation and microvascular maturation.

The main contribution of secondary septation is increasing the number and reducing the size of the alveoli, eventually leading to an increase of the gas exchange surface area of the lung [5, 16]. While a human lung at birth contains up to 50 million alveoli [17-19], this number increases greatly postnatally, with an average of 480 million alveoli (range of 300-800 million) reported in an adult lung [7, 20, 21]. The dramatic increase in the number of alveoli and overall surface area happens through the formation of secondary septa. At this stage of lung development, distal airspaces are lined by thick walls consisting of two external capillary layers and a single central connective tissue layer. Ridges of secondary septa (or crests) arise from primary septa just before term in humans, and at P7 in mice. Initiation sites of these crests are typically rich in elastic fibers and myofibroblasts expressing  $\alpha$ -smooth muscle actin ( $\alpha$ SMA), which secrete numerous proteins of the extracellular matrix (ECM) facilitating crest protrusion [1, 5, 7, 13, 22].

The process of microvascular maturation occurs in parallel with alveolarization and is mainly concluded within the first two to three years of age. During this process double capillary layer matures into a single capillary network facilitating the faster gas diffusion [7, 13]. It is largely accepted, that once the single capillary network is formed, no more alveolarization can occur in the lung [9].

The process of alveolarization remains poorly understood but is thought to be carefully coordinated by the combined action of various gene expression programs (comprised of transcription factors and epigenetic effects) and both contact-mediated and growth factor-mediated cell-to-cell communication. The development and maturation of the lung structure is also driven in part by physical forces caused by breathing motions and the production and remodeling of the ECM scaffold [1, 2, 23-26].

## 1.2 Bronchopulmonary dysplasia

Multiple diseases are either caused by, or by themselves cause disturbances to lung development resulting in malformation of the lung architecture, and defects in gas exchange. Depending on the severity of the damage, serious disturbances to respiratory function, as well as long-term consequences may occur [3].

The most common neonatal form of chronic lung disease (CLD) is bronchopulmonary dysplasia (BPD) [27], which was first described in study by William Northway in 1967, in the lungs of prematurely born infants, treated for the severe respiratory distress syndrome (RDS) [28]. Oxygen supplementation and positive pressure mechanical ventilation received by these patients, however lifesaving, was associated with oxygen toxicity and disturbed postnatal lung development, leading to a consecutive injury, characterized by an interstitial and alveolar edema, persistent inflammation and parenchymal fibrosis [5, 28, 29].

Characteristics of BPD have gradually changed over the past several decades. Improvements in the medical management of BPD led to a considerable increase in the survival of infants with extremely low birth weight, resulting in an increase in BPD incidence. On account of these changes, the definition as well as diagnostic criteria of BPD have been eventually altered [3, 27, 29, 30]. Nowadays, the disease, also known as “new BPD”, is clinically defined by the need for supplemental oxygen and/or mechanical ventilation for more than 28 days, or at the 36<sup>th</sup> week postmenstrual age [27]. Lungs of BPD patients are now histologically characterized less by fibrosis and fibroproliferative airway damage. Instead, the lung structure is more often characterized by defects in alveolar and septal formation (leading to alveolar hypoplasia), thickening of alveolar walls, a dysmorphic pulmonary circulation and ECM remodeling. In comparison to “old BPD”, BPD today is therefore described largely as a disease of arrested lung development (Figure 2) [3, 27, 31, 32].

Despite improvements in clinical care, BPD still remains one of the major causes of morbidity and mortality of infants in a neonatal intensive care unit [3, 27, 29, 30]. Moreover, studies suggest possible long-term consequences of BPD persisting later into the adulthood [33-35]. Although the pathogenic pathways involved in BPD are not well-understood, several hypotheses have been formed about the processes involved in the development of BPD. Processes known to play role in the pathology of BPD include: abnormal shifts in physical forces, failures in the development of pulmonary vasculature, altered cellular composition of

the developing alveoli, increase of inflammatory cell infiltration, perturbed gene expression and growth factor signaling, aberrant cell-to-cell communication, and dysfunctional ECM architecture and metabolism, particularly changes in the abundance and organization of collagen and elastin fibers and deregulation of ECM-remodeling enzymes [5, 36-40].

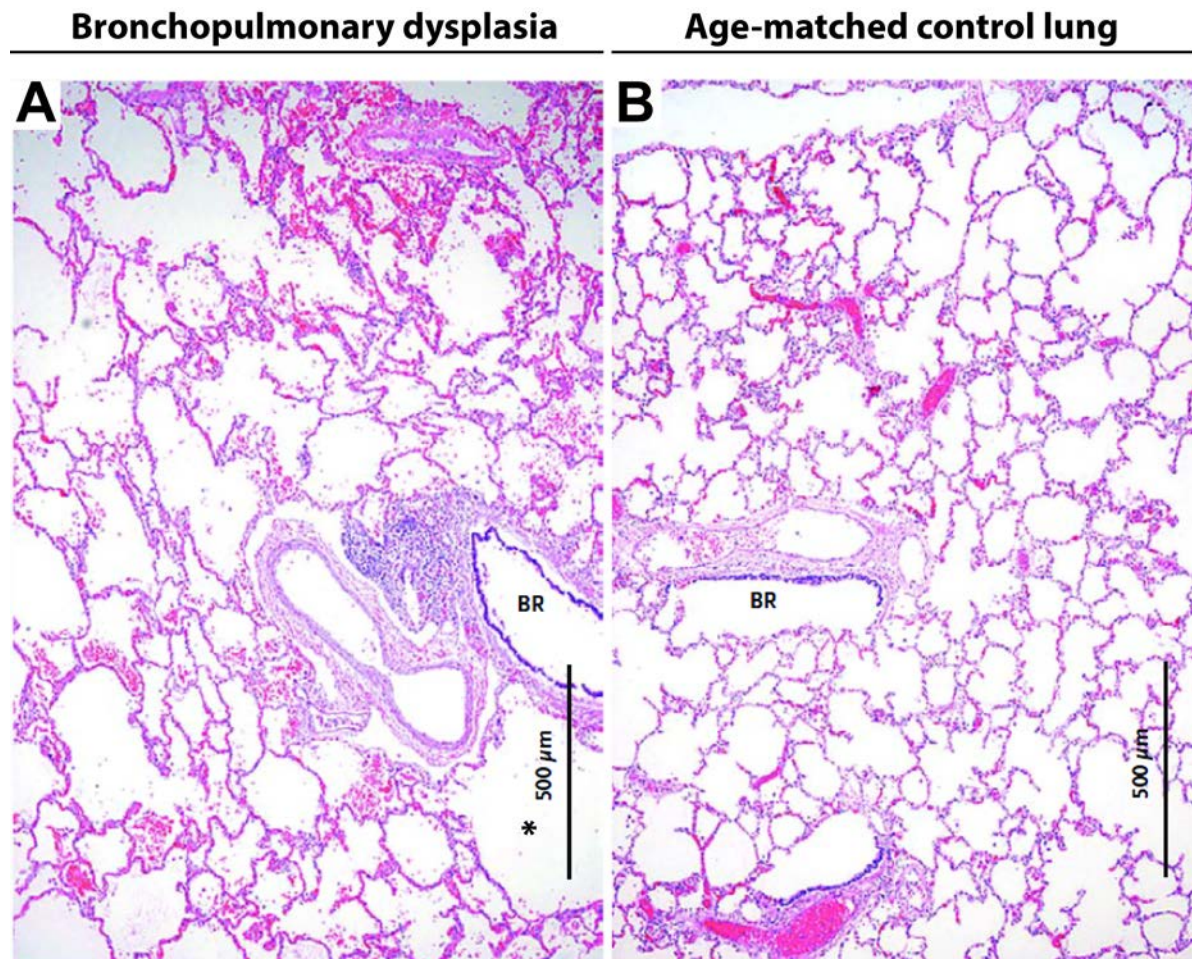


**Figure 2. Histological structure of the lung of a patient with bronchopulmonary dysplasia and a healthy age-matched control lung.**

Comparison of hematoxylin and eosin stained peripheral lung structure in a 12-year old male patient with bronchopulmonary dysplasia (A) and a comparable area of lung tissue from an age-matched control lung with normal alveolarization (B) [41]. Asterisk marks abnormally enlarged air space. *BR*, bronchiole.

### **1.3 The extracellular matrix in context of normal and aberrant lung development**

Branching morphogenesis and alveolarization are characterized by intensive growth and remodeling of newly forming parenchymal structures. This process requires precisely timed mesenchymal-to-epithelial interactions, which cannot occur in the absence of a functional ECM compartment [42, 43].

The first observations regarding the remodeling of ECM structures during lung development, namely collagen and elastin, were made in the 1970's and 1980's [44, 45]. While the ECM plays a mainly supporting role in adult lung, it provides a crucial mechanical support for the developing epithelium, mesenchyme and the capillary network [4, 5]. During the alveolar stage of lung development, collagen is mainly present within the alveolar walls, while elastin is deposited more specifically in areas of so-called "foci" at the tips of protruding secondary septa, suggesting the importance of elastin in the process of septal formation [13, 46] (Figure 3). The expression of collagen and elastin is strongly regulated throughout the course of lung development in various experimental animals, including mice [46-49]. While expression of both basement membrane and fibrillary collagens peaks at P7, the peak of elastin expression coincides with the burst of secondary septation around P14 [5, 48]. The importance of collagen and elastin in postnatal lung maturation was further proven in studies using lathyrogens, pharmaceutical lathyrisms-inducing agents, namely  $\beta$ -aminopropionitrile (BAPN), which disrupted normal ECM deposition and led to an arrest in alveolarization [50, 51].

A failure of alveolar septation in both a clinical and an experimental setting is accompanied by changes in ECM production and deposition. Perturbed ECM structures have been repeatedly reported in disorders of lung development, including BPD. Collagen fibers in the lung parenchyma in these studies are often described as "disorganized, tortuous, and thickened" [37, 38]. Elastin fibers also exhibit an abnormal structure formation both in the parenchyma [52-54] and the vasculature [55] of patients with BPD, and animal models of BPD alike (Figure 3).

Despite the considerable effort made in order to understand the changes in ECM production and metabolism in the developing lung parenchyma, the underlying reasons for these perturbations are still not fully known [5]. However, ECM homeostasis throughout lung development and a balance between ECM production by cells and degradation and

remodeling of ECM components by enzymatic machinery seems to play a key role in processes of alveolar and septal formation.

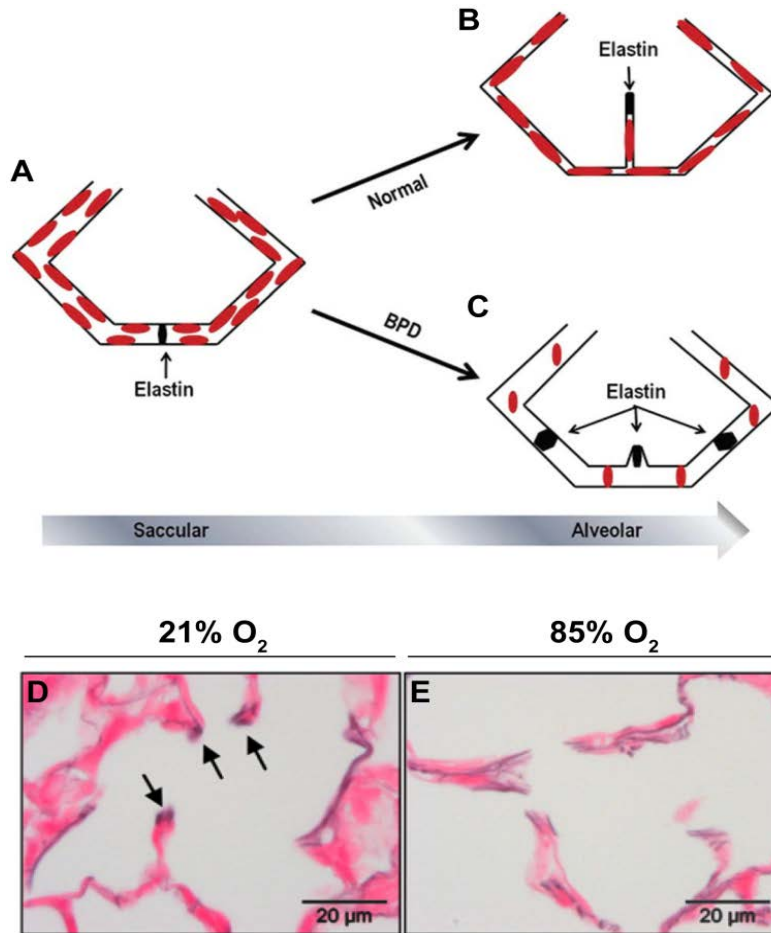


**Figure 3. Elastin deposition during lung formation in bronchopulmonary dysplasia and in the hyperoxia-based mouse model of bronchopulmonary dysplasia.**

(A-C) Schematic representation of elastin deposition and capillary network formation during normal and aberrant alveolarization. (A) Initial elastin deposition within the alveolar wall, prior to the formation of secondary septa in the normally developing lung. A double capillary network is present. (B) Elastin localizes to the top of newly forming secondary septa in the normally developing lung. A single capillary network is present. (C) Deposition of elastin at the top of secondary septa is disturbed during aberrant alveolar formation associated with bronchopulmonary dysplasia (BPD). Elastin is partially deposited within thickened septa. The alveolar microvasculature is malformed [13]. (D-E) Elastin foci in the hyperoxia-based mouse model of BPD. (D) Elastin fibers form foci at the top of secondary septa in mice exposed to 21% O<sub>2</sub>. (E) Elastin fibers fail to form foci in the lungs of mice exposed to 85% O<sub>2</sub> from the day of birth up to, and including postnatal day 28. Elastin fibers appear disorganized and malformed. Elastin visualized by Hart's stain [46].

### **1.3.1 Key components of extracellular matrix in the context of lung development**

The ECM forms a complex, large network of multiple heterogeneous components with diverse structural, mechanical and biochemical properties [56]. Within these structural elements of ECM the most abundant are collagen and elastin which represent 50% [57] and 18% [58], respectively, of the lung ECM. Other components include microfibrils, glycoproteins fibrillin [59] and fibulin [60], integrins and integrin ligands [61].

The ECM structure, which serves as a scaffold, is constantly remodeled during lung development [42, 43]. Therefore, the production of structural components which form ECM, as well as the enzymatic systems involved in regulation of ECM deposition and stability, must be considered. This machinery include members of families of enzymes involved in the post-translational modulations of various ECM components on one hand, and degradation of the ECM on the other hand. Together this actions of ECM-remodeling enzymes enable natural processes of the ECM renewal [5].

#### **Collagen**

The most abundant protein within the interstitial ECM, collagen, is produced by fibroblasts [62-64]. Collagen fibers in the lung, which are represented predominantly by collagen types I and III, are found mainly within blood vessels, bronchi and alveolar septa [65-67]. Quantity of collagen in the lung fluctuates throughout the period of lung development, with a peak in expression at P7 in mice. Parenchymal collagen forms a fine network of fibers. Collagen has been attributed with a major role in processes of alveolar septation [38, 48].

Numerous studies using various animal models of BPD and emphysema have demonstrated the presence of abnormal collagen structures and failures in integrity of collagen network. These changes are thought to be associated not only with defects in formation of new alveoli, but also in the destruction of pre-existing alveoli [38, 46, 68]. Furthermore, studies performed in animal models of BPD report an increase in collagen production accompanied with a formation of thicker collagen fibers, which was associated with decrease in lung elasticity [46, 68].

Observations along this line were also made in clinical studies. Lungs of the patients diagnosed with BPD exhibited an increase in the abundance of fibrillar collagens (collagen I and III) and collagen I/collagen III ratio. In addition the number of collagen-positive cells

was also increased [65, 69]. Thickened, disorganized and misshapen collagen fibers were also observed in lungs of patients diagnosed with BPD who received positive pressure ventilation. It is possible that the increase in the size of the alveoli due to the ventilation causes a compression and damage to ECM network surrounding the alveoli, eventually corrupting the normal course of septation [38].

*In vitro*, collagen production can be regulated by growth factors, including transforming growth factor (TGF)- $\beta$  [70, 71]. Supporting the findings *in vitro* are the reports of increased levels of TGF- $\beta$  in preterm infants with BPD [72]. Moreover, TGF- $\beta$  was casually implicated in arrest of alveolar formation in animal model of BPD where an increase in TGF- $\beta$  activation led to an increase in a collagen production by fibroblasts and in the consecutive collagen deposition [46, 73, 74]. Similarly, TGF- $\beta$  over-expressed in the lungs *in utero* led to pulmonary hypoplasia, collagen deposition was increased in the developing alveolar septa and animals developed thickened collagen fibers [75]. Furthermore, it has been shown that TGF- $\beta$  modulates expression levels of multiple matrix-remodeling enzymes, further regulating collagen formation and metabolism [70, 76-78].

## **Elastin**

Elastic fibers are formed by thoroughly cross-linked microfibrils of elastin and fibrillin associated with several accessory molecules, including latent TGF- $\beta$ -binding protein (LTBP), fibulins and emilins [59]. Elastin in the developing lungs is produced by fibroblasts and smooth muscle cells (SMC). Elastic fibers in the lung are present predominantly in the conducting airways, alveolar ducts, alveoli and in the developing lung vasculature [62, 64, 79]. The expression of elastin and formation of elastin network in lungs begins in the pseudoglandular stage. Elastin (*Eln*) expression peaks between the saccular and alveolar stage and remain high throughout the period of secondary septation (P5–P15 in mice). Throughout the alveolar stage, elastin is found specifically at the tips of the developing septa, where it forms elastin foci. This pattern of deposition indicates that elastin could play a role in the formation of secondary septa and in the alveolarization [13, 46, 80]. The expression of elastin eventually decreases after the process of alveolarization is completed [48, 81].

Although the expression of elastin in adult lungs is low, reactivation of elastin synthesis can occur in various pathological situations. For example, disorganized and unusually shaped elastic fibers were described in emphysema and pulmonary fibrosis [39,

81]. Similarly, abnormal elastin fiber structure and deposition was observed within the parenchyma of prematurely-born ventilated neonates [82].

The importance of elastin in the development of the lung is further emphasized by studies on elastin deficient (*Eln*<sup>-/-</sup>) or haploinsufficient (*Eln*<sup>+/-</sup>) mice. Complete deletion of elastin causes perinatal lethality and lungs of *Eln*<sup>-/-</sup> mice show an impaired distal airway development [83]. While retaining a normal lung development and lung structure, elastin haploinsufficient mice express 50% lower elastin levels, and two-fold increase in levels of collagen and lysyl oxidase (LOX). This observations were accompanied by an increase in lung compliance and decrease in stiffness when compared to wild-type (WT) mice [84, 85]. Along the same line, transgenic mice with elastin expression decreased to 37% of normal levels, had good survival, but exhibited a significant increase in lung size and a pronounced arrest in alveolar formation [85].

Over the past decade, elastin has been studied at length in multiple animal models of lung development and BPD. Both perinatal hyperoxia and mechanical ventilation were shown to increase elastin production. Elastin fibers in these lungs are often described as disturbed and fragmented and are largely localized within alveolar walls instead of septal tips [46, 64, 86-88]. Abnormalities in elastin fibers formation probably leads to a further fiber disintegration and malfunction.

Although the mechanisms behind the elastin regulation are not fully understood, multiple studies highlight the possible roles of TGF- $\beta$  and platelet-derived growth factor (PDGF) in these processes. While TGF- $\beta$  seems to be involved in induction of elastin expression [76, 89, 90], certain forms of PDGF suppressed elastin production [91]. This data from experimental models supports observations made in clinical studies, where increase in the abundance of TGF- $\beta$  [72] and decrease in abundance of PDGF were observed in BPD patients [92].

While both, studies employing mechanical ventilation, and perinatal hyperoxia models report an increase in elastin mRNA levels, controversy exists about the status of mature elastin, where different observations have been made in respect to the methods employed (analysis of tropoelastin by immunoblot, vs. histological staining, vs. analysis of elastin cross-links) [88, 93-95].

## **Extracellular matrix remodeling enzymes**

Although many studies focus on ECM components synthesis and production, only few studies to date have explored the subsequent ECM processing and remodeling. However, due to the long half-life of ECM fibers in the lung (up to several years in mice), more importance has recently been given to formation of elastin and collagen fibers, their remodeling and maturation, rather than the gene and protein expression *per se* [4, 46, 96-98].

It is likely that the formation of elastin and collagen fibers with abnormal structure and properties is a result of dysregulated activity of large amount of matrix-remodeling enzymes. Possible candidate enzymes include: matrix metalloproteinases (MMPs), tissue inhibitors of matrix metalloproteinases (TIMPs), and members of transglutaminase (TGM), lysyl hydroxylase (Procollagen-lysine, 2-oxoglutarate 5-dioxygenase; PLOD) and the lysyl oxidase family. Interestingly in addition to an ability to modulate expression levels of elastin and collagen itself, TGF- $\beta$  was also shown to impact the expression levels of above-listed matrix remodeling enzymes [70, 76-78, 97, 98]. Therefore, it has been proposed that an arrest in lung alveolarization and proper matrix formation may occur as a consequence of a protease/anti-protease imbalance and changes in collagen/elastin ratio introduced by increased levels of TGF- $\beta$  [99].

### **1.4 The lysyl oxidase family**

Several recent studies have revealed the importance of matrix remodeling enzymes in ECM deposition and remodeling during both normal and aberrant lung development associated with BPD [46, 58, 97, 98]. Among these are elastin and collagen cross-linking enzymes of the lysyl oxidase family.

The lysyl oxidase family comprises of five copper-dependent amine oxidases: lysyl oxidase (LOX) and four lysyl oxidase-like enzymes (LOXL1-LOXL4) [100, 101]. All members of the family catalyze the process of oxidative deamination of lysine and hydroxylysine residues (Figure 4). Deamination generates semialdehydes, which are highly reactive and spontaneously form intramolecular and intermolecular covalent cross-links in elastin and collagen molecules [100, 101].

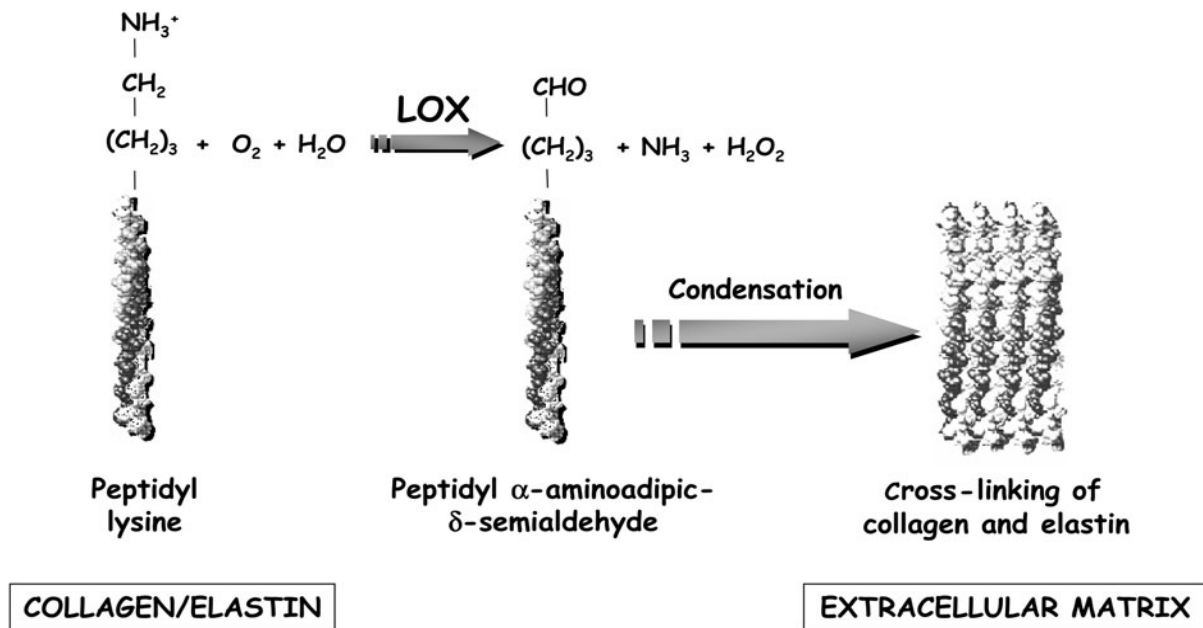


**Figure 4. Chemical reaction catalyzed by lysyl oxidase.**

Schematic representation of lysyl oxidase (LOX)-mediated oxidative deamination. Primary amines in elastin and collagen molecules are oxidized by LOX and other members of lysyl oxidase family to reactive semialdehydes. Reactive semialdehydes further form covalent intramolecular and intermolecular cross-links [102].

Lysyl oxidases play a crucial role in the processes of normal lung development as demonstrated by studies in knock-out animals. Lysyl oxidase-deficient mice exhibit perinatal lethality due to aortic aneurism and severe cardio-respiratory dysfunction. Lungs of *Lox*<sup>-/-</sup> mice are characterized by an arrest in alveolarization and elastic and collagen fibers in these lungs were described as “fragmented and disperse” [58, 103, 104]. In addition, desmosine (a measure of elastin cross-links) and hydroxylysinonorleucine (HLNL) and hydroxyproline (HP) crosslinks (both measures of collagen cross-linking status), were severely decreased in lungs of *Lox*<sup>-/-</sup> mice when compared to wild-type mice [104]. Moreover, lysyl oxidase enzymatic activity was rapidly decreased in the absence of *Lox* expression. This suggests that LOX alone might serve as the main contributor to overall catalytic activity of this enzymatic family. Unlike *Lox*<sup>-/-</sup> mice, mice deficient in *Loxl1* survived to adulthood. However *Loxl1*<sup>-/-</sup> mice are characterized by decreased connective tissue strength leading to a formation of redundant skin and pelvic organ prolapse. Lungs of *Loxl1*<sup>-/-</sup> mice also had enlarged airspaces and exhibited a decrease in desmosine, but not HP levels, suggesting that LOXL1 plays a role exclusively in elastin (but not collagen) metabolism [105].

The role of lysyl oxidases have been implicated in the development of several lung diseases, including pulmonary arterial hypertension, lung adenocarcinoma, lung fibrosis, and BPD [46, 106-108]. The role of lysyl oxidases in BPD has also been investigated in several animal models. Gene expression of *Lox* and *Loxl1* was increased in the lungs of pre-term ventilated lambs [109]. Although the expression of *Lox* in the lung was similarly increased in mechanically ventilated mouse pups, *Loxl1* levels were decreased [93]. An increase in lung gene expression and protein abundance of LOX, LOXL1, LOXL2 and LOXL3 was noted in the hyperoxia-based mouse model of BPD, accompanied by increase in overall lysyl oxidase enzymatic activity [46]. Exposure of developing mouse pups to increased concentrations of oxygen was additionally associated with arrest in alveolar formation and a severe defect in elastin foci formation. Similarly, *Lox* and *Loxl1* levels were increased in lung of patients diagnosed with BPD [46].

In addition, localization of LOX in the nuclei of fibrogenic [110] and LOXL2 in the nuclei of epithelial cells [111] has recently been discovered. This findings suggests the existence of “non-matrix” roles for at least some members of lysyl oxidase family [112]. For example, LOX could drive the transcription of collagen III $\alpha$ 1 (*Col3a1*) gene in fibroblasts [113]. LOX was also found to increase the activity of *Eln* promoter in human embryonic kidney (HEK) 293T cells [114]. Furthermore, LOXL2 was associated with Snail1, suggesting a possible role in *Cdh* expression regulation [111]. LOXL2 was also found to catalyze the deamination of trimethylated Lys4 in histone H3, therefore modulating epigenetic effects in the nucleus [115], which was associated with epithelial-to-mesenchymal transition (EMT).

It is therefore possible that lysyl oxidases play a dual role in the processes of lung development and pathogenesis of BPD. It is likely that dysregulation in the gene and protein expression of lysyl oxidases (and potentially expression of other matrix remodeling enzymes) leads to formation of over cross-linked elastin and collagen fibers in the parenchyma of the developing lung. This way excessively stabilized ECM network would be unable to undergo native processes of ECM remodeling leading to an increase in lung stiffness. This would impact the elastic properties of the lung, possibly causing an arrest in alveolarization and formation of secondary septa. Alternatively, unbalance in expression of lysyl oxidases could drive further changes in the expression of potential lysyl oxidase target genes, including essential components of ECM network *Eln* and *Col*, contributing even more to the disturbances in ECM formation and remodeling. However, the causal role of lysyl oxidases in

formation of ECM structures and perturbed gene regulation in the context of BPD has not yet been fully adressed.

## 2 AIMS OF THE STUDY

Bronchopulmonary dysplasia presents a common complication of preterm birth with significant morbidity and mortality. Pathogenic pathways behind the development of BPD are not well understood, however, the importance of proper formation and metabolism of the ECM in the context of normal and aberrant lung development is well known. Abnormal formation and deposition of two main structural components of ECM, collagen and elastin fibers, represent a pathological feature of both clinical and experimental BPD.

The correct temporal and spatial coordination of the activity of matrix remodeling enzymes plays a crucial role in elastin and collagen metabolism and remodeling. Among these are lysyl oxidases, amine oxidases catalyzing the formation of covalent crosslinks in elastin and collagen molecules. Dysregulated expression and activity of lysyl oxidases have been reported to play a role in pathogenesis of BPD, as well as in various animal models of BPD.

In this context, the main aims of this study were:

- i.) To characterize the expression profile of lysyl oxidase family members in mouse lungs during normal and aberrant lung development.
- ii.) To investigate a causal role for the lysyl oxidase family in experimental hyperoxia-based mouse model of BPD.
- iii.) To assess the impact of lysyl oxidase activity on the formation of elastin and collagen fibers in mice lungs during normal and aberrant lung development.
- iv.) To assess the impact of lysyl oxidase activity on lung alveolarization in mice lungs during normal and aberrant lung development.
- v.) To explore the possible “non-matrix” roles for lysyl oxidases *in vitro*.

### 3 MATERIALS AND METHODS

#### 3.1 Materials

##### 3.1.1 Equipment

<b>Name</b>	<b>Company</b>
Autoclave	Systec, Germany
Agar embedding moulds	custom made
Agar cutting mould	custom made
Bacteria culture incubator	Heareus, Germany
Blotting membrane, Trans-Blot <sup>®</sup> Turbo <sup>™</sup> Transfer Pack	Bio-Rad, Germany
Camera, D5300	NIKON, USA
Cell counter, Countess <sup>®</sup>	Invitrogen, UK
Cell culture dish, 100 mm	Greiner Bio-One, Germany
Cell culture dish for bacteria	Greiner Bio-One, Germany
Cell culture flask, 250 ml	Greiner Bio-One, Germany
Cell culture incubator	Thermo Fisher Scientific, USA
Cell culture plates, 6-well	Greiner Bio-One, Germany
Cell culture plates, 6-well, Snapwell Permeable Support	Costar, USA
Cell culture sterile working bench	Thermo Fisher Scientific, USA
Cell scrapers, 25 cm	Sarstedt, Germany
Cell strainers, 100, 40 µm	BD Biosciences USA
Cover slides	Roth, Germany
Digital slide scanner, NanoZoomer-XR C12000	Hamamatsu, Germany
<i>Eco</i> RI enzyme	Promega, USA
Electrophoresis chambers, Wide Mini-Sub <sup>®</sup> Cell GT	Bio-Rad, Germany
Electrophoresis chambers, Mini Protean <sup>®</sup> Tetra system	Bio-Rad, Germany
Espresso personal microcentrifuge	VWR, USA
Feather <sup>®</sup> trimming blade	Pfm medical, Germany
FIA 96-well plate, black	Greiner Bio-One, Germany
Filter tips, 10 µl, 100 µl, 200 µl, 300 µl, 1000 µl	Sarstedt, Germany
Fully Automated Rotary Microtome	Leica Biosystems, Germany
Fume hood	Vinitex, Netherlands

<b>Name</b>	<b>Company</b>
Heating plate	Medax, Germany
High speed micro centrifuge	Hitachi, Japan
Histobloc	Heareus, Germany
Histoform Q mould	Heareus, Germany
Homogenizing kit for soft tissue, Precellys <sup>®</sup>	PEQLAB, Germany
Homogenyzer, Precellys <sup>®</sup> 24-Dual homogenizer	PEQLAB, Germany
Imager ImageQuant <sup>®</sup> LAS 4000	GE health care, USA
Infinite <sup>®</sup> 200 PRO multimode reader	TECAN, Switzerland
Inoculation loops, 10 µl	Sarstedt, Germany
InoLab <sup>®</sup> pH meter	WTW, Germany
Knife holder NZ RM2200 silver	Leica Biosystems, Germany
Light microscope	Leica, Germany
Magnetic Dynabeads <sup>®</sup> , streptavidin-coupled	Thermo Fisher Scientific, USA
Magnetic separator	Thermo Fisher Scientific, USA
MicroAmp <sup>®</sup> Optical 96-Well Reaction Plate	Thermo Fisher Scientific, USA
Microcentrifuge tubes, 0.5, 1.5, 2 ml	Eppendorf, Germany
Microplate reader, VersaMax ELISA	Molecular devices, USA
Microscope slides, SUPERFROST ULTRA PLUS <sup>®</sup>	Thermo Fisher Scientific, USA
Microtome blade S-35 pfm,	Pfm medical, Germany
Microtome knife, 16cm long, profile d, steel assy	Leica Biosystems, Germany
Multifuge 3 S-R centrifuge	Heraeus, Germany
NanoDrop <sup>®</sup> ND-1000 spectrophotometer	Thermo Fisher Scientific, USA
Nitrocellulose membrane, 0.2 µm	Bio-Rad, Germany
Objective, AF-S DX Micro NIKKOR, 85mm	NIKON, USA
Paraffin embedding station	Leica Biosystems, Germany
Pasteur pipette, 3.5 ml	Sarstedt, Germany
PCR-thermocycler, peqSTAR	VWR, USA
Pipetboy <sup>®</sup>	Integra, Switzerland
Pipettes, automatic, 10 µl, 100 µl, 300 µl	Eppendorf, Germany
Pipettes, manual, 10 µl, 20 µl, 100 µl, 200 µl, 1000 µl	Eppendorf, Germany
Pipettes, multichannel, 300 µl	Eppendorf, Germany

<b>Name</b>	<b>Company</b>
Pipettes, serological, 2 ml, 5 ml, 10 ml, 25 ml, 50 ml	Falcon, USA
Polyvinylidene difluoride (PVDF) membranes, 0.2 µm	Bio-Rad, Germany
Real-Time PCR system, StepOnePlus™	Applied Biosystems, USA
Refrigerated microcentrifuge CT15RE	VWR, USA
Rotilabo® embedding cassettes	Roth, Germany
Routine Stereomicroscope	Leica Biosystems, Germany
Single use needles, FINE-JECT®	HENKE SASS WOLF, Germany
Snap-cap vials, Rotilabo®	Roth, Germany
Snap-on lids	Roth, Germany
Standard analog shaker	VWR, USA
Standard Clamp w/Adapter 40×40 mm Silver	Leica Biosystems , Germany
Surgical instruments – scissors, tweezers	F.S.T., Germany
Thermo shaker, MS-100	Universal labortechnik, Germany
Test tubes, 15 ml, 50ml	Greiner Bio-One, Germany
Tissue processor	Leica Biosystems, Germany
Ultraviolet (UV) Transilluminator, Gel Imager	Intas, Germany
Unneeded polyamide suture, SUPRAMID	SERAG, Germany
VisiopharmNewCast software	Visiopharm, Denmark
Vortex mixer	VWR, USA
Waterbath, for cell culture	Lauda, USA
Water bath, for histological slides	Vogel, Germany
Western blot transfer system, Trans-Blot® Turbo™	Bio-Rad, Germany
White light transilluminator, TW-26	UVP, UK

### 3.1.2 Reagents

<b>Name</b>	<b>Company</b>
Accutase <sup>®</sup> solution	Sigma-Aldrich, Germany
Acetone, > 99.7% (vol/vol)	Roth, Germany
Acrylamide solution, Rotiphorese Gel 30	Roth, Germany
Agar for microbiology (Agar-agar)	Sigma-Aldrich, Germany
Agarose	Promega, Germany
Agarose, low melting point	Sigma-Aldrich, Germany
Ammonium persulfate (APS)	Promega, Germany
Ampicillin sodium salt	Sigma-Aldrich, Germany
Azure II	Sigma-Aldrich, Germany
Borax, di-Natriumtetraborate Decahydrate	Roth, Germany
Bovine serum albumin (BSA)	Thermo Fisher Scientific, USA
Collagenase	Sigma-Aldrich, Germany
Complete macrophage medium	CellBiologics, USA
Complete mouse endothelial cell medium	CellBiologics, USA
Complete <sup>®</sup> protease inhibitor	Roche, Germany
Dispase	BD Biosciences, USA
1,4-Dithiothreitol (DTT)	Promega, USA
DNase I	Serva, Germany
Dulbecco's modified Eagle medium (DMEM), 1 g/l glucose	Thermo Fisher Scientific, USA
Dulbecco's modified Eagle's medium (DMEM), 4.5 g/l glucose	Thermo Fisher Scientific, USA
Dulbecco's phosphate buffered saline (DPBS)	Sigma-Aldrich, Germany
Elastase	Sigma-Aldrich, Germany
Ethanol, 70% (vol/vol)	Roth, Germany
Ethanol, absolute	Roth, Germany
Ethidium bromide	Promega, USA
Ethylenediaminetetraacetic acid (EDTA)	Sigma-Aldrich, Germany
Ethylene glycol-bis ( $\beta$ -aminoethyl ether)- <i>N,N,N',N'</i> -tetraacetic acid (EGTA)	Sigma-Aldrich, Germany

<b>Name</b>	<b>Company</b>
Fetal bovine serum (FBS)	PAA Laboratories, Austria
Gelatin-Based Coating Solution	CellBiologics, USA
GeneRuller™, DNA ladders	Thermo Fisher Scientific, USA
Glutaraldehyde	Serva, Germany
Glycine	Roth, Germany
Hank's balanced salt solution (HBSS)	PAA Laboratories, Austria
Hematoxylin	Waldeck, Germany
HEPES	Sigma-Aldrich, Germany
Isofluran-CP®, 1ml/ml	Cp-pharma®, Germany
LB-Agar, Lurria/Muller	Roth, Germany
4× Laemmli Sample Buffer	Bio-Rad, Germany
Lipofectamine® 2000	Thermo Fisher Scientific, USA
Liquid nitrogen	Air Liquide, Germany
Magnesium chloride (25 nM)	Applied Biosystems, USA
Magnesium chloride (50 nM)	Thermo Fisher Scientific, USA
2-Mercaptoethanol	Bio-Rad, Germany
Methanol	Sigma-Aldrich, Germany
Methylene blue	Roth, Germany
MuLV reverse transcriptase	Applied Biosystems, USA
m-Xylol, > 98.5% (vol/vol)	Roth, Germany
NARCOREN®, Pentobarbital Sodium	Merial GmbH
Non-fat dry milk powder	Roth, Germany
Nuclease-free water	Ambion, USA
OptiMEM® medium	Thermo Fisher Scientific, USA
Osmium tetroxide	Roth, Germany
Paraformaldehyde (PFA)	Sigma-Aldrich, Germany
Paraplast®, paraffin	Leica, Biosystems, Germany
PCR-Buffer II 10×	Applied Biosystems, USA
PCR Nucleotide Mix (10 mM)	Promega, USA
pCR™2.1-TOPO® Gateway Entry	Thermo Fisher Scientific, USA
Pencillin – Streptomycin (100×)	AppliChem, Germany

<b>Name</b>	<b>Company</b>
Pertex, mounting media	Medite, Germany
Phosphate buffered saline (PBS) 1×, 10×	Sigma-Aldrich, Germany
Platinum <sup>®</sup> SYBR <sup>®</sup> Green qPCR SuperMix UDG kit	Invitrogen, USA
pLenti7.3/V5DESTTM	Thermo Fisher Scientific, USA
Polybrene, hexadimethrine bromide	Sigma-Aldrich, Germany
Ponceau S	Sigma-Aldrich, Germany
Precision Plus Protein <sup>®</sup> Dual color standard	Bio-Rad, Germany
Propane/Butane	Campin Gaz, Germany
2-Propanol	Merck, Germany
Proteinase K	Promega, USA
QIAquick gel extraction kit	Qiagen, Netherlands
QIAquick PCR purification kit	Qiagen, Netherlands
QIAprep <sup>®</sup> SpinMiniprep/Maxiprep kit	Qiagen, Netherlands
QuickStart <sup>®</sup> Bradford 1×Dye Reagent	Bio-Rad, Germany
Random hexamers, 50 μM	Thermo Fisher Scientific, USA
Resorcin-Fuchsin	Waldeck, Germany
RIPA <sup>®</sup> buffer	Sigma-Aldrich, Germany
RNase free water	Qiagen, Germany
Roti <sup>®</sup> -Histol	Roth, Germany
RNase inhibitor	Applied Biosystems, USA
Select agar	Sigma-Aldrich, Germany
SmGm-2 Supplements	Lonza, Switzerland
Smooth muscle growth medium (SmGM)-2	Lonza, Switzerland
Sodium cacodylate	Serva, Germany
Sodium dodecyl sulfate (SDS), 10× solution	Promega, USA
Sodium orthovanadate	Sigma-Aldrich, Germany
Spectinomycin dihydrochloride pentahydrate	Sigma-Aldrich, Germany
Super Optimal Broth (S.O.C)	Thermo Fisher Scientific, USA
SuperSignal <sup>®</sup> West femto maximum sensitivity substrate	ThermoFisher Scientific, USA
Tris-acetate-EDTA (TAE) buffer, 50×	Roth, Germany
Tris-EDTA (TE) buffer	ThermoFisher Scientific, USA

<b>Name</b>	<b>Company</b>
Technovit 3040	HeareusKulzer, Germany
Technovit 7100	HeareusKulzer, Germany
Technovit, universal liquid	Heareus Kulzer, Germany
Tetramethylethylenediamine (TEMED)	Bio-Rad, Germany
Tris	Roth, Germany
Trypsin-EDTA	ThermoFisher Scientific, USA
Trypan blue solution 0.4% (vol/vol)	ThermoFisher Scientific, USA
TurboFect™	ThermoFisher Scientific, USA
Tween® 20	Sigma-Aldrich, Germany
Uranyl acetate	Serva, Germany
Van Gieson stain	Roth, Germany
Water for injections	ThermoFisher Scientific, USA

### 3.1.3 Purchased primary cells and cell-lines

NIH/3T3, fibroblasts, mouse embryonic cells	American Type Culture Collection, USA
HEK 293T, human embryonic kidney cells, epithelial cells	American Type Culture Collection, USA
TheTransform One Shot <sup>®</sup> DH5 $\alpha$ <sup>™</sup> -T1R, TOP10 Competent Cells, <i>E.coli</i> cells	ThermoFisher Scientific, USA
Bone marrow macrophages, bone marrow derived mouse macrophages	Cell Biologics, USA
Primary lung vascular endothelial cells, primary mouse cells	Cell Biologics, USA

## 3.2 Methods

### 3.2.1 Animal experiments

All animal procedures were approved by the local authorities, *Regierungspräsidium Darmstadt* (approval numbers B2/329; B2/1029 and B2/277).

#### 3.2.1.1 Pilot study

Prior to intervention studies, a pilot study was performed in order to determine the tolerance of mice to BAPN treatment. Two different doses of BAPN, as well as control injections with vehicle were employed, and animals were observed for duration of five days. Three animals per group were injected intraperitoneally (i.p.) daily with either vehicle [1× phosphate buffered saline (PBS)], or BAPN (diluted in vehicle) at a dose of 15 or 150 mg·kg<sup>-1</sup>·day<sup>-1</sup>. All animals were euthanized at P5.5 with an overdose of pentobarbital (500 mg·kg<sup>-1</sup>, i.p.).

#### 3.2.1.2 Normobaric hyperoxia-based mouse model of BPD

An arrest in the alveolarization in the lungs of newborn mouse pups was induced by continuous exposure of animals to normobaric hyperoxia, more precisely 85% O<sub>2</sub> (FiO<sub>2</sub> 0.85) from the day of birth (P1). This model of BPD recapitulates a several major hallmarks seen in human BPD, including morphological changes, such as a decrease in the number of alveoli, an associated decrease of overall gas-exchange surface area and an increase in the septal thickness, as well as inflammation and perturbations to ECM deposition and remodeling.

Newborn C57BL/6J mice were randomized to equal-sized litters (average eight pups per litter) and placed into either a normoxic (21% O<sub>2</sub>) or a hyperoxic (85% O<sub>2</sub>) environment within 2 h after birth. Newborn pups were exposed from the day of birth (P1.5), continuously up to and including P9.5 or P19.5, when experiments were terminated.

In order to minimize oxygen toxicity and potential confounders of milk production caused by hyperoxia, nursing dams were rotated between normoxia and hyperoxia on 24 h : 24 h cycle. Mice were maintained on 12 h : 12 h light-dark cycle and received food *ad libitum*. All animals were euthanized at P9.5 or P19.5 with an overdose of pentobarbital (500 mg·kg<sup>-1</sup>, i.p.).

### **3.2.1.3 Treatment of hyperoxia-exposed newborn mice with $\beta$ -aminopropionitrile**

Based on the observations made during the pilot study BAPN was administered at a dose of  $15 \text{ mg}\cdot\text{kg}^{-1}\cdot\text{day}^{-1}$  in a hyperoxia-based BPD model. Newborn C57BL/6J mice were randomized to equal-sized litters and placed into either a normoxic (21%  $\text{O}_2$ ) or a hyperoxic (85%  $\text{O}_2$ ) environment within 2 h after birth. Both groups were further subdivided into two groups, treated with daily i.p. injections of either vehicle (1 $\times$ PBS), or BAPN (diluted in vehicle) at a dose of  $15 \text{ mg}\cdot\text{kg}^{-1}\cdot\text{day}^{-1}$  for either 9 or 19 days. Experiments were terminated on P9.5 or P19.5.

### **3.2.1.4 Organ isolation**

All animals were euthanized with an overdose of pentobarbital ( $500 \text{ mg}\cdot\text{kg}^{-1}$ , i.p.). Subsequently, the abdomen was opened and the diaphragm was punctured to allow the lungs to retract. The chest wall was opened by cutting through sternum, but ribs remained intact in their original position in order to preserve the natural size of the chest cavity. Lungs were isolated for further stereological analysis, RNA and protein analysis, collagen and elastin measurements or tissue staining.

#### **Lungs isolated for embedding in plastic resin and stereological analysis**

In order to preserve the blood in the tissue, lungs of animals used for stereological analysis were not perfused and animals were not exsanguinated. Instead, lungs were instillation-fixed via a tracheal cannula under a 20 cm  $\text{H}_2\text{O}$  hydrostatic pressure with fixation solution containing 1.5% (wt/vol) paraformaldehyde (PFA) and 1.5% (wt/vol) glutaraldehyde in 150 mM HEPES-PBS. Lungs were excised and stored at 4 °C in fixation solution for 24 h.

#### **Lungs isolated for future RNA and protein analysis**

Animals were exsanguinated and lungs were perfused with 1 $\times$ PBS via the right heart ventricle. Lungs were removed and immediately frozen in liquid nitrogen. Samples were kept at -80 °C for further processing.

### **Lungs isolated for collagen and elastin crosslinks analysis**

Animals were exsanguinated and lungs were perfused with 1×PBS via the right heart ventricle, excised, transferred to 1.5 ml tube containing 1×PBS and frozen in liquid nitrogen. Samples were stored at -80 °C for further processing.

### **Lungs isolated for embedding in paraffin and staining of elastin fibers**

Animals were exsanguinated and lungs were perfused with 1×PBS via the right heart ventricle. The trachea was cannulated and lungs were instillation-fixed under a 20 cm H<sub>2</sub>O hydrostatic pressure with 4% (wt/vol) PFA in 1×PBS. Lungs were excised and stored at 4 °C in fixation solution for 24 h prior to paraffin embedding.

#### **3.2.1.5 Embedding in agar and lung volume estimation**

Following 24 h of fixation, lungs were cleaned of any remains of the trachea, thymus, heart or blood clots and embedded *in toto* in 2% (wt/vol) agar-agar for at least 6 h. Agar blocks were then cut into 2-mm thick sections and always the same side of each section was photographed for calculations of lung volume. Individual pieces of each lung were retrieved from agar slices for further embedding in plastic resin.

The reference lung volume was estimated from photographs of lung sections embedded in agar by the Cavalieri principle using Visiopharm NewCast computer-assisted stereology system. Briefly, point counting was performed on a point grid. Counting was performed within 100% of each lung section. Volume of the lung was estimated based on the number of points counted, size of the surface area/point and thickness of the section.

#### **3.2.1.6 Embedding in plastic resin**

All individual pieces of one lung were transferred into Snap-cap vials and further processed inside a fume hood. Buffers required for treatment of the lungs prior to embedding are listed in Table 1. Briefly, lungs were washed 4 × 5 min with 0.1 M sodium cacodylate buffer and treated with 1% osmium tetroxide (OsO<sub>4</sub>) in 0.1 M sodium cacodylate buffer for 2 h. Afterwards lungs were washed 4 × 5 min with 0.1 M sodium cacodylate buffer, washed 4 × 5 min with ddH<sub>2</sub>O. Samples were then protected from light and treated overnight with half-saturated uranyl acetate (UrAc) buffer. Afterwards, samples were washed with double

distilled (ddH<sub>2</sub>O) and dehydrated in increasing concentration of acetone. Lungs were first incubated overnight in 1:1 solution of 100% acetone and Technovit 7100-Hardener I and eventually Technovit 7100-Hardener I solution. Finally, lungs were incubated in Technovit 7100-Hardener I-Hardener II solution for 5 min. Over this time vials with samples were constantly stirred. Individual pieces of lung, together with the buffer were transferred into a Histoform Q mould and allowed to solidify for at least 48 h. Plastic blocks were removed from moulds with Technovit universal liquid and Technovit 3040 using the Histobloc adaptors.

**Table 1. Buffers required for treatment of lungs and embedding in Technovit 7100.**

<b>Buffer</b>	<b>Dilution</b>
Sodium cacodylate	0.1 M, in ddH <sub>2</sub> O
Osmium tetroxide	2% (wt/vol) stock solution, in water for injections 1% (wt/vol) working solution, in 0.1 M sodium cacodylate
Uranyl acetate	saturated stock solution, in ddH <sub>2</sub> O half-saturated working solution, in ddH <sub>2</sub> O
Acetone	70% (vol/vol), 90% (vol/vol), 100% (vol/vol), in ddH <sub>2</sub> O
Technovit 7100	undiluted solution
Technovit 7100-Hardener I	1% (wt/vol) Hardener I, in Technovit 7100
Technovit 7100-Hardener I-Hardener II	200 µl Hardener II in 3 ml Technovit 7100-Hardener I
Technovit 3040-Technovit universal liquid	2:1 ratio

### **3.2.1.7 Embedding in paraffin**

Lungs were instillation-fixed with 4% (wt/vol) PFA in 1×PBS for 24 h. Afterwards lungs were cleaned of any remains of trachea, thymus, heart or blood clots, transferred in embedding moulds and stored in 1×PBS for up to 1 week prior to processing. Tissue was then dehydrated by ethanol, cleared by xylene to remove alcohol and infiltrated with molten paraffin wax. Finally, tissue was embedded in moulds in paraffin and allowed to solidify on a cooling plate. Material was stored at 4 °C for further use.

### **3.2.1.8 Paraffin and plastic sectioning**

Paraffin and plastic embedded lungs were sectioned with fully automated rotary microtome. For paraffin embedded lungs, 3- $\mu\text{m}$  sections were cut using a Feather microtome blade and collected on Superfrost Ultra Plus adhesion slides. Slides were allowed to dry on a heating plate at 40 °C overnight.

For plastic embedded lungs, blocks were cut into 2- $\mu\text{m}$  sections using a, profile d steel assy microtome knife. Forty sections were cut and every tenth section was collected for staining. In addition, for the estimation of the alveolar number, three consecutive sections were cut and first and third sections were collected on the same adhesion slide. Slides were allowed to dry on a heating plate at 65 °C.

### **3.2.1.9 Hart's elastin staining**

The deposition of elastin fiber structures was visualized in 3- $\mu\text{m}$  thick lung tissue sections from paraffin embedded mouse lungs by Hart's elastin stain. Shortly, paraffin sections were brought to water via xylene and ethanol and incubated in Hart's solution overnight. Subsequently, the slides were washed and counterstained with iron hematoxylin and van Gieson solution. Finally sections were dehydrated with ethanol, clear with xylene and covered with cover slips using a mounting medium.

### **3.2.1.10 Richardson's staining**

Lung structure was visualized in 2  $\mu\text{m}$  thick lung tissue sections from plastic-embedded mouse lungs by Richardson's staining. Briefly, plastic sections were stained in warm Richardson's stain (65 °C) for 30 s, washed briefly in cold tap water and rinsed in hot tap water. Subsequently, sections were washed briefly in ddH<sub>2</sub>O and rinsed in Xylol. All slides were scanned at 60 $\times$  magnification using a NanoZoomer-XR C12000 digital slide scanner.

Richardson's stain – stock solution:

ddH<sub>2</sub>O

0.25% (wt/vol) methylene blue

0.22% (wt/vol) Borax (di-Sodium tetraborate)

0.5% (wt/vol) Azur II

The stock solution must be filtered through filter paper and diluted 1:1 with tap water prior to use.

### **3.2.2 Design-based stereology**

Methods of lung structure analysis were based on the American Thoracic Society/European Respiratory Society recommendations for quantitative assessment of lung structure [116] and according to systematic uniform random sampling for stereological analysis.

Analyses were performed using Visiopharm NewCast computer-assisted stereology system. Analysis of lung structure included four main parameters: gas-exchange surface area, septal thickness, mean linear intercept (MLI) and number of alveoli. In addition, lung volume was estimated by the Cavalieri principle using the same software. The parenchymal fraction, as well as airspace and septal fraction within the parenchyma were counted by point counting on a corresponding point grid (Figure 5A-5B). Surface density was assessed by point and intersection counting on a “line grid” of known length (Figure 5E-5F). Approximately 40-60 lung sections were evaluated on total of four scanned slides and 2-3% of each section was analyzed. The alveolar density was assessed by counting of newly appearing alveolar bridges using a physical dissector, where the height of the dissector was 4 μm (Figure 5C-5D). Approximately 10 sections were evaluated for each lung and 2% of each section was analyzed. In order to determine the absolute number of alveoli and absolute size of gas-exchange surface area in the lung, alveolar density and surface density, respectively were normalized to reference lung volume.

For each stereological parameter, the coefficient of error (CE), the coefficient of variation (CV), and the squared ratio between both ( $CE^2/CV^2$ ) were calculated in order to confirm the measurement precision. The quotient threshold was set at 0.5.

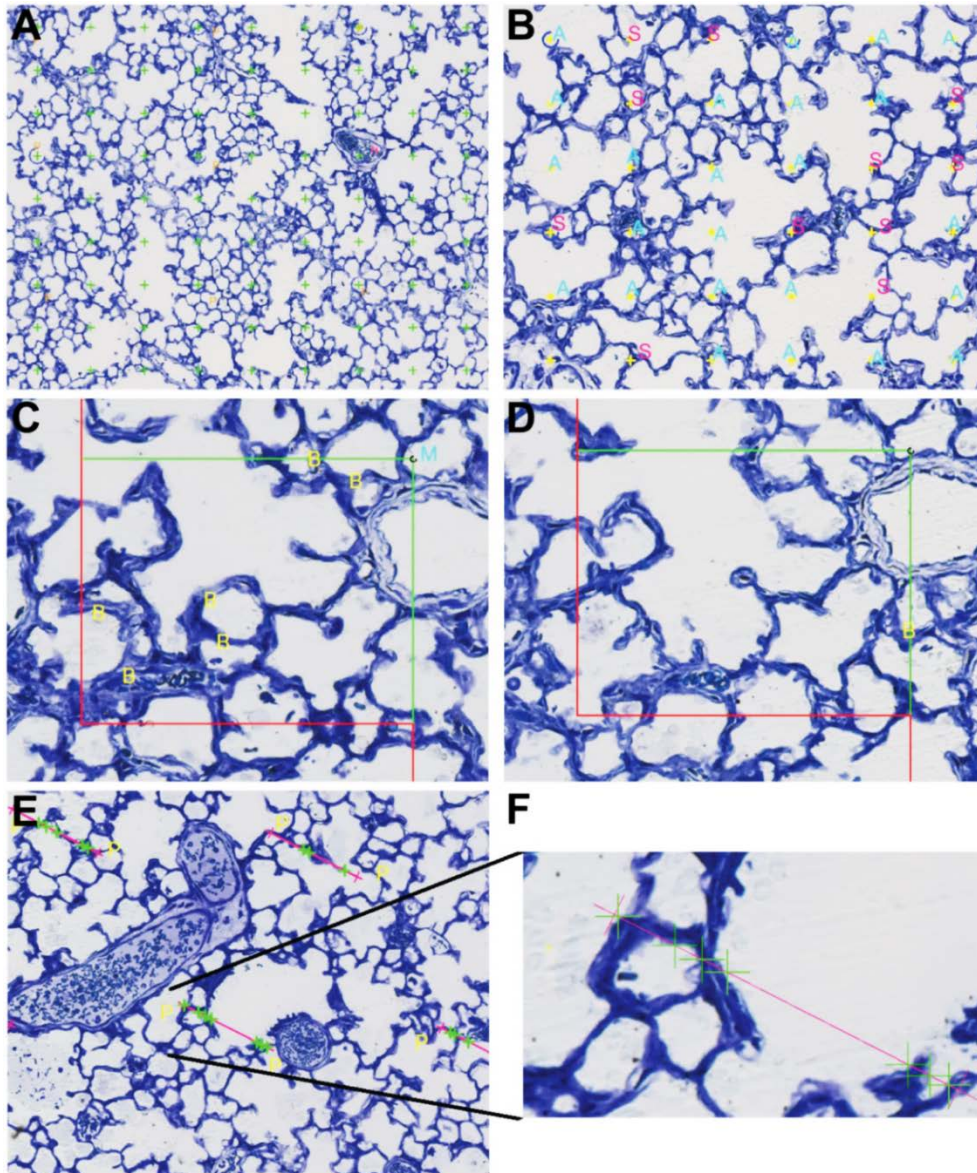


**Figure 5. Visiopharm NewCast counting tools used in the stereological analysis of lung structure.**

Lungs were installation-fixed under 20 cm H<sub>2</sub>O hydrostatic pressure with fixation solution and treated with sodium cacodylate, OsO<sub>4</sub> and uranyl acetate and embedded in plastic resin. Blocks were cut to 2- $\mu$ m sections, stained with Richardson's stain and lung structure was analyzed using the Visiopharm NewCast computer-assisted stereology system. (A-B) An example of a parenchymal fraction estimation (A), and estimation of airspace and septal fraction within parenchymal region (B) by point counting on a corresponding point grid. Magnification 10 $\times$  (A) and 20 $\times$  (B). (C-D) Estimation of alveolar density assessed by two-sided counting of newly forming alveolar bridges. The height of the physical disector was 4  $\mu$ m. Magnification 40 $\times$ . (E) Example of surface density estimation by point and intersection counting on a line grid. Magnification 20 $\times$ . (F) Detail of point and intersection counting from panel E.

### **3.2.3 Cell culture and cell treatments**

#### **3.2.3.1 NIH/3T3 cell culture**

The mouse embryonic fibroblast cell-line NIH/3T3 was cultured in Dulbecco's modified Eagle's medium (DMEM) supplemented with 10% (vol/vol) fetal bovine serum (FBS) and 1% (vol/vol) penicillin/streptomycin (P/S) in incubator at 37 °C with a humidified 5% (vol/vol) CO<sub>2</sub> atmosphere. When the culture reached a confluency of approximately 70%, cells were washed with PBS and treated with 5 ml of acutase solution for 5 min at 37 °C. The activity of acutase was inhibited with 5 ml of culture media and required portion of de-attached cells was transferred into a new culture flask or a 6-well plate.

#### **3.2.3.2 HEK293T cell culture**

Human embryonic kidney (HEK) 293T cells were cultured in DMEM supplemented with 10% (vol/vol) FBS in incubator at 37 °C and humidified in 5% (vol/vol) CO<sub>2</sub> atmosphere. Cells were passaged at 70% confluency. Shortly, cells were washed with 1×PBS and treated with 5 ml of acutase solution for 5 min at 37 °C. Acutase activity was inhibited with culture media and required portion of cells was transferred into a new culture flask or a Petri dish.

#### **3.2.3.3 Bone marrow-derived macrophages culture**

Mouse (C57BL/6) bone marrow-derived macrophages were cultured in gelatine-coated culture flasks in complete macrophage medium and maintained in incubator at 37 °C with a humidified 5% (vol/vol) CO<sub>2</sub> atmosphere.

#### **3.2.3.4 Lung vascular endothelial cells culture**

Primary mouse (C57BL/6) lung microvascular epithelial cells were cultured in gelatine-coated culture flasks in complete mouse endothelial cell medium and maintained in incubator at 37 °C with a humidified 5% (vol/vol) CO<sub>2</sub> atmosphere. Cells were passaged into a new culture flask when confluency reached approximately 70% using trypsin-ethylenediaminetetraacetic acid (EDTA).

### **3.2.3.5 Isolation and culture of primary mouse lung fibroblasts**

Primary mouse lung fibroblasts were isolated from adult female C57BL/6J mice. Briefly, mice were euthanized with an overdose of pentobarbital (500 mg·kg<sup>-1</sup>, i.p), the abdomen was opened and mice were exsanguinated. Subsequently, the diaphragm was punctured to allow the lungs to retract and the chest was opened. Lungs were perfused with 1×PBS via the right heart ventricle, and excised. Lungs were then minced using surgical scissors, transferred into a 50-ml falcon tube containing pre-heated collagenase and stirred for 45 min at 37 °C. A crude tissue suspension was then re-suspended using a 20 ml syringe with 20 G needle and filtered through a 40 µm filter into a new 50-ml falcon tube. The resulting suspension was centrifuged at 400 × g for 8 min at 4 °C and the pellet was re-suspended in 5 ml of DMEM supplemented with 10% (vol/vol) FBS and 1% (vol/vol) P/S.

Cells were cultured in a cell culture flask in incubator at 37 °C with a humidified 5% (vol/vol) CO<sub>2</sub> atmosphere. When the culture reached a confluency of approximately 70%, cells were washed with 1×PBS and treated with 5 ml of acutase solution for 5 min at 37 °C. Activity of acutase was inhibited with 5 ml of culture media and the required portion of de-attached cells was transferred into a new culture flask or a 6-well plate.

### **3.2.3.6 Isolation and culture of primary mouse alveolar epithelial type II cells**

Primary mouse alveolar epithelial type II cells (AECII) were isolated using the modified protocol published by Corti and collaborators [117]. Briefly, C57BL/6J female mice were euthanized with an overdose of pentobarbital (500 mg·kg<sup>-1</sup>, i.p), the abdomen was opened and mice were exsanguinated. Subsequently, the diaphragm was punctured to allow the lungs to retract and the chest was opened. Lungs were perfused with Hank's balanced salt solution (HBSS) via the right heart ventricle. The trachea was cannulated and 2 ml of dispase followed by 0.5 ml of 1% low-melting point agarose was injected into the lungs. Lungs were removed after 5 min and incubated in 3 ml of dispase at room temperature (RT) for 45 min.

The lungs were transferred into a Petri dish containing 7 ml of DMEM without FBS, containing DNaseI (isolation medium I) and the bronchial tree was carefully removed. The crude tissue suspension was incubated for 10 min at RT and sequentially filtered through 100 µm and 40 µm cell strainers and a 20 µm nylon membrane. The resulting cell suspension was centrifuged twice at 130×g for 8 min at 4 °C and the pellet was re-suspended in 5 ml of

DMEM containing FBS (isolation medium II). Cells were stained with trypan blue and counted using a Countess<sup>®</sup> Cell Counter. Cells were then incubated with 0.75 µl biotinylated anti-CD16/32, 0.9 µl biotinylated anti-CD45 and 0.4 µl biotinylated anti-CD31 antibodies per 1 million cells, for 30 min in a water bath at 37 °C, after which cells were centrifuged at 130×g for 8 min at 4 °C. Antibodies required for AECII selection are listed in Table 2. The resulting pellet was resuspended in DMEM without FBS (isolation media III), combined with Streptavidin-coupled Dynabeads<sup>®</sup> magnetic beads and incubated for 30 min at RT followed by 15 min of separation in magnetic separator. After the separation, the supernatant was carefully collected and centrifuged at 130×g for 8 min at 4 °C. Pellet was resuspended in DMEM with 10% (vol/vol) FBS and 1% (vol/vol) P/S (culture media). All media required for AECII isolation are listed in Table 3.

Cells were seeded in 6-well plate with 24-mm diameter Snapwell<sup>™</sup> inserts. After 24 h, the culture medium was removed from the apical compartment and the cells were grown on an air-liquid interface. During the culture cells were stored in incubator at 37 °C and humidified in 5% (vol/vol) CO<sub>2</sub> atmosphere.

**Table 2. Antibodies used for alveolar epithelial type II cells isolation.**

Antibody	Company	Catalog number	Amount (µl)	Origin
anti-CD45	BD Biosciences	553078	(cells in millions) × 0.900	rat
anti-CD16/32	BD Biosciences	553143	(cells in millions) × 0.675	rat
anti-CD31	BD Biosciences	553371	(cells in millions) × 0.400	rat

**Table 3. Media used for alveolar epithelial type II cells isolation and culture.**

Isolation medium I	Isolation medium II	Isolation medium III	Culture medium
DMEM, 4.5 g/l glucose	DMEM, 4.5 g/l glucose	DMEM, 4.5 g/l glucose	DMEM, 4.5 g/l glucose
HEPES, 2% (vol/vol)	FBS, 10% (vol/vol)	P/S, 1% (vol/vol)	FBS, 10% (vol/vol)
P/S, 0.1% (vol/vol)	P/S, 1% (vol/vol)		P/S, 1% (vol/vol)
DNaseI, 0.01% (vol/vol)			

### 3.2.3.7 Isolation and culture of pulmonary arterial smooth muscle cells

Murine pulmonary arterial smooth muscle cells (PASMC) were isolated from C57BL/6J adult mice. Shortly, mice were euthanized with an overdose of pentobarbital (500 mg·kg<sup>-1</sup>, i.p) and the abdomen was open. Mice were then exsanguinated, the diaphragm

was punctured to allow the lungs to retract and the chest was opened. Lungs were perfused with 1×PBS via the right heart ventricle. Lung, heart and aorta were removed together and pulmonary artery was dissected and adventitial layer was removed. Pulmonary arteries were then transferred in 2 ml of HBSS with 1 mg/ml collagenase and 10 mg/ml elastase and digested by shaking at 37 °C for 25 min. Subsequently, the cell suspension was vortexed and supplemented with 1 ml of fresh media. Cells were centrifuged for 5 min at  $2,564 \times g$  and pellet was washed by centrifugation with additional 2 ml of media.

Cells were seeded in a cell culture flask coated with 0.75% gelatine in an incubator at 37 °C with a humidified 5% (vol/vol) CO<sub>2</sub> atmosphere. When the culture reached a required confluency, cells were washed with PBS and treated with 5 ml of acutase solution for 5 min at 37 °C. Activity of acutase was inhibited with 5 ml of culture media and required portion of de-attached cells was transferred into a new culture flask.

#### PASMC culture media:

Smooth muscle growth medium (SmGM)-2

SmGm-2 Supplements

#### **3.2.3.8 Treatment of primary mouse lung fibroblasts with $\beta$ -aminopropionitrile**

Primary mouse lung fibroblasts were cultured in DMEM supplemented with 10% (vol/vol) FBS and 1% (vol/vol) P/S in incubator at 37 °C with a humidified 5% (vol/vol) CO<sub>2</sub> atmosphere. Cells were seeded into a 6-well plate and starved for 24 h prior to BAPN treatment in DMEM containing 0.1% (vol/vol) FBS and 1% (vol/vol) P/S. Afterwards, cells were treated either with vehicle (1×PBS) or 1 mM BAPN, both dissolved in 2 ml of DMEM supplemented with 10% (vol/vol) FBS and 1% (vol/vol) P/S for 24 h prior to harvest.

#### **3.2.3.9 Transient transfection with short interfering RNA**

Primary mouse lung fibroblasts were seeded one day prior to transfection into 6-well cell culture plates, until they reached confluency of approximately 70%. Cells were transfected using TurboFect™ transfection reagent according to manufacturer's instructions. Shortly, cells were incubated with 1900  $\mu$ l of DMEM medium supplemented with 10% (vol/vol) FBS and 1% (vol/vol) P/S. Meanwhile, 100  $\mu$ l of short interfering (si)RNA,

TurboFect™ and Opti-MEM® serum-free medium mixture was incubated for 20 min. The mixture was added to the cells drop-wise. Overall, cells were transfected with 50 nM siRNA, using 6 µl TurboFect™ transfection reagent/well in 2 ml of media. Oligonucleotide sequences of siRNA used in knockdown experiments are specified in Table 4. Unspecific, scrambled (scr.) siRNA sequence and mock transfection served as a control. Following transfection, cells were cultured in incubator at 37 °C with a humidified 5% (vol/vol) CO<sub>2</sub> atmosphere, and harvested 48 h after the transfection.

**Table 4. List of siRNA oligonucleotides used in knockdown experiments.**

Target	Company	Catalog number	Duplex sequence, 5' – 3'
<i>Lox</i>	Santa Cruz Biotechnology, USA	sc-45219	CCA GUG GAU UGA UAU UAC Att UGU AAU AUC AAU CCACUG Gtt
			GUA GAA CGA UCC UUU CAA Att UUU GAA AGG AUC GUU CUA Ctt
			CCA AGC UAGUCU AAC CAA Att UUU GGU UAG ACU AGC UUG Gtt
<i>Loxl1</i>	Santa Cruz Biotechnology, USA	sc-45221	GUG UAC AGC UUGCUC AAC Utt AGU UGA GCA AGC UGU ACA Ctt
			GGA UCG ACA UAA CUG AUG Ut ACA UCA GUU AUGUCG AUC Ctt
			CGC UAC GUU UCU ACA ACA Att UUG UUG UAG AAA CGU AGC Gtt
<i>Loxl2</i>	Santa Cruz Biotechnology, USA	sc-45223	CAA GCA CAC UGA AGA CGUUt AAC GUC UUC AGU GUG CUU Gtt
			CAU GUA CCG UCA UGA CAU Utt AA UGU CAU GAC GGU ACAUGtt
			GAA GAA AGG UGC UCA UUC Att UGA AUG AGC ACC UUU CUU Ctt
scrambled control	Santa Cruz Biotechnology, USA	sc-37007	unknown

### 3.2.4 Gene expression analysis

#### 3.2.4.1 Deoxyribonucleic acid isolation

Genomic DNA was isolated from tail biopsies. Briefly, tails were digested shaking at 540 revolutions per minute (rpm) (mixing orbit 2 mm) in 500 µl Tens buffer containing 1% proteinase K (200 mg/ml) overnight at 56 °C . Samples were then centrifuged and supernatant transferred to a new 1.5 ml tube and combined with 400 µl of isopropanol. Samples were vortexed and centrifuged at 16,200 × g for 15 min at 4 °C in refrigerated microcentrifuge CT15RE. The resulting pellet was diluted in 500 µl of 70% ethanol (EtOH)

(70% EtOH in nuclease-free H<sub>2</sub>O) and centrifuged for 1 min. The EtOH was removed and samples were allowed to dry at RT for approximately 10 min, after which the pellet were resolved in 80 µl of TE buffer. Finally, samples were shaken for additional 30 min at 56 °C and 540 rpm (mixing orbit 2 mm). The purity and quantification of isolated DNA was determined with a NanoDrop<sup>®</sup> ND 1000.

### 3.2.4.2 Sex determination in mouse pups

Genomic DNA obtained from tail biopsies was screened by polymerase chain reaction (PCR) reaction to detect the presence of the *Ilf3* gene in both male and female sex and the male-only *Sry* locus (primer sequences are listed in Table 5.). The reaction conditions were: 95 °C for 4.5 min, followed by 33 cycles of 95 °C for 35 s to achieve denaturation, 50 °C for 1 min for primers annealing and 72 °C for 1 min to allow product elongation. Finally 5 min incubation at 72 °C was performed after the last cycle was concluded.

Following PCR reaction, resulting amplicons were resolved on a 1.5% (wt/vol) agarose gel containing 0.002% (vol/vol) ethidium bromide in 1×TAE buffer using the Wide Mini-Sub<sup>®</sup> Cell GT electrophoresis chambers. Amplicons were visualized in Intas UV Transilluminator.

Reaction mix used for sex determination (per one reaction):

5× Green GoTaq flexi PCR buffer	10 µl
MgCl <sub>2</sub> (25 mM)	4 µl
dNTP mix (10 mM)	1 µl
GoTaq polymerase (5 U/µl)	0.25 µl
<i>Ilf3</i> primer mix (10 µM)	0.6 µl
<i>Sry</i> primer mix (10 µM)	1 µl
Nuclease-free H <sub>2</sub> O	31.15 µl
<u>DNA</u>	<u>2 µl</u>
Total volume/reaction	50 µl

**Table 5. Primers employed for sex determination.**

Gene	Primer	Primer sequence, 5' - 3'	Primer size, bp	Amplicon size, bp
<i>Il3</i>	Forward	GGGACTCCAAGCTTCAATCA	20	544
	Reverse	TGGAGGAGGAAGAAAAGCAA	20	
<i>Sry</i>	Forward	TGGGACTGGTGACAATTGTC	20	402
	Reverse	GAGTACAGGTGTGCAGCTCT	20	

*bp*, base pairs

### 3.2.4.3 Total RNA isolation from cell culture and lung tissue

For total (t)RNA isolation from cells, cells were homogenized by scraping in RNA lysis buffer (part of the PeqGoldTotal RNA Kit). For isolation from lung, approximately 50 mg of lung tissue was homogenized in RNA lysis buffer using a Precellys 24-Dual homogenizer. The resulting suspension was centrifuged for 1 min at  $10,000 \times g$  at RT in an Espresso personal microcentrifuge and supernatant was used for subsequent tRNA isolation using the PeqGold Total RNA Kit according to manufacturer's instructions. The final pellet was dissolved in 30  $\mu$ l of nuclease-free H<sub>2</sub>O. The purity and quantification of isolated tRNA was determined with a NanoDrop<sup>®</sup> ND 1000.

### 3.2.4.4 Complementary DNA synthesis

The complementary (c)DNA was synthesized from RNA preparations with  $A_{260/280}$  absorbance ratio above 1.90. To perform a cDNA synthesis, 1000 ng of tRNA (diluted in nuclease-free H<sub>2</sub>O) from each sample was transcribed using MuLV reverse transcriptase and random hexamer oligodeoxyribonucleotides. Briefly, 20  $\mu$ l of tRNA was denatured at 70 °C for 10 min and subsequently supplemented with 20  $\mu$ l of reverse transcription mixture. The mixture was then incubated at 21 °C for 10 min, followed by a cDNA synthesis at 43 °C for 1 h and 15 min. Eventually, MuLV reverse transcriptase was inactivated by 5 min incubation at 99 °C.

Reverse transcription mixture used for cDNA synthesis (per one reaction):

10× PCR bufferII	4 µl
MgCl <sub>2</sub> (25 mM)	8 µl
Nuclease-free H <sub>2</sub> O	1 µl
Random hexamers (50 µM)	2 µl
dNTP mix (10 mM)	2 µl
RNase inhibitor (20 U/µl)	1 µl
<u>MuLV reverse transcriptase (50 U/µl)</u>	<u>2 µl</u>
Total volume/reaction	20 µl

### 3.2.4.5 Quantitative real-time reverse transcription-PCR

Quantitative gene expression analyses were performed by quantitative real-time reverse transcription (RT)-PCR using a Platinum<sup>®</sup> SYBR<sup>®</sup> Green qPCR SuperMix UDG kit and a StepOnePlus<sup>™</sup> Real-Time PCR System. Primer pairs specific to the target mRNA sequence were obtained from previously published publications, from online PrimerBank database (<https://pga.mgh.harvard.edu/primerbank/>) or designed using Primer-BLAST software (<http://www.ncbi.nlm.nih.gov/tools/primer-blast/>) and are listed in Table 6.

The reaction conditions were: polymerase activation at 50 °C for 2 min, 95 °C for 5 min, 40 cycles of 95 °C for 5 s to achieve denaturation, primers annealing at 59 °C for 5 s and 72 °C for 30 s to allow the product elongation. Melting curve analysis was performed to confirm an amplification of a specific product and absence of primer-dimer formation. The  $\Delta$ CT values were calculated as mean Ct (reference gene) – mean Ct (gene of interest), where the *Polr2a* gene always served as reference gene.

Master mix mixture used for real-time RT-PCR (per one reaction):

Platinum <sup>®</sup> SYBR <sup>®</sup> Green qPCR SuperMix-UDG	13 µl
MgCl <sub>2</sub> (50 mM)	1 µl
Primer mix, forward and reverse primer (10 µM each)	1 µl
Nuclease-free H <sub>2</sub> O	8 µl
<u>cDNA</u>	<u>2 µl</u>
Total volume/reaction	23 µl

**Table 6. Primers employed for a real-time RT-PCR analysis.**

Gene	Primer	Primer sequence, 5' - 3'	Primer size, bp	Amplicon size, bp	T <sub>m</sub> , °C	Location, bp
<i>Lox</i>	Forward	CAG CCA CAT AGA TCG CAT GGT	21	133	60.54	579 - 599
	Reverse	GCC GTA TCC AGG TCG GTT C	19		60.23	711 - 693
<i>Loxl1</i>	Forward	GAG TGC TAT TGC GCT TCC C	19	225	58.98	1675 - 1693
	Reverse	GGT TGC CGA AGT CAC AGG T	19		60.23	1899 - 1881
<i>Loxl2</i>	Forward	ATT AAC CCC AAC TAT GAA GTG CC	23	130	58.72	2280 - 2302
	Reverse	CTG TCT CCT CAC TGA AGG CTC	21		59.50	2409 - 2389
<i>Loxl3</i>	Forward	CTA CTG CTG CTA CAC TGT CTG T	22	133	59.77	133 - 154
	Reverse	GAC CTT CAT AGG GCT TTC TAG GA	23		59.03	265 - 243
<i>Loxl4</i>	Forward	GCC AAC GGA CAG ACC AGA G	19	139	60.37	216 - 234
	Reverse	CCA GGT CAA GGC TGA CTC AAA	21		60.20	354 - 334
<i>Lcel</i>	Forward	AAG TGC CCT CCT GTG TCT TC	20	223	61.50	118 - 137
	Reverse	CAC AAC AGT CAC TGC TAC CAC	21		60.80	340 - 320
<i>Mmp9</i>	Forward	GCG TCG TGA TCC CCA CTT AC	20	88	62.60	644 - 663
	Reverse	CAG GCC GAA TAG GAG CGT C	19		62.20	731 - 713
<i>Rbm33</i>	Forward	TGC AGA ACG GTC CTG GAG AA	20	119	63.00	75 - 94
	Reverse	CAT CTG ACA AAT CCG ACT GGT T	22		63.00	193 - 172
<i>Cage1</i>	Forward	AAT GTC AAT GGT CCC TCT CAA GA	23	139	61.00	22 - 44
	Reverse	CAG AGA ACG TGT GTG TAG ACT C	22		60.00	160 - 139
<i>Rarres1</i>	Forward	AAT GTT CTG CGA GGG TGT TTT	21	201	60.40	341 - 361
	Reverse	ACA GGG GTC TCA GTG AAT TAT CA	23		60.50	541 - 519
<i>Adrald</i>	Forward	CGG ACC TTC TGC GAC GTA TG	20	124	62.60	478 - 497
	Reverse	TGG CTG GAT ACT TGA GCG AGT	21		63.00	601 - 581
<i>Prkcz</i>	Forward	GCG TGG ATG CCA TGA CAA C	19	191	61.80	89 - 107
	Reverse	AAT GAT GAG CAC TTC GTC CCT	21		61.20	279 - 259
<i>Cobl</i>	Forward	CTT AGG GGG AAG CTA TGG ACT	21	92	60.10	2307 - 2327
	Reverse	ACA CAT CCC TGT CAT AAC ACC T	22		60.80	2398 - 2377
<i>Lcn12</i>	Forward	CAG TTT CAG GGA GAG TGG TTT G	22	142	60.80	112 - 133
	Reverse	CCC GAG TCA TGG AGT TGG T	19		61.00	253 - 235
<i>Akr1c18</i>	Forward	TCC CAT CGT CCA GAG TTG GT	20	141	62.40	165 - 284
	Reverse	TCC ATG CTC ATC TTT AGG CAA AA	23		60.20	405 - 383
<i>Gdf10</i>	Forward	CAG GAC ATG GTC GCT ATC CAC	21	128	62.30	202 - 222
	Reverse	ACA GGC TTT TGG TCG ATC ATT TC	23		61.40	329 - 307
<i>Mmp3</i>	Forward	ACA TGG AGA CTT TGT CCC TTT TG	23	192	60.70	507 - 529
	Reverse	TTG GCT GAG TGG TAG AGT CCC	21		60.70	698 - 678
<i>Ifnb1</i>	Forward	CAG CTC CAA GAA AGG ACG AAC	21	138	60.90	82 - 102
	Reverse	GGC AGT GTA ACT CTT CTG CAT	21		60.00	219 - 199
<i>Cxcl9</i>	Forward	CCG AGG CAC GAT CCA CTA C	19	114	59.90	164 - 182
	Reverse	AGG CAG GTT TGA TCT CCG TT	20		59.30	277 - 258
<i>Csf2</i>	Forward	GGC CTT GGA AGC ATG TAG AGG	21	104	62.50	83 - 103
	Reverse	GGA GAA CTC GTT AGA GAC GAC TT	23		61.10	186 - 164
<i>Eln</i>	Forward	TGT CCC ACT GGG TTA TCC CAT	21	92	62.40	792 - 812
	Reverse	CAG CTA CTC CAT AGG GCA ATT TC	23		60.70	883 - 861
<i>Cdh18</i>	Forward	ATT ACG AGC ACA TCT TGC ATC TG	23	127	61.00	7 - 29
	Reverse	TTT CCC CTT CAG TGT GTT TGG	21		60.40	133 - 113
<i>Oxct2b</i>	Forward	GGG AGT GTC CAT TTC TAC ACG	21	239	60.10	112 - 132
	Reverse	CCC AGG TAG GAG CAC ACC A	19		62.90	350 - 332
<i>Slc15a5</i>	Forward	CCG GAA CTG GGG TGG ATT TTC	21	128	63.00	993 - 1013
	Reverse	GTC CAT CTC TCT TAG AGG GAA GT	23		60.00	1120 - 1098
<i>Lrig2</i>	Forward	AGC CTG GAT TTG AGT CAT AAC CG	23	200	62.20	232 - 254
	Reverse	GCA GAA TAA AGC TCG AAT GCT TC	23		60.20	431 - 409
<i>Cd8a</i>	Forward	CCG TTG ACC CGC TTT CTG T	19	121	62.50	10 - 28
	Reverse	CGG CGT CCA TTT TCT TTG GAA	21		61.40	130 - 110
<i>Kcnj11</i>	Forward	CCT TTT CTC CAT CGA GGT CCA	21	107	61.20	102 - 122
	Reverse	GCC CGA CGA TAT TCT GCA CA	20		62.30	208 - 189
<i>Polr2a</i>	Forward	CTA AGG GGC AGC CAA AGA AAC	21	209	59.45	808 - 828
	Reverse	CCA TTC AGC ATA CAA CTC TAG GC	23		59.19	1016 - 994

*bp*, base pairs; *T<sub>m</sub>*, melting temperature

### 3.2.4.6 Microarray analysis

Following siRNA knockdown and BAPN treatment, tRNA was isolated from primary lung mouse fibroblasts using a PeqGold Total RNA Kit and subjected to microarray analysis. Analysis were performed by IMG Laboratory (Martinsried, Germany) using an Agilent SurePrint G3 Mouse Gene Expression Microarray in combination with a one-color based hybridization protocol. Detected induced and repressed genes were further categorized based on the PANTHER analysis.

### 3.2.5 Analysis of protein expression, activity and deposition

#### 3.2.5.1 Protein isolation from cell culture and lung tissue

For protein isolation from cells, cells were homogenized by scraping in protein lysis buffer (100  $\mu$ l of buffer/well) and collected in a 1.5 ml tube. For isolation from lungs, approximately 50 mg of lung tissue was homogenized in 300  $\mu$ l protein lysis buffer using a Precellys 24-Dual homogenizer. Resulting suspension was centrifuged for 1 min at  $10,000 \times g$  at RT in an Espresso personal microcentrifuge and the supernatant was transferred into 1.5 ml tube. Suspensions were incubated on ice for 30 - 60 min, and vortexed every 10 minutes. Samples were then centrifuged at  $16,200 \times g$  for 15 min at 4 °C in refrigerated microcentrifuge CT15RE and the supernatant was collected into a new 1.5 ml tube. In order to prevent protein degradation, the entire protein isolation procedure was carried out on ice.

#### Protein lysis buffer:

20 mM Tris-Cl, pH 7.5

150 mM NaCl

1 mM EDTA

1 mM EGTA

1% (vol/vol) NP-40

#### Immediately before use lysis buffer was supplemented with:

1 $\times$ Complete™ protease inhibitor cocktail

1 mM Na<sub>3</sub>VO<sub>4</sub>

#### 3.2.5.2 Bradford assay

Protein concentration was determined by Bradford assay. Samples, as well as lysis buffer (first blank control) were diluted with ddH<sub>2</sub>O in a 1:10 ratio in case of cell protein lysates, or a 1:50 ratio in the case of proteins obtained from tissue homogenates. A total of

10 µl of each diluted sample and lysis buffer were transferred to 96-well plate. In order to determine the standard curve, 10 µl of bovine serum albumin (BSA) protein standards as well as second blank control (ddH<sub>2</sub>) was included on the plate. All the samples and standards were analyzed in triplicates. Subsequently 200 µl of Quick Start™ Bradford dye reagent was added to each well using a multichannel pipette. After 5 min the absorbance was measured at wavelength of 570 nm in a VersaMax ELISA Microplate reader using a SoftMax® Pro Software. Protein concentrations were determined using the standard curve.

### 3.2.5.3 Protein electrophoresis and western blot analysis

A fixed amount of protein was always mixed with 4× sample buffer supplemented with 10% (vol/vol) β-mercaptoethanol. Proteins were resolved in polyacrylamide gel by gel electrophoresis at 110 mV in running buffer.

Proteins were transferred onto a 0.2 µm nitrocellulose or polyvinylidene difluoride (PVDF) membrane using the western blot transfer system, Trans-Blot® Turbo™. Successful protein transfer was validated by Ponceau S protein staining. In order to avoid unspecific binding of antibody, the membrane was "blocked" for 1 h in blocking buffer at RT and subsequently incubated with primary antibody diluted in blocking buffer at 4 °C overnight. List of primary antibodies used in the western blot analysis is provided in Table 7.

After the incubation with primary antibody, the membrane was rinsed in washing buffer. Six washings of 5 min each were performed. The membrane was then incubated with the horseradish peroxidase-conjugated secondary antibody diluted in blocking buffer for 1 h at RT, after which another round of washing was performed. Finally, the membrane was incubated in SuperSignal® West Femto chemiluminescent substrate and the protein bands were visualized with a LAS-4000 luminescent image analyzer.

#### SDS-resolving gel (10%):

ddH<sub>2</sub>O  
10% (vol/vol) acrylamide  
375 mM Tris-Cl, pH 8.8  
0.05% (vol/vol) SDS  
0.05% (vol/vol) APS  
0.065% (vol/vol) TEMED

#### SDS-stacking gel:

ddH<sub>2</sub>O  
5% (vol/vol) acrylamide  
125 mM Tris-Cl, pH 6.8  
0.1% (vol/vol) SDS  
0.1% (vol/vol) APS  
0.1% (vol/vol) TEMED

SDS-running buffer:

ddH<sub>2</sub>O

192 mM glycine

25mM Tris-Cl, pH 7.5

1% (vol/vol) SDS

Washing buffer:

1× PBS

0.1% (vol/vol) Tween 20

Blocking buffer:

1×PBS

5% (wt/vol) non-fat dry milk

Ponceau S staining:

0.1% (wt/vol) Ponceau S

5% (vol/vol) acetic acid

**Table 7. Primary and secondary antibodies used for western blot analysis.**

<b>Antibody</b>	<b>Company</b>	<b>Catalog number</b>	<b>Dilution</b>	<b>Host</b>
anti-LOX	LSBio	LS-C143168	1:2,500	rabbit
anti-LOX	Abcam	ab31238	1:500, tissue homogenates 1:1,000, cell homogenates	rabbit
anti-LOXL1	Abcam	ab81488	1:750	rabbit
anti-LOXL2	Abcam	ab113960, tissue and cell homogenates ab179810, cell homogenates	1:750	rabbit
anti-LOXL3	Abcam	ab122263	1:250	rabbit
anti-LOXL4	Abcam	ab130646	1:100	rabbit
anti-β-ACTIN	Cell Signaling Technology	4967	1:5,000	rabbit
Anti-rabbit IgG	Thermo Scientific	31460	1:3,000	goat

**3.2.5.4 Analysis of collagen and elastin protein and cross-links**

For the isolation of material for collagen and elastin measurements in lung homogenates lungs were perfused with PBS via the right heart ventricle, excised, transferred to 1.5 ml tube containing 1×PBS, and frozen in liquid nitrogen. Samples were stored at -80 °C for further

processing. Analysis of collagen and elastin protein and cross-links were performed by Prof. Dr. Med. Jürgen Brinckman and Dipl.-Ing. Heiko Steenbock from the Institute of Virology and Cell Biology of University of Lübeck.

### **3.2.5.5 Lysyl oxidase activity assay.**

Lysyl oxidase activity from whole-lung homogenates and cell homogenate extracts was assessed using a Lysyl Oxidase Activity Assay Kit. A total of 10 µg of freshly isolated protein served as an enzyme source. Lysyl oxidase activity is reported as the BAPN-sensitive fraction determined in the presence of 500 mM BAPN. Fluorescence was measured during the exponential phase of enzymatic reaction using Infinite<sup>®</sup> 200 PRO multimode reader.

### **3.2.6 Cloning and lentiviral production**

The generation and use of S2-level genetically modified viruses was approved by local authorities, the *Regierungspräsidium* Gießen (approval number IV44-53r30.03.MPP07.13.15). The *Lox*-, *Loxl1*- and *Loxl2*-encoding lentivirus particles were constructed using the Gateway<sup>®</sup> cloning technology.

#### **3.2.6.1 Amplification and isolation of *Lox*, *Loxl1* and *Loxl2* sequences**

First, cDNA was amplified by RT-PCR from tRNA pools isolated from mouse lung or heart tissue homogenates. Murine *Lox*, *Loxl1* and *Loxl2* coding sequences were amplified with specific primers by PCR reaction. Primer sequences are provided in Table 8. The reaction conditions were: 95 °C for 5 min, followed by 39 cycles of 95 °C for 30 s to achieve denaturation, 60 °C for 40 s for primer annealing and 72 °C for 1 min to allow product elongation. Finally, 10-min final extension at 72 °C was performed after the last cycle in order to allow for the clearance of the replication machinery.

Following the PCR reaction, the resulting amplicons were resolved on a 1.5% (wt/vol) agarose gel containing 0.002% (vol/vol) ethidium bromide in 1×TAE buffer using Wide Mini-Sub<sup>®</sup> Cell GT electrophoresis chambers. Amplicons were visualized in an Intas UV Transilluminator. Bands migrating at 1,235 bp, 1,823 bp and 2,330 bp corresponding to *Lox*,

*Lox11* and *Lox2*, respectively, were carefully excised with a scalpel. Excised bands were purified using a QIAquick gel extraction kit.

Reaction mix (per one reaction):

10× PfuUltra™ High Fidelity reaction buffer	5 µl
dNTP mix (10 mM)	1 µl
PfuUltra™ High Fidelity polymerase (2.5 U/µl)	1 µl
Forward primer mix (10 µM)	1.5 µl
Reverse primer mix (10 µM)	1.5 µl
Nuclease-free H <sub>2</sub> O	39.0 µl
<u>cDNA (100 ng/µl)</u>	<u>1 µl</u>
Total volume/reaction	50 µl

**Table 8. Primers used for amplification of *Lox*, *Lox11* and *Lox12* sequences.**

Gene	Primer	Primer sequence, 5' - 3'	Primer size, bp	Amplicon size, bp
<i>Lox</i>	Forward	ATG CGT TTC GCC TGG GCT	18	1,235
	Reverse	CTA ATA CGG TGA AAT TGT GCA GCC T	25	
<i>Lox11</i>	Forward	ATG GCT CTG GCC GGA GCC	18	1,823
	Reverse	TCA GGA CTG GAC GAT TTT GCA GTT TG	26	
<i>Lox12</i>	Forward	ATG GAG CTC CAT TTT GGC TC	20	2,330
	Reverse	TTA CTG TAC AGA GAG CTG GTT ATT T	25	

*bp*, base pairs

### 3.2.6.2 Ligation into the intermediate (entry) vector

A total of approximately 100 ng gene-specific DNA was mixed in 1.5 ml tube with 10 ng pCR™2.1-TOPO® Gateway Entry vector, 1 µl of salt solution (1.2 M NaCl, 0.06 M MgCl<sub>2</sub>) and nuclease-free water in total volume of 6 µl and left to ligate for 1 h at RT.

### 3.2.6.3 Entry plasmid transformation of competent cells

The Transform One Shot® DH5α™-T1R, TOP10 Competent Cells were transformed by heat shock. Briefly, 50 µl of competent cells and 2 - 6 µl of ligation product were first incubated on ice for 30 min. Afterwards, cells underwent heat shock in 42 °C for 30 s and were subsequently incubated on ice for an additional 2 min. Cells were then mixed with

250 µl of Super Optimal Broth (S.O.C.) medium and incubated for 1 h at 37 °C and 200 rpm (mixing orbit 2 mm), after which they were centrifuged in microcentrifuge for 4 min at  $1,534 \times g$ . The pellet was re-suspended in approximately 50 µl of media and plated on 10 cm Petri dishes coated with LB-Agar, supplemented with 50 µg/ml spectinomycin. Culture was incubated overnight in incubator at 37 °C with a humidified 5% (vol/vol) CO<sub>2</sub> atmosphere.

LB media:

LB media	2.5 g
Agarose	1.5 g
Spectinomycin; 50 mg/ml	100 µl
ddH <sub>2</sub> O	100 ml

#### **3.2.6.4 Plasmid mini-preparation**

Selected single bacterial colonies were inoculated in 5 ml LB media containing 50 µg/ml spectinomycin and incubated at 37 °C and shaking at 180 rpm (mixing orbit 2 mm) for 8 h. Afterwards, 2 ml of the bacterial culture was transferred into 200 ml of fresh medium and incubated overnight at 37 °C with shaking at 180 rpm (mixing orbit 2 mm). Plasmid constructs were then extracted from bacterial cultures using a NucleoBond<sup>®</sup> Xtra Mini kit.

In order to confirm the presence of the desired sequence in the plasmid, constructs were digested with EcoRI enzyme for 2 h at 37 °C and resolved on a 1.5% (wt/vol) agarose gel containing 0.002% ethidium bromide in 1×TAE buffer using the Wide Mini-Sub<sup>®</sup> Cell GT electrophoresis chambers. Amplicons were visualized in Intas UV Transilluminator. Correct nucleotide sequence of the insert was confirmed by sequencing.

Plasmid digestion reaction:

Plasmid	7 µl
Buffer H	2 µl
EcoRI	1 µl
ddH <sub>2</sub> O	up to 20 µl of total volume

### **3.2.6.5 Ligation into the final (destination) vector**

A total of approximately 100 ng pCR<sup>TM</sup>2.1-TOPO<sup>®</sup> containing the gene of interest was mixed in 1.5 ml tube with 150 ng pLenti7.3/V5DEST<sup>TM</sup> destination vector, 6 µl TE buffer and 2 µl LR-clonase and incubated at RT for 4 h. The reaction was stopped by the addition of 1 µl of proteinase K.

### **3.2.6.6 Final plasmid transformation of competent cells**

Heat shock of competent cells was performed exactly as described above. After centrifugation, the pellet was resuspended in 50 µl of media and plated on a 10 cm Petri dishes coated with LB-Agar, supplemented with 0.1% (vol/vol) ampicillin. The culture was incubated overnight in an incubator at 37 °C with a humidified 5% (vol/vol) CO<sub>2</sub> atmosphere.

### **3.2.6.7 Plasmid maxi-preparation**

Selected bacterial colonies were inoculated exactly as described above into LB media containing 1 µl/ml ampicillin. Plasmid constructs were then extracted from bacterial culture using a NucleoBond<sup>®</sup> Xtra Maxi kit.

### **3.2.6.8 Lentivirus production in HEK293T cells**

First, HEK293T cells were seeded in 10 cm Petri dishes and incubated in DMEM supplemented with 10% FBS in an incubator at 37 °C with a humidified 5% (vol/vol) CO<sub>2</sub> atmosphere. After 24 h, medium was carefully aspirated and 10 ml of fresh media was added. Cells were then co-transfected with 3 µg *Lox*-, *Lox11*- or *Lox12*-encoding pLenti7.3/V5DEST<sup>TM</sup> destination vector together with 9 µg of ViraPower<sup>TM</sup> Packaging Vector Mix diluted in 3 ml OptiMEM. Transfection was undertaken with 36 µl Lipofectamine<sup>®</sup> transfection reagent. The mixture was added to the cells drop-wise after 20 min incubation. After 72 h medium was collected and stored at -80 °C for further use. The lentivirus particle concentration was not assessed, instead HEK293T cell medium containing viral particles was used as a source of virus.

### **3.2.6.9 Lentivirus-mediated overexpression of *Lox*, *Lox11* and *Lox12* in NIH/3T3 cells**

Mouse NIH/3T3 cells were seeded into 6-well plates and cultured in DMEM supplemented with 10% (vol/vol) FBS and 1% P/S (vol/vol) in incubator at 37 °C with a humidified 5% (vol/vol) CO<sub>2</sub> atmosphere for 24 h. Afterwards, cell media was aspirated and cells were transduced with 500-700 µl of *Lox*-, *Lox11*- or *Lox12*-expressing lentivirus particles for 72 h. Transduction was carried out using 8 µg/ml polybrene (hexadimethrine bromide). Both empty lentivirus and media without lentiviral particles were employed as controls.

### **3.2.7 Statistical analysis**

Data are presented as mean ± SD. Data in tables 9-12 are presented as mean ± SE. All statistical analyses were performed with GraphPad Prism 6.0. The presence of potential statistical outliers was determined by Grubbs' test. Differences in the case of two-group comparisons were evaluated by unpaired Student's *t*-test, while differences in the case of three-group comparisons were evaluated by one-way ANOVA with Tukey's multiple comparisons (post hoc) test. *P* values < 0.05 were considered as significant.

## 4 RESULTS

### 4.1 Exposure of immature mouse lungs to 85% O<sub>2</sub> dysregulates lysyl oxidase expression

Previous studies of lung formation in mice by our group suggested the regulation of the lysyl oxidase family members in both normal and aberrant late lung development [46]. Therefore, we wanted to confirm the regulation of these enzymes at gene and protein expression levels. Newborn mouse pups were exposed to normoxic (21% O<sub>2</sub>) or hyperoxic (85% O<sub>2</sub>) conditions from the day of birth for either nine or 19 days. Exposure of newborn pups to 85% O<sub>2</sub> led to an increase in the gene expression of *Lox* and *Loxl2* at both P9.5 and P19.5 (Figure 6A-B). Although no apparent change in LOXL2 expression could be detected by immunoblot, increase of protein expression of LOX was evident by immunoblot at P19.5 (Figure 6C). Moreover, an increase of protein expression of LOXL2 and LOXL4 in lungs after hyperoxia exposure was also detected (Figure 6C-D). Expression of *Loxl3* was not significantly altered by hyperoxia exposure.

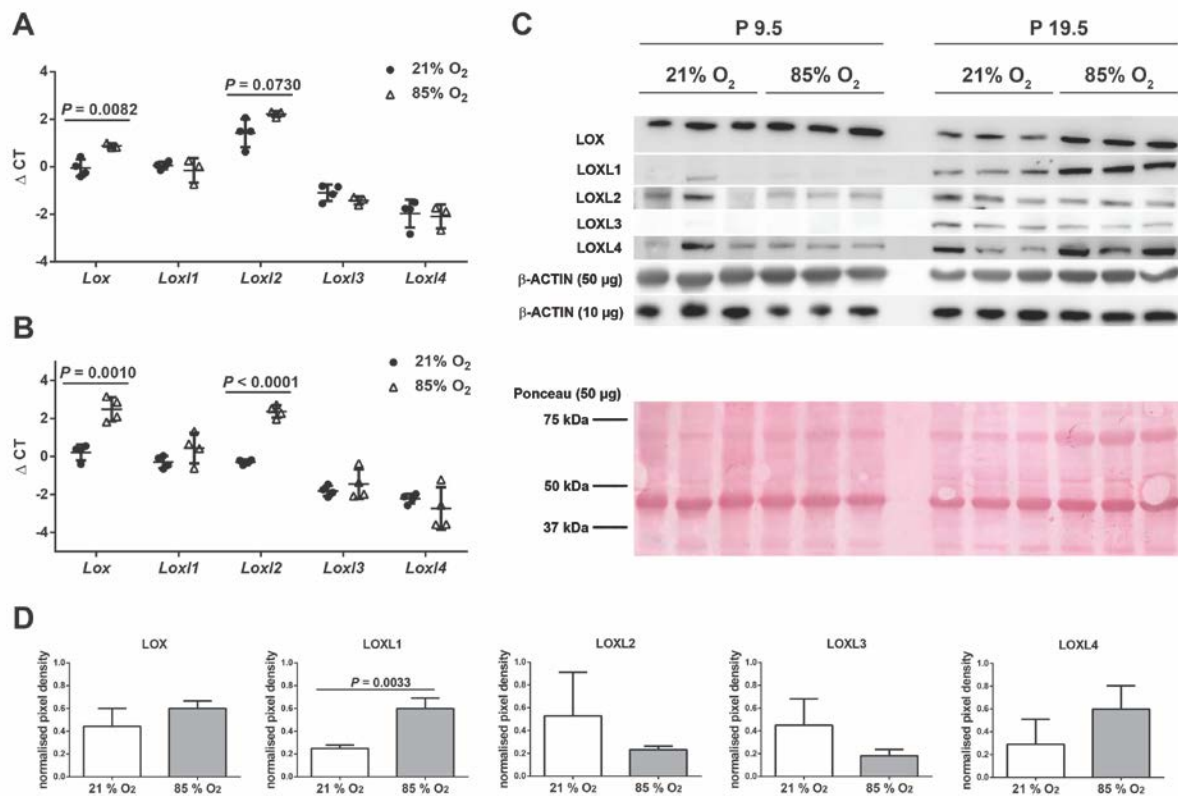


**Figure 6. The expression of lysyl oxidase family members is dysregulated during aberrant late lung development.**

(A-B) Gene expression levels of all five members of the lysyl oxidase family were assessed in lung homogenates from mouse pups exposed to 21% O<sub>2</sub>, or 85% O<sub>2</sub> from the day of birth, at P9.5 and P19.5, by real-time RT-PCR. Values represent mean  $\pm$  SD ( $n = 3-5$ , per group). The  $P$  values were determined by unpaired Student's  $t$ -test. (C) Protein expression levels of lysyl oxidases were assessed in lung homogenates from mouse pups exposed to 21% O<sub>2</sub> or 85% O<sub>2</sub> from the day of birth, by immunoblot at P9.5 and P19.5. For the detection of lysyl oxidases, 50  $\mu$ g of protein was loaded. Loading equivalence was controlled by  $\beta$ -ACTIN abundance. In addition, a Ponceau S-stained immunoblot membrane, as well as a second loading control, in which 1/5 of protein (10  $\mu$ g) was used, are also shown. (D) Densitometric analysis of the protein expression in mice at P19.5. Pixel densities for the bands representing individual lysyl oxidase family members were normalized for the pixel density of the  $\beta$ -ACTIN bands from the same sample. Values represent mean  $\pm$  SD ( $n = 3$ , per group). The  $P$  values were determined by unpaired Student's  $t$ -test.

## **4.2 Inhibition of lysyl oxidase activity in the lungs of developing mice exposed to 85% O<sub>2</sub>**

High doses of lathyrogens, including BAPN, can be toxic to multiple organs and are known to cause disturbances to lung maturation and normal ECM deposition [50, 51]. To avoid any morbidity or mortality associated with potential drug overdose, a five-day long pilot study was first performed to evaluate the impact of different doses of BAPN on developing mouse pups. Newborn pups were injected intraperitoneally, on a daily basis, from the day of birth with either vehicle (1×PBS) or the pan-lysyl oxidase inhibitor BAPN, diluted in 1×PBS at two different concentrations. Daily administration at a dose of 150 mg·kg<sup>-1</sup> significantly reduced animal viability and motility. Milk intake of the pups injected with 150 mg·kg<sup>-1</sup> BAPN was visibly reduced, and the body weight was decreased when compared with vehicle-treated littermates (Figure 7A-B). However, a ten-times lower dose of BAPN (15 mg·kg<sup>-1</sup>·day<sup>-1</sup>) was well tolerated by the developing pups, and did not lead to any visible perturbations in growth, motility or milk intake (Figure 7A-B). A dose of 15 mg·kg<sup>-1</sup>·day<sup>-1</sup> was therefore employed in further studies. Newborn mouse pups were divided to two groups and exposed from the day of birth continuously for nine or 19 days to either normoxic (21% O<sub>2</sub>) or hyperoxic (85% O<sub>2</sub>) conditions, as illustrated in Figure 7C. Both groups were further subdivided into vehicle (1×PBS) and BAPN-treated group (15 mg·kg<sup>-1</sup>·day<sup>-1</sup> BAPN diluted in 1×PBS).

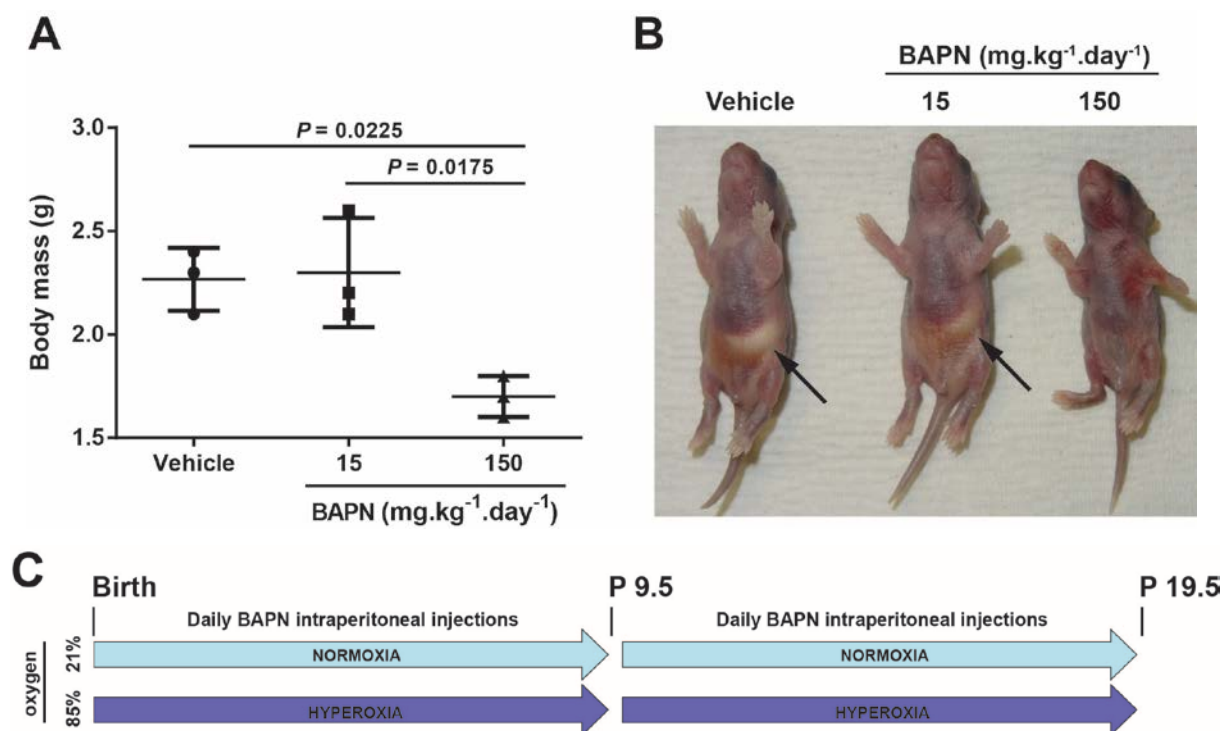


**Figure 7. Effect of  $\beta$ -aminopropionitrile administration on mouse viability.**

A pilot study was performed, where newborn mouse pups were injected intraperitoneally on daily basis, for five days with solvent vehicle or  $\beta$ -aminopropionitrile (BAPN) diluted in vehicle at two different doses. (A) Body mass measured at P5.5. (B) Representative images of mice from each treatment group observed at P5.5. Arrows indicate the milk spot. (C) The experimental protocol employed in subsequent studies. Values represent mean  $\pm$  SD ( $n = 3$ , per group). The  $P$  values were determined by one-way ANOVA with Tukey's multiple comparisons test.

In order to confirm the inhibitory effect of BAPN, a lysyl oxidase activity assay was performed. Activity was assessed in whole-lung homogenates from 9-days old developing mouse pups exposed to normoxic (21% O<sub>2</sub>) or hyperoxic (85% O<sub>2</sub>) conditions and concomitantly treated with daily injection (i.p.) of either vehicle alone or 15 mg.kg<sup>-1</sup> BAPN. As expected, hyperoxia exposure caused a considerable increase in lysyl oxidase activity in the developing mouse lungs. Importantly, the daily BAPN treatment at the dose of 15 mg.kg<sup>-1</sup> was sufficient to preserve the normal levels of lysyl oxidase enzymatic activity in the lungs of hyperoxia-exposed animals when compared to vehicle-treated normoxia-exposed control animals (Figure 8).

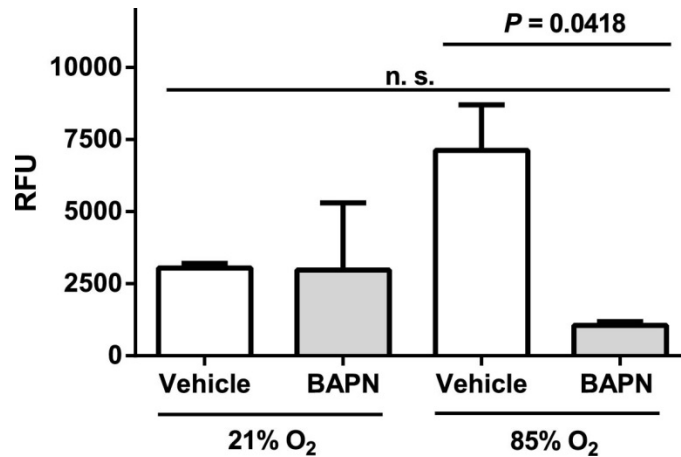


**Figure 8. Lysyl oxidase enzymatic activity was normalized by the administration of  $\beta$ -aminopropionitrile.**

Lysyl oxidase enzymatic activity was measured in total of 10  $\mu$ g of protein extract from lung homogenates. Measurements were performed using a Lysyl Oxidase Activity Assay Kit. Activity is reported as the  $\beta$ -aminopropionitrile (BAPN)-sensitive fraction in the presence of 500 mM BAPN. Values are represented as means  $\pm$  SD. RFU, relative fluorescent units. n.s., not significant ( $P > 0.05$ ). The  $P$  values were determined by one-way ANOVA with Tukey's multiple comparisons test.

#### **4.3 Cross-linking of collagen and elastin in the lungs of developing mouse pups upon hyperoxia exposure and treatment with $\beta$ -aminopropionitrile**

Lysyl oxidases act as copper-dependent enzymes catalyzing the oxidative deamination of lysine and hydroxylysine residues. This process generates reactive semialdehydes, which form intramolecular and intermolecular covalent cross-links in both elastin and collagen molecules. In order to evaluate the impact of hyperoxia and lysyl oxidase activity inhibition on collagen formation we quantified the total amount of collagen and elastin as well as different types of collagen and elastin cross-links in lung homogenates of 19 days-old mouse pups after the exposure to hyperoxia and/or treatment with BAPN.

The abundance of the non-collagen-non-elastin proteins was not altered in the lungs of developing mouse pups after 19 days of hyperoxia exposure. However, a pronounced three-fold increase in the collagen/elastin ratio was observed. This increase was partially blunted when BAPN was administered (Table 9). The increase in the collagen/elastin ratio was accompanied by a 63%-increase in total lung collagen protein levels. Similarly, collagen

fraction in total lung protein was increased by 42% in the animals exposed to hyperoxia when compared to normoxia-exposed control animals. This increase was at least partially restored when the developing hyperoxia-exposed pups were also treated with BAPN (Figure 9A-9B).

Both hyperoxia exposure and daily BAPN administration had a considerable effect on collagen cross-linking in the developing mouse lungs. Although hyperoxia exposure didn't alter the abundance of hydroxylysinoxorleucine (HLNL) and hydroxylysylpyridinoline (HP) cross-links, an 11% increase in the abundance of dihydroxylysinoxorleucine (DHLNL) cross-links was observed. Moreover, exposure of developing mouse pups to hyperoxia led to an increase in the DHLNL/HLNL ratio, which reflects the lysyl hydroxylation status in collagen cross-links [118] and indicates the fibrotic nature of the tissue [119]. Daily administration of BAPN to normoxia-exposed developing mouse pups did not affect neither the total collagen levels in the lungs, nor the collagen fraction within the total lung protein (Figure 9A-9B). The abundance of DHLNL was also not impacted (Figure 9C), however BAPN administration caused a significant increase in the abundance of HLNL cross-links, resulting in a decrease of DHLNL/HLNL ratio (Figure 9E-9F). In addition, BAPN administration decreased the abundance of HP cross-links in both normoxia-exposed and hyperoxia-exposed mouse pups (Figure 9C). Moreover, daily treatment of developing mouse pups with BAPN reversed the increase in DHLNL/HLNL ratio induced by exposure of the mice to hyperoxia (Figure 9F).

**Table 9. Effect of hyperoxia exposure and  $\beta$ -aminopropionitrile administration on deposition of collagen in the developing mouse lungs at postnatal day 19.5.**

Parameter	21% O <sub>2</sub>		85% O <sub>2</sub>			
	Vehicle	BAPN	Vehicle		BAPN	
	mean $\pm$ S.E.	mean $\pm$ S.E.	mean $\pm$ S.E.	<i>P</i> value vs. Vehicle, 21% O <sub>2</sub>	mean $\pm$ S.E.	<i>P</i> value vs. Vehicle, 85% O <sub>2</sub>
nc-ne-protein/lung [ $\mu$ g]	2387 $\pm$ 128.50	2575 $\pm$ 81.40	2784 $\pm$ 140.30	0.1763	2440 $\pm$ 184.90	0.3143
collagen/elastin, %	68.29 $\pm$ 5.19	64.60 $\pm$ 2.11	180.40 $\pm$ 12.18	< 0.0001	144.00 $\pm$ 15.36	0.0723

Additional cross-link data are presented in Figure 9. *BAPN*,  $\beta$ -aminopropionitrile; *nc-ne protein*, non-collagen-non-elastin-proteins. Values represent mean  $\pm$  S.E, ( $n = 6-7$ , per group). The *P* values were determined by one-way ANOVA with Tukey's multiple comparisons test.

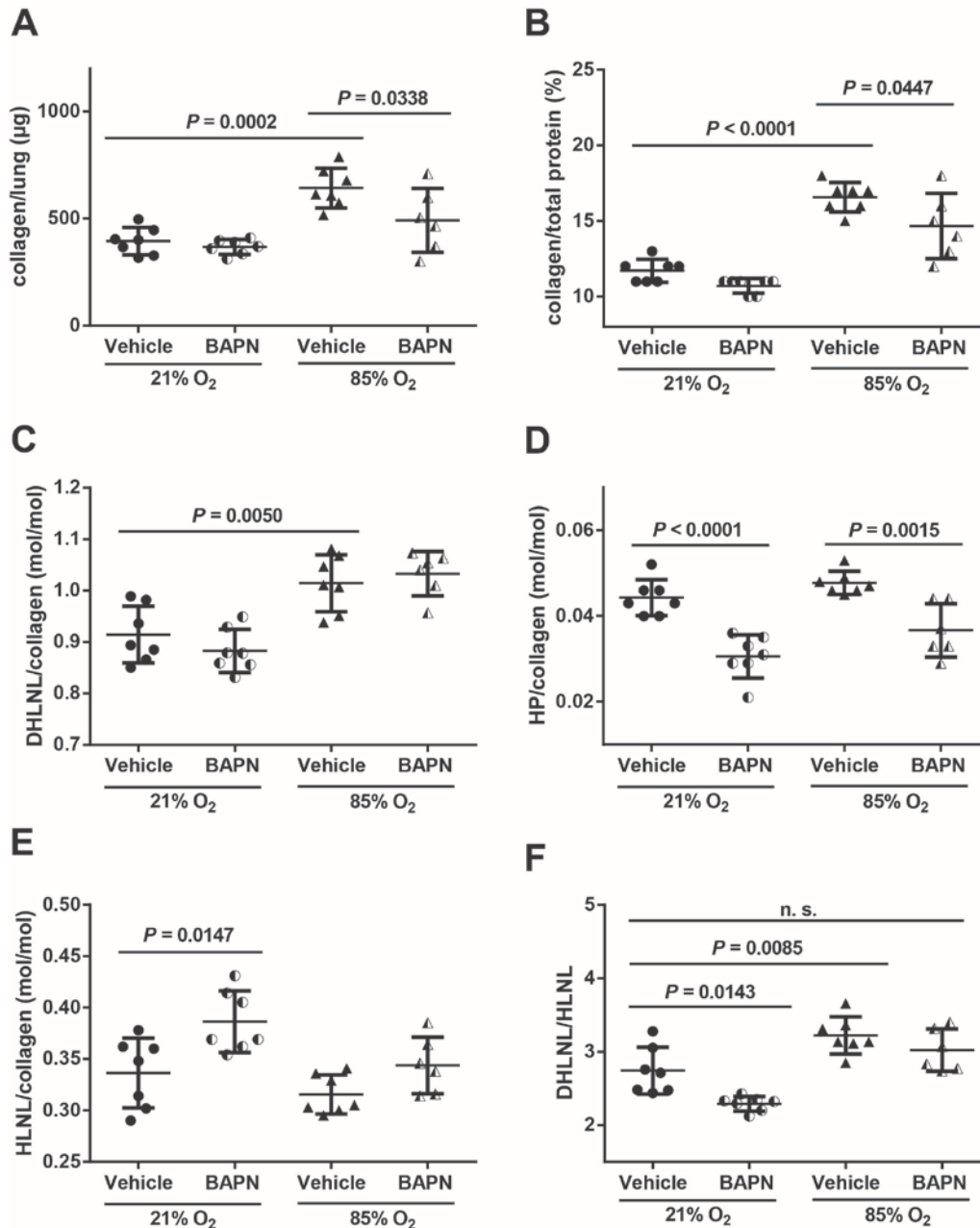


**Figure 9. Effect of hyperoxia exposure and  $\beta$ -aminopropionitrile administration on the levels of collagen and formation of collagen cross-links in the lungs of developing mouse pups at postnatal day 19.5.**

(A) The abundance of total collagen in the lung. (B) Abundance of collagen per unit total protein. (C-E) The abundance of collagen cross-links, dihydroxylysinonorleucine (DHLNL) (C), hydroxylysylpyridinoline (HP) (D), and hydroxylysinonorleucine (HLNL) (E) per total collagen. (F) The DHLNL-to-HLNL ratio. Analysis of the lungs of 19 days-old, vehicle or  $\beta$ -aminopropionitrile (BAPN)-treated mouse pups concomitantly exposed to either 21% O<sub>2</sub> or 85% O<sub>2</sub>. Values represent mean  $\pm$  SD ( $n = 6-7$ , per group). n.s., not significant ( $P > 0.05$ ). The  $P$  values were determined by one-way ANOVA with Tukey's multiple comparisons test.

Similar to collagen, the abundance of elastin and elastin cross-links was severely altered by exposure of newborn mouse pups to 85% O<sub>2</sub>. The amount of total insoluble elastin protein in the lung was significantly decreased when compared to healthy animals of the same age (Table 10), and the proportion of elastin per total lung protein was decreased by one third (Figure 10A). Moreover, hyperoxia exposure led to a significant reduction in the levels of elastin cross-links; desmosine (by 30%) and isodesmosine (by 21%); as well as the ratio between the two (Figure 10B-10D).

Daily administration of BAPN to normoxia-exposed animals reduced the levels of insoluble elastin in the lungs, although no such effect was observed in the lungs of animals concomitantly exposed to hyperoxia (Figure 10A). However, BAPN administration to the developing mouse pups had partially recovered the levels of desmosine and isodesmosine cross-links, which were decreased by the exposure of vehicle-treated newborn pups to 85% O<sub>2</sub>. In addition, increases in desmosine and isodesmosine levels led to an improvement in the desmosine/isodesmosine ratio, which was partially restored in hyperoxia-exposed pups after BAPN treatment, compared to normoxia-exposed vehicle-treated animals (Figure 10B-10D).

**Table 10. Effect of hyperoxia exposure and  $\beta$ -aminopropionitrile administration on deposition of elastin in developing mouse lungs at postnatal day 19.5.**

Parameter	21% O <sub>2</sub>		85% O <sub>2</sub>			
	Vehicle	BAPN	Vehicle		BAPN	
	mean $\pm$ S.E.	mean $\pm$ S.E.	mean $\pm$ S.E.	<i>P</i> value vs. Vehicle, 21% O <sub>2</sub>	mean $\pm$ S.E.	<i>P</i> value vs. Vehicle, 85% O <sub>2</sub>
elastin/lung [ $\mu$ g]	582.7 $\pm$ 16.00	569.1 $\pm$ 10.24	359.7 $\pm$ 14.75	< 0.0001	350.9 $\pm$ 23.14	0.9815
(des+isodes)/elastin[pmol/ $\mu$ g]	14.14 $\pm$ 0.364	15.45 $\pm$ 0.317	10.55 $\pm$ 0.383	< 0.0001	12.28 $\pm$ 0.276	0.0098

Additional cross-link data are presented in Figure 10. *BAPN*,  $\beta$ -aminopropionitrile; *des*, desmosine; *isodes*, isodesmosine. Values represent mean  $\pm$  S.E, (*n* = 6-7, per group). The *P* values were determined by one-way ANOVA with Tukey's multiple comparisons test.

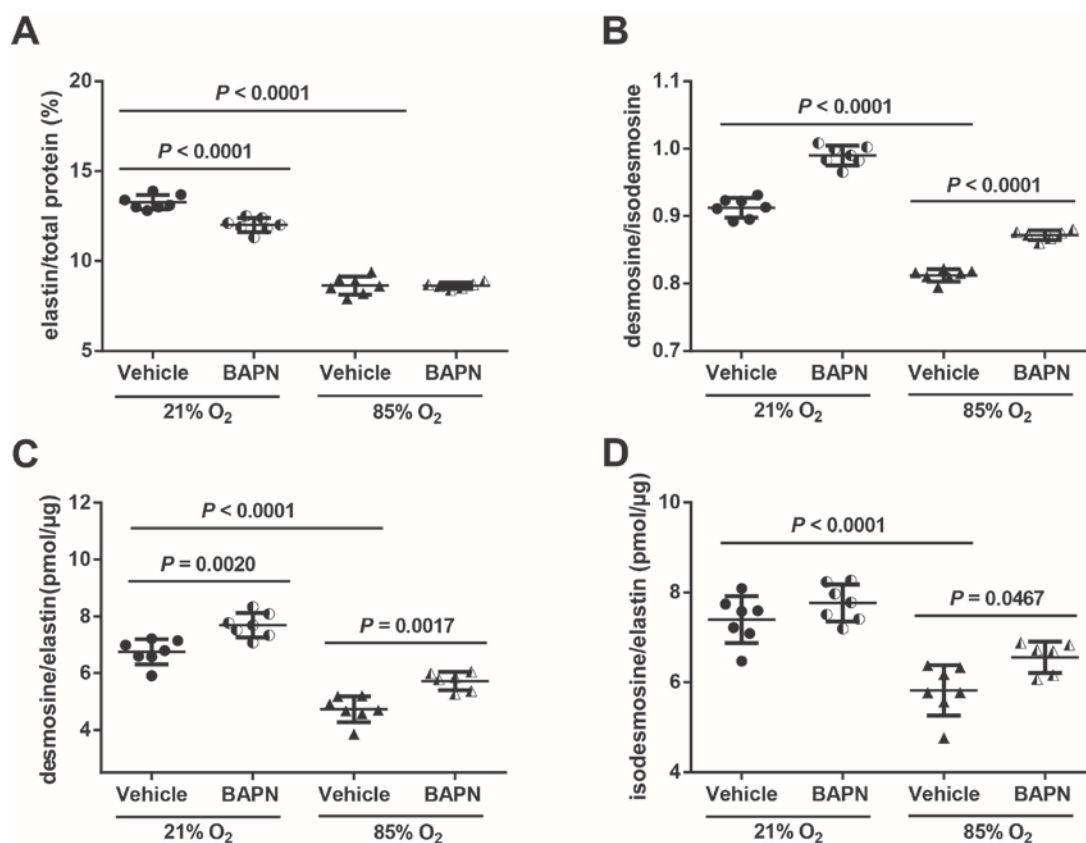


**Figure 10. Effect of hyperoxia-exposure and  $\beta$ -aminopropionitrile administration on the levels of elastin and elastin cross-links in the lungs of developing mouse pups at postnatal day 19.5.**

(A) The abundance of insoluble elastin per unit total protein. (B) Desmosine/isodesmosine ratio. (C) The abundance of desmosine per total elastin. (D) The abundance of isodesmosine per total elastin. Analysis of the lungs of 19 day-old, vehicle or  $\beta$ -aminopropionitrile (BAPN)-treated mouse pups concomitantly exposed to either 21% O<sub>2</sub> or 85% O<sub>2</sub>. Values represent mean  $\pm$  SD ( $n = 6-7$ , per group). The  $P$  values were determined by one-way ANOVA with Tukey's multiple comparisons test.

#### 4.4 The impact of hyperoxia exposure and $\beta$ -aminopropionitrile administration on elastin fibers formation in the parenchyma of the developing mouse lung

During the development of the lung, elastin is organized into specific structures, so-called "foci", deposited on the tips of the developing alveolar septa, suggesting the role of elastin in the septal formation [13, 46, 80]. In contrast, elastin fibers in the lungs of mechanically ventilated or hyperoxia-exposed animals are often described as disrupted and fragmented [46, 64, 86-88]. In the present study the formation of elastin foci in the lungs of

the developing mouse pups was considerably altered by hyperoxia exposure (85% O<sub>2</sub>) at both, P9.5 (Figure 11A vs. 11B) and P19.5 (Figure 11E vs. 11F) when compared with control normoxia-exposed animals. Elastin fibers in the lungs of hyperoxia-exposed mice formed fewer foci and appeared disorganized and “brush-like” (Figure 11F).

The daily administration of BAPN did not visibly alter the appearance of the elastin foci formation in the lungs of normally-developing mouse pups at P9.5 and P19.5, when compared with the vehicle-treated control animals (Figure 11A vs. 11C and Figure 11E vs. 11G). Daily administration of BAPN to the developing mouse pups concomitantly exposed to 85% O<sub>2</sub> from the day of birth did not improve the formation of the elastin foci in the developing alveolar septa at P9.5 (Figure 11C vs. 11D). However, when BAPN was administered for an additional ten days (up to and including P19.5), formation of the elastin foci was partially preserved (Figure 11H), although overall structure and thickness of the alveolar septa remained unchanged when compared with the vehicle-treated hyperoxia-exposed animals (Figure 11F vs. 11H).

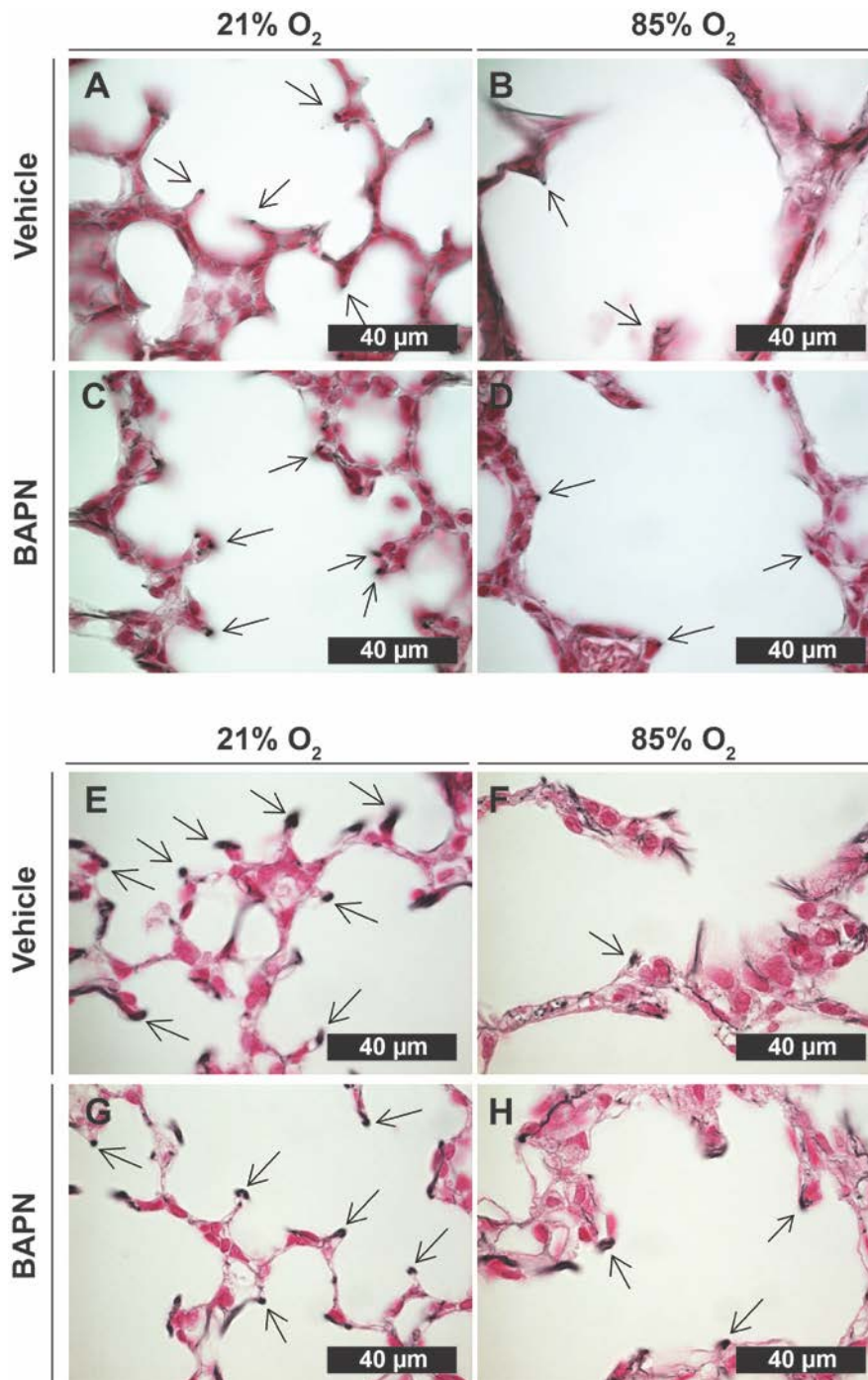


**Figure 11. Hyperoxia-exposure and  $\beta$ -aminopropionitrile administration alter the formation of elastin foci in developing alveolar septa.**

Representative paraffin embedded lung tissue sections from animals exposed to 21% O<sub>2</sub> (A, C, E, G) or 85% O<sub>2</sub> (B, D, F, H), concomitantly treated with either vehicle (A, B, E, F) or  $\beta$ -aminopropionitrile (BAPN) (C, D, G, H) for the first 9 (A-D) or 19 (E-H) days of life. Arrows indicate elastin foci.

#### **4.5 Treatment of hyperoxia-exposed mouse pups did not preserve normal lung architecture**

The exposure of mouse pups to 85% O<sub>2</sub> from the day of birth for nine (Figure 12) or 19 (Figure 13) days resulted in an arrest in alveolarization, characterized by a decrease in gas-exchange surface area, thickening of the alveolar septa and a substantial decrease in the number of alveoli in lung as seen by visual inspection. We further quantified these parameters using the stereological analysis. The full list of stereo-morphometric parameters is provided in Table 11 for lungs of mice at P9.5 and in Table 12 for lungs from mice at P19.5.

Exposure of developing mouse pups to hyperoxia (85% O<sub>2</sub>) from day of birth until P9.5 had a striking impact on lung architecture (Figure 12A vs. 12B). The gas-exchange surface area was decreased in hyperoxia-exposed mouse pups when compared with normally-developing animals [ $57.89 \pm 7.26 \text{ cm}^2$  vs.  $91.98 \pm 27.77 \text{ cm}^2$  (Figure 12E)]. Similarly, number of alveoli decreased from  $1.746 \pm 0.4495 \times 10^6$  in normoxia-exposed mouse pups to  $1.11 \pm 0.27 \times 10^6$  in hyperoxia-exposed mouse pups (Figure 12H). In contrast, the mean linear intercept (MLI) was increased by hyperoxia exposure from  $39.27 \pm 7.51 \mu\text{m}$  in normally-developing lungs to  $65.39 \pm 6.547 \mu\text{m}$  in the lungs of hyperoxia-exposed pups (Figure 12G).

Although the visual inspection of the lungs from developing mouse pups at P9.5 suggested a formation of a more complex lung structure in the BAPN-treated normoxia-exposed mice (Figure 12C), when compared to vehicle-treated mice (Figure 12A), no significant changes assessed by stereological analysis were found (Figure 12E-12H). Similarly, treatment with BAPN appeared to improve the lung structure of hyperoxia-exposed mice when compared with vehicle-treated hyperoxia-exposed mice (Figure 12B vs. 12D). However, no significant improvement in any of the parameters investigated could be validated by stereological analysis, where the gas-exchange surface area, septal thickness, MLI and number of alveoli remained unchanged upon the BAPN-treatment (Figure 12E-12H). However, a tendency towards an improvement was observed in the estimates of alveolar surface area (Figure 12E), MLI (Figure 12G) and number of alveoli (Figure 12H). Based on the trends toward an improvement in lung structure observed after the BAPN-treatment in hyperoxia-exposed lungs on P9.5, and the improvement of elastin foci formation observed on P19.5 (Figure 11), it was speculated, that longer intervention with

BAPN and analysis at a later time point may emphasize the corrective effects of BAPN on the lung structure of hyperoxia-exposed mouse pups.

**Table 11. Stereo-morphometric parameters of developing mouse lungs after hyperoxia exposure and  $\beta$ -aminopropionitrile administration assessed at postnatal day 9.5.**

Parameter	21% O <sub>2</sub>		85% O <sub>2</sub>			
	Vehicle mean $\pm$ S.E.	BAPN mean $\pm$ S.E.	Vehicle		BAPN	
			mean $\pm$ S.E.	<i>P</i> value vs. Vehicle, 21% O <sub>2</sub>	mean $\pm$ S.E.	<i>P</i> value vs. Vehicle, 85% O <sub>2</sub>
V (lung) [cm <sup>3</sup> ]	0.16 $\pm$ 0.011	0.18 $\pm$ 0.013	0.15 $\pm$ 0.006	0.9696	0.17 $\pm$ 0.011	0.4473
CV [V (lung)]	0.07	0.03	0.06		0.05	
V <sub>V</sub> (par/lung) [%]	88.81 $\pm$ 2.06	90.27 $\pm$ 1.11	88.19 $\pm$ 1.84	0.9936	87.13 $\pm$ 1.38	0.9688
V <sub>V</sub> (non-par/lung) [%]	11.19 $\pm$ 2.06	9.73 $\pm$ 1.11	11.81 $\pm$ 1.84	0.9936	12.87 $\pm$ 1.37	0.9688
N <sub>V</sub> (alv/par)10 <sup>7</sup> [cm <sup>-3</sup> ]	1.25 $\pm$ 0.07	1.21 $\pm$ 0.07	0.84 $\pm$ 0.06	0.0021	0.94 $\pm$ 0.08	0.7935
S <sub>V</sub> [cm <sup>-1</sup> ]	651.46 $\pm$ 22.8	635.00 $\pm$ 14.68	438.51 $\pm$ 22.05	< 0.0001	491.63 $\pm$ 23.47	0.0890
V <sub>V</sub> (alvair/par) [%]	62.99 $\pm$ 2.67	61.39 $\pm$ 1.11	71.41 $\pm$ 1.60	0.0234	70.69 $\pm$ 1.73	0.9935
V (alv air, lung) [cm <sup>3</sup> ]	0.087 $\pm$ 0.006	0.098 $\pm$ 0.006	0.094 $\pm$ 0.005	0.7823	0.106 $\pm$ 0.006	0.4985
CV [V (alv air, lung)]	0.18	0.17	0.13		0.16	
V (sep, lung) [cm <sup>3</sup> ]	0.051 $\pm$ 0.007	0.062 $\pm$ 0.005	0.013 $\pm$ 0.001	< 0.0001	0.016 $\pm$ 0.002	0.9392
CV [V (sep, lung)]	0.38	0.22	0.23		0.33	

*BAPN*,  $\beta$ -aminopropionitrile *V*, volume; *V<sub>V</sub>*, volume density; *S<sub>V</sub>*, surface density; *N<sub>V</sub>*, numerical density; *CV*, coefficient of variation; *par*, parenchyma; *non-par*, non-parenchyma; *sep*, septa; *alv air*, alveolar airspaces; *alv*, alveoli. Values represent mean  $\pm$  S.E. (*n* = 6-7, per group). The *P* values were determined by one-way ANOVA with Tukey's multiple comparisons test.

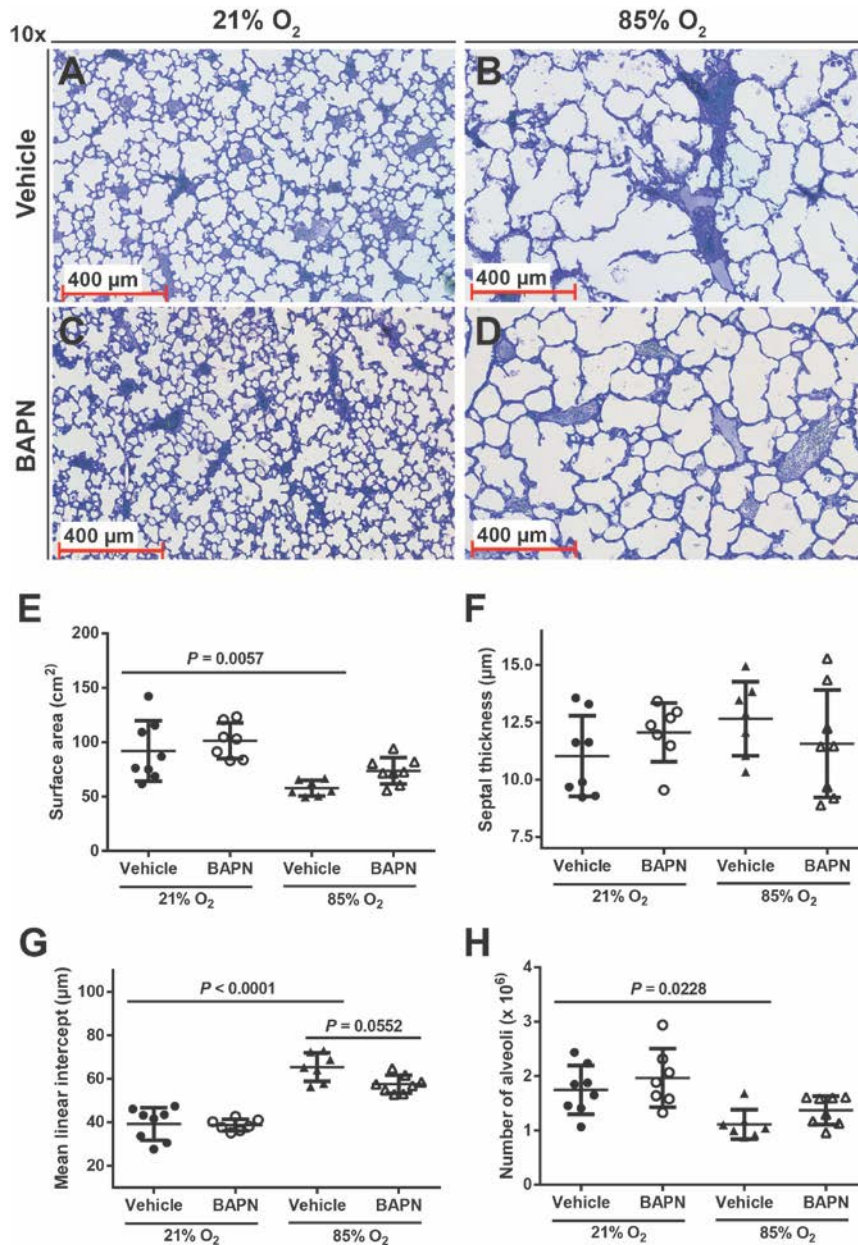


**Figure 12. Impact of the hyperoxia-exposure and  $\beta$ -aminopropionitrile administration on the lung architecture at postnatal day 9.5.**

Representative plastic-embedded lung tissue sections from animals exposed to 21% O<sub>2</sub> (A, C) or 85% O<sub>2</sub> (B, D), concomitantly treated with either vehicle (A, B) or  $\beta$ -aminopropionitrile (BAPN) (C, D) for the first 9 days of life. The alveolar surface area (E), septal thickness (F), mean linear intercept (MLI) (G) and total number of alveoli in the lung (H) were determined by stereo-morphometric analysis. Sex was determined by polymerase chain reaction and no clustering on the basis of sex was observed. Values represent mean  $\pm$  SD ( $n = 7-8$ , per group). The  $P$  values were determined by one-way ANOVA with Tukey's multiple comparisons test. Additional stereo-morphometric parameters are present in Table 11.

The duration of the intervention study was prolonged for an additional 10 days and the developing mouse lungs were harvested at P19.5 (Figure 13). As expected, exposure of mouse lungs to 85% O<sub>2</sub> once again resulted in an arrest in alveolarization (Figure 13A vs. 13B). The gas-exchange surface area was decreased from 203.80 ± 11.71 cm<sup>2</sup> in the lungs of normally-developing mouse pups to 115.00 ± 11.36 cm<sup>2</sup> in the lungs of the hyperoxia-exposed mouse pups (Figure 13F) and the number of alveoli was decreased from 7.05 ± 1.10 × 10<sup>6</sup> in normally-developing pups to 2.33 ± 0.43 × 10<sup>6</sup> in hyperoxia-exposed animals (Figure 13I). Contrariwise, an increase in both, the thickness of the alveolar septal wall [(8.80 ± 0.5 μm (21% O<sub>2</sub>) vs. 13.20 ± 0.96 μm (85% O<sub>2</sub>); Figure 13G] and MLI [28.06 ± 0.69 μm (21% O<sub>2</sub>) vs. 57.75 ± 5.22 μm (85% O<sub>2</sub>); Figure 13H] was observed in the hyperoxia-exposed developing pups when compared to normoxia-exposed control animals.

**Table 12. Stereo-morphometric parameters of developing mouse lungs after hyperoxia exposure and β-aminopropionitrile administration assessed at postnatal day 19.5.**

Parameter	21% O <sub>2</sub>		85% O <sub>2</sub>			
	Vehicle	BAPN	Vehicle		BAPN	
	mean ± S.E.	mean ± S.E.	mean ± S.E.	<i>P</i> value vs. Vehicle, 21% O <sub>2</sub>	mean ± S.E.	<i>P</i> value vs. Vehicle, 85% O <sub>2</sub>
V (lung) [cm <sup>3</sup> ]	0.26 ± 0.007	0.28 ± 0.011	0.27 ± 0.014	0.9669	0.26 ± 0.016	0.9851
CV [V (lung)]	0.07	0.09	0.12		0.14	
V <sub>V</sub> (par/lung) [%]	90.30 ± 0.969	90.22 ± 1.354	91.24 ± 0.922	0.9161	89.47 ± 0.767	0.6240
V <sub>V</sub> (non-par/lung) [%]	9.70 ± 0.969	9.78 ± 1.354	8.76 ± 0.922	0.9161	10.53 ± 0.767	0.6239
N <sub>V</sub> (alv/par) 10 <sup>7</sup> [cm <sup>-3</sup> ]	3.03 ± 0.21	3.44 ± 0.11	0.98 ± 0.10	< 0.0001	1.11 ± 0.06	0.8811
S <sub>V</sub> [cm <sup>-1</sup> ]	877.20 ± 13.17	845.10 ± 17.15	476.40 ± 12.09	< 0.0001	437.10 ± 17.85	0.3009
V <sub>V</sub> (alvair/par) [%]	61.50 ± 0.55	61.70 ± 1.46	68.52 ± 1.28	0.0075	66.80 ± 1.65	0.7874
V (alv air, lung) [cm <sup>3</sup> ]	0.143 ± 0.004	0.157 ± 0.006	0.167 ± 0.013	0.3043	0.156 ± 0.012	0.8356
CV [V (alv air, lung)]	0.06	0.08	0.17		0.18	
V (sep, lung) [cm <sup>3</sup> ]	0.090 ± 0.002	0.098 ± 0.005	0.076 ± 0.003	0.0543	0.076 ± 0.002	0.9993
CV [V (sep, lung)]	0.05	0.12	0.09		0.07	

*BAPN*, β-aminopropionitrile *V*, volume; *V<sub>V</sub>*, volume density; *S<sub>V</sub>*, surface density; *N<sub>V</sub>*, numerical density; *CV*, coefficient of variation; *par*, parenchyma; *non-par*, non-parenchyma; *sep*, septa; *alv air*, alveolar airspaces; *alv*, alveoli. Values represent mean ± S.E. (*n* = 5, per group). The *P* values were determined by one-way ANOVA with Tukey's multiple comparisons test.

No apparent differences in alveolar formation were observed in the lungs of BAPN-treated normoxia-exposed animals when compared to vehicle-treated controls by visual inspection (Figure 13B vs. 13D). However, a significant increase in the number of alveoli following the administration of BAPN was revealed when stereological analysis of the lung structure was employed (Figure 13I). On the contrary, no increase in the number of alveoli could be found following the BAPN-treatment in the lungs of hyperoxia-exposed pups when compared with vehicle-treated hyperoxia-exposed controls (Figure 13B vs. 13D). Moreover, the administration of BAPN to the animals exposed to 85% O<sub>2</sub> caused a further thickening of the alveolar wall septa from  $13.20 \pm 0.96\mu\text{m}$  to  $15.18 \pm 0.43\mu\text{m}$  when compared to vehicle-treated animals within the same oxygen-exposure group (Figure 13E and 13G).

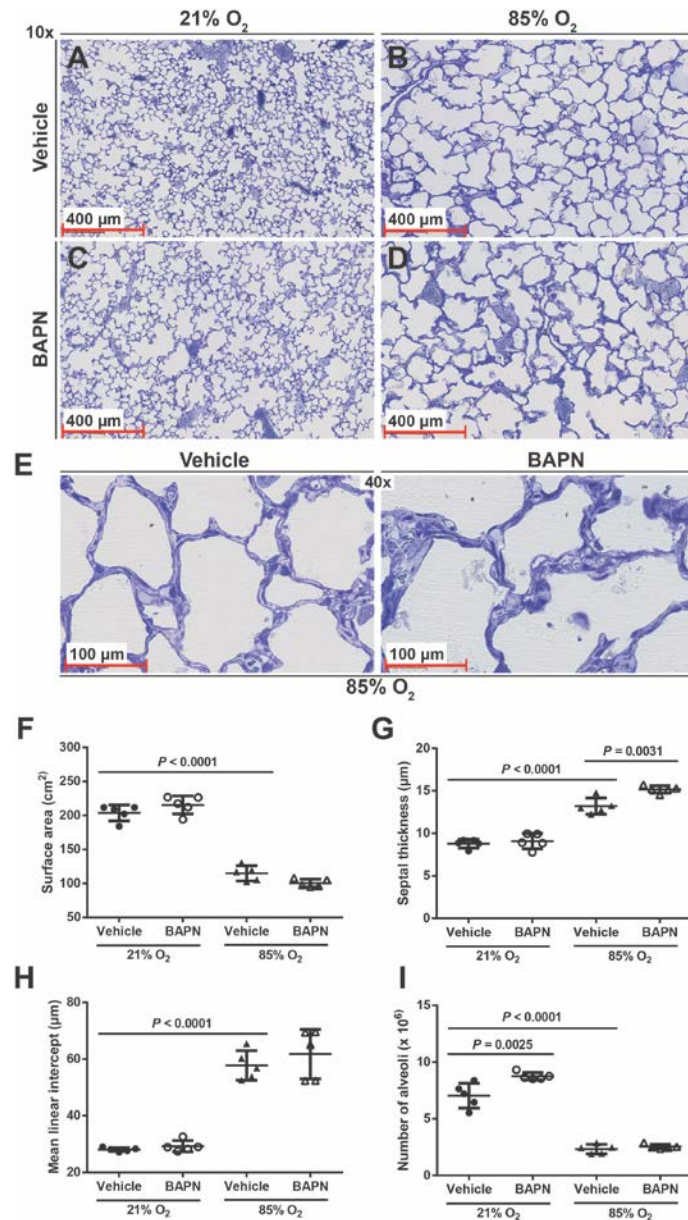


**Figure 13. Impact of the hyperoxia-exposure and  $\beta$ -aminopropionitrile administration on the lung architecture at postnatal day 19.5.**

Representative plastic-embedded lung tissue sections from animals exposed to 21% O<sub>2</sub> (A, C) or 85% O<sub>2</sub> (B, D), concomitantly treated with either vehicle (A, B) or  $\beta$ -aminopropionitrile (BAPN) (C, D) for the first 19 days of life. (E) Higher magnification images emphasizing the changes in septal thickness between vehicle and BAPN-treated hyperoxia-exposed mice. The alveolar surface area (F), septal thickness (G), mean linear intercept (MLI) (H) and total number of alveoli in the lung (I) were determined by stereo-morphometric analysis. Sex was determined by polymerase chain reaction and no clustering on the basis of sex was observed. Values represent mean  $\pm$  SD ( $n = 5$ , per group). The  $P$  values were determined by one-way ANOVA with Tukey's multiple comparisons test. Additional stereo-morphometric parameters are present in Table 12.

#### 4.6 Expression profile of lysyl oxidase family members in various cell-types present in the lung

Although the role of lysyl oxidases in ECM formation and metabolism is well known, multiple studies have recently focused on so-called “non-matrix” roles for some of the members of the lysyl oxidase family. These roles include control of intracellular signaling and transcriptional regulation, including regulation of expression of several structural and enzymatic components of the ECM network, such as *Cdh*, *Eln* and *Col3a1*. In order to define a cell-type suitable for investigation of the possible non-matrix roles for lysyl oxidases in the context of lung development, a lysyl oxidase family expression screening was performed in different cell-types present in the lung. Cell-types investigated included primary mouse lung fibroblasts, epithelial cells, PASMCs, microvascular endothelial cells and bone marrow-derived macrophages (Figure 14).

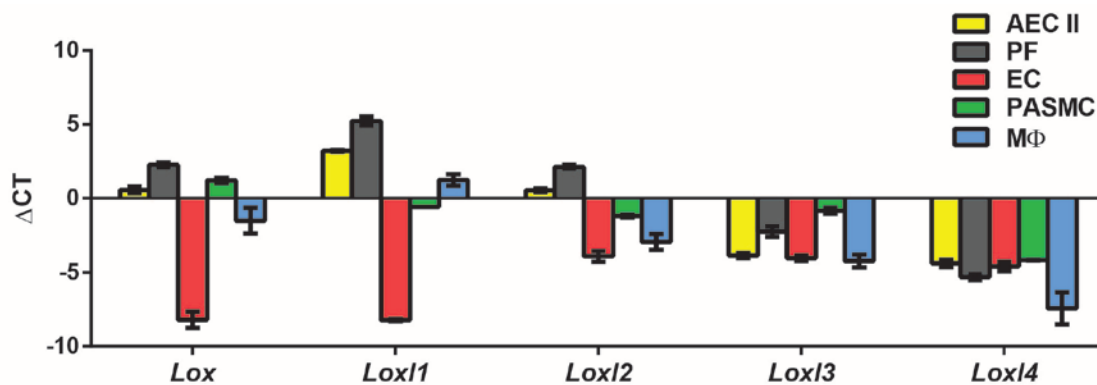


**Figure 14. Relative expression of lysyl oxidase family members in various mouse lung cell-types cultured *in vitro*.**

The gene expression of *Lox*, *Loxl1*, *Loxl2*, *Loxl3* and *Loxl4* was evaluated by real-time RT-PCR. The total RNA was obtained from various mouse primary cells. *AECII*, type II alveolar epithelial cells; *PF*, pulmonary fibroblasts, *EC*, pulmonary microvascular endothelial cells; *PASMC*, pulmonary arterial smooth muscle cells; *M $\Phi$* , bone marrow-derived macrophages. Values represent mean  $\pm$  SD, ( $n = 4$  cell cultures, per group).

Gene expression analyses in controlled cell culture conditions may lead to various artifacts due to the absence of cells natural environment including a functional ECM network. However the screening performed in this study outlined a rather constant pattern in the expression of members of the lysyl oxidase family. A variable expression of individual members was observed in different cell-types, with highest expression levels detected in

fibroblasts and lowest expression levels detected in endothelial cells. The first three family members, *Lox*, *Loxl1* and *Loxl2* all exhibited the most differential expression across the various lung cell-types. Moreover, *Lox*, *Loxl1* and *Loxl2* all exhibited the highest expression in lung fibroblasts, the leading collagen-producing and elastin-producing cell-type in the lung. Therefore, the consecutive studies of the possible non-matrix regulatory properties focused exclusively on the first three members of the lysyl oxidase family and were limited to the context of pulmonary mouse fibroblasts.

#### **4.7 Knockdown of *Lox*, *Loxl1* and *Loxl2* expression impacts the transcriptome of primary mouse lung fibroblasts**

In order to assess whether lysyl oxidase family members have any gene regulatory roles in primary mouse lung fibroblasts, an siRNA-mediated knockdown of *Lox*, *Loxl1* and *Loxl2* was performed and any impact on gene regulation was evaluated by subsequent microarray screening. Both gene and protein expression levels of LOX (Figure 15A-15B), LOXL1 (Figure 15E-15F) and LOXL2 (Figure 15I-15J) were successfully depleted in primary mouse pulmonary fibroblasts after a transfection with a respective siRNA.

In order to explore a possible compensatory regulation of other lysyl oxidase family members, the expression of remaining two members of interest was also assessed for each knockdown. Interestingly, although a siRNA-mediated knockdown of *Lox* did not have any effect on the gene expression of *Loxl1* (Figure 15C), a significant down-regulation in *Loxl2* gene expression was observed (Figure 15D). Both *Loxl1* and *Loxl2* knockdown caused a significant increase of *Lox* mRNA expression (Figure 15G and 15K). Moreover, the knockdown of *Loxl1* led to a down-regulation of *Loxl2* expression (Figure 15H), while *Loxl2* knockdown had no effect on mRNA expression levels of *Loxl1* (Figure 15L), suggesting a possible interplay between the *Loxl1* and *Loxl2* gene expression. It is worth to note, that all siRNA sequences used in this experiment did not share any regions of homology with the sequences of the other two lysyl oxidase members. The expression levels of *Lox*, *Loxl1* and *Loxl2* in primary mouse lung fibroblasts therefore influence each other. It is not yet apparent whether the interplay between the gene expression of individual lysyl oxidases is a compensatory effect, or rather a direct effect, where one member of the family regulates the transcription of another member.

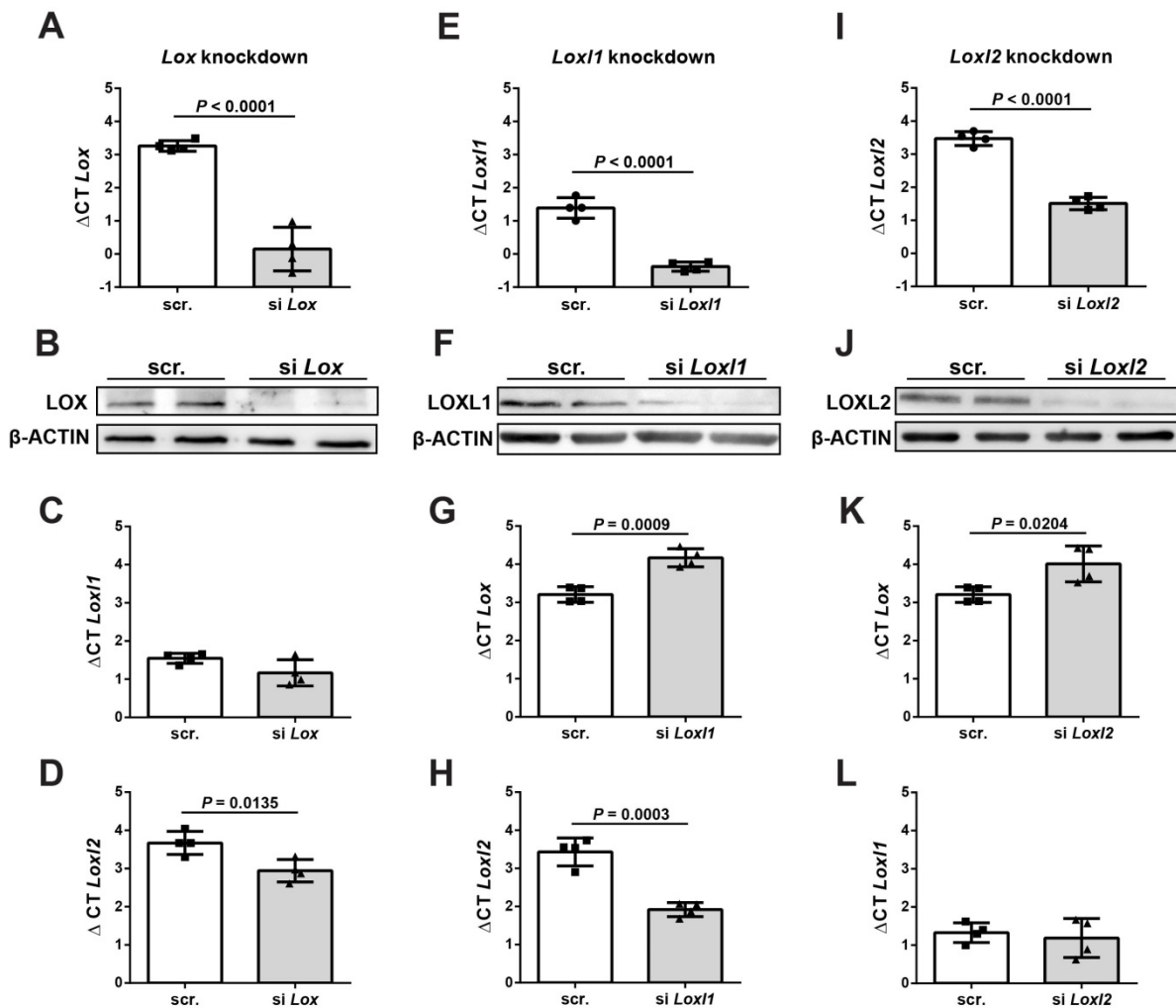


**Figure 15. Short interfering RNA-mediated knockdown of lysyl oxidases in primary mouse lung fibroblast cultures.**

The short interfering (si)RNA-mediated knockdown of lysyl oxidase (LOX) was evaluated by real-time RT-PCR (A) and immunoblot (B). Additionally, possibility of the compensatory effects of LOX knockdown on lysyl oxidase-like 1 (*Loxl1*) (C) and lysyl oxidase-like 2 (*Loxl2*) (D) expression was evaluated by real-time RT-PCR. The siRNA-mediated knockdown of LOXL1 was evaluated by real-time RT-PCR (E) and immunoblot (F). Additionally, possibility of the compensatory effects of LOXL1 knockdown on *Lox* (G) and *Loxl2* (H) expression was evaluated by real-time RT-PCR. The siRNA-mediated knockdown of LOXL2 was evaluated by real-time RT-PCR (I) and immunoblot (J). Additionally, possibility of the compensatory effects of LOXL2 knockdown on *Lox* (K) and *Loxl1* (L) expression was evaluated by real-time RT-PCR. Values represent mean means  $\pm$  SD, ( $n = 4$ , per group). The  $P$  values were determined by unpaired Student's  $t$ -test. Immunoblots are representative of expression observed in at least three immunoblots in total. Loading equivalence was controlled by  $\beta$ -ACTIN.

After the efficiency of transfection and knockdown were confirmed, total RNA pools from transfected mouse primary pulmonary fibroblasts were screened for potential transcriptomic changes by microarray. The siRNA-mediated knockdown of *Lox* led to an up-regulation of 85 and down-regulation of 49 genes. Among the dysregulated genes, *Lox* itself was the single most down-regulated gene. The ten most up-regulated and most down-regulated genes following the *Lox* knockdown are listed in Table 13, and others listed include the ECM-related genes *Mmp9* and *Rarres1*. Expression changes of four most up-regulated and the four most down-regulated genes were evaluated by real-time RT-PCR and all but one were confirmed (Figure 16A).

**Table 13. List of differentially up- and down-regulated genes after a *Lox* knockdown as assessed by microarray analysis.**

Most up-regulated genes					
n.	P <sub>(corr)</sub>	FC	Log FC	Gene Symbol	Gene name
1	0.027154	3.908041	1.966445	<b>Lce1l</b>	late cornified envelope 1L
2	0.016138	3.889547	1.959602	<b>Mmp9</b>	matrix metalloproteinase 9
3	0.007329	3.464999	1.792855	<b>Rbm33</b>	RNA binding motif protein 33
4	0.022728	3.405689	1.767947	<b>Gm6712</b>	predicted gene 6712 (Gm6712)
5	0.002383	3.269200	1.708938	<b>Zfp951</b>	zinc finger protein 951 (Zfp951)
6	0.006838	3.257450	1.703743	<b>Zfp960</b>	zinc finger protein 960 (Zfp960), transcript variant 1
7	0.005427	3.240398	1.696171	<b>Zfp458</b>	zinc finger protein 458 (Zfp458)
8	0.029255	2.970390	1.570653	<b>Cage1</b>	cancer antigen 1
9	0.002799	2.928108	1.549969	<b>Gm14325</b>	predicted gene 14325 (Gm14325)
10	0.044686	2.846928	1.509406	<b>Gm14432</b>	predicted gene, OTTMUSG00000016609
Most down-regulated genes					
n.	P <sub>(corr)</sub>	FC	Log FC	Gene Symbol	Gene name
1	0.037609	-4.6165500	-2.206820	<b>Lox</b>	lysyl oxidase
2	0.047584	-3.4912100	-1.803730	<b>Rarres1</b>	retinoic acid receptor responder (tazarotene induced) 1
3	0.027323	-3.1600500	-1.659950	<b>Adra1d</b>	adrenergic receptor, alpha 1d
4	0.031039	-3.1526300	-1.656550	<b>Prkcz</b>	protein kinase C, zeta
5	0.038292	-3.046400	-1.607110	<b>Cobl</b>	cordón-bleu WH2 repeat
6	0.028848	-2.974400	-1.572600	<b>Ces2e</b>	carboxylesterase 2E
7	0.044987	-2.78087	-1.475540	<b>Cbr2</b>	carbonyl reductase 2
8	0.035204	-2.72894	-1.448340	<b>Serpib9</b>	serine (or cysteine) peptidase inhibitor, clade B, member 9
9	0.030026	-2.64904	-1.405470	<b>Mamstr</b>	MEF2 activating motif and SAP domain containing transcriptional regulator
10	0.042531	-2.62607	-1.392910	<b>Adora2a</b>	adenosine A2a receptor

*n*, number; *P*<sub>(corr)</sub>, corrected *P* value; *FC*, fold change;

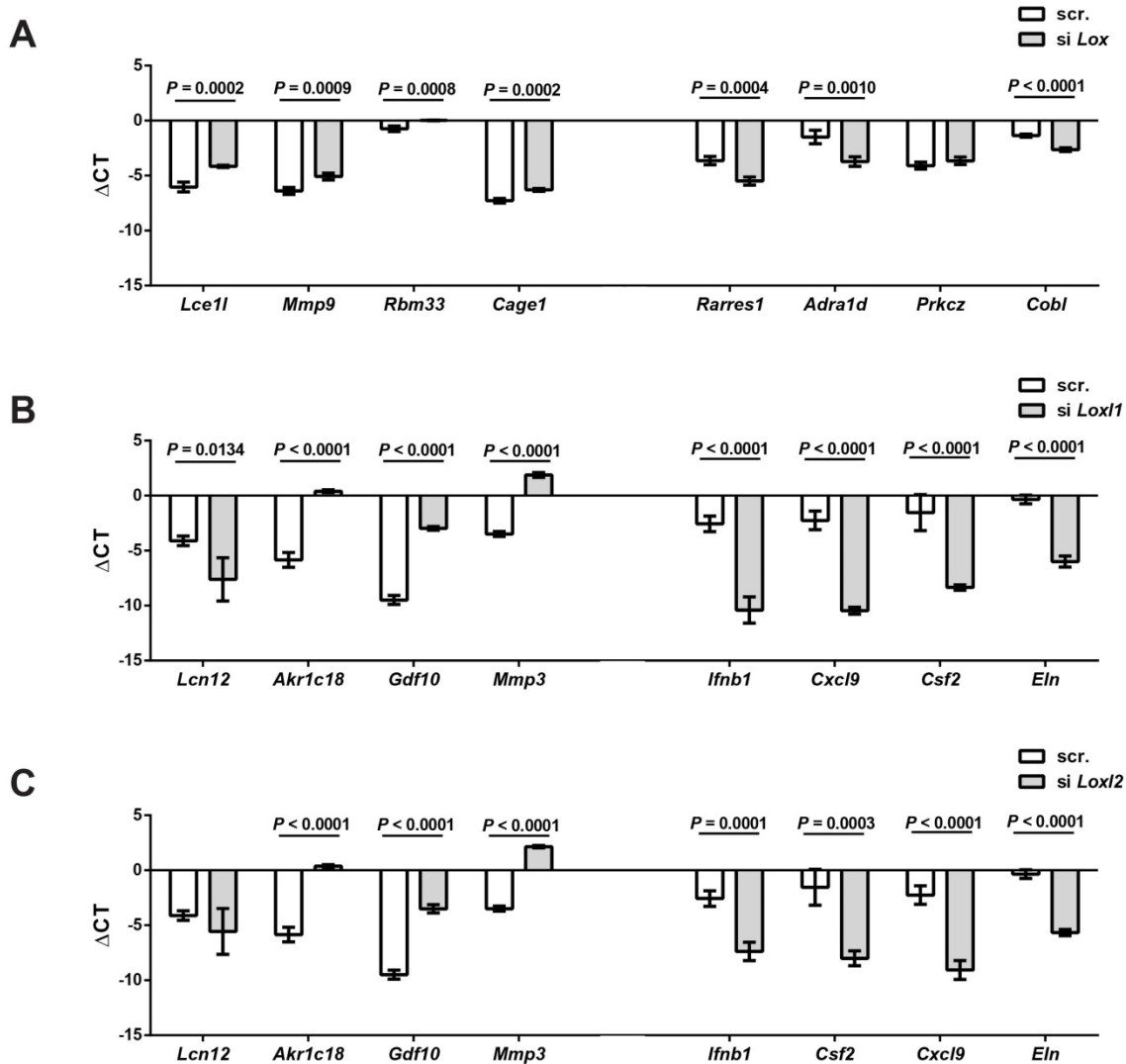


**Figure 16. Microarray analysis validation following the short interfering RNA-mediated knockdown of lysyl oxidases in primary mouse lung fibroblasts.**

Microarray data presented in tables 13, 14 and 15 were validated by real-time RT-PCR. (A) Expression of the most up-regulated and the most down-regulated genes identified by microarray analysis after *Lox* short interfering (si)RNA-mediated knockdown in primary mouse pulmonary fibroblasts. (B) Expression of the most up-regulated and the most down-regulated genes identified by microarray analysis after *Lox1* siRNA-mediated knockdown in primary mouse pulmonary fibroblasts. (C) Expression of the most up-regulated and the most down-regulated genes identified by microarray analysis after *Lox2* siRNA-mediated knockdown in primary mouse pulmonary fibroblasts. *scr.*, control scrambled siRNA sequence; *si*, gene-specific siRNA sequence; Values are represented as means  $\pm$  SD, (n = 4, per group). The *P* values were determined by unpaired Student's *t*-test.

Knockdown of *Lox11* led to a dysregulation of an even higher number of genes than the knockdown of *Lox*. From the pool of dysregulated genes 1,988 were up-regulated and 1,773 were down-regulated. *Lox11* was identified as the 1222<sup>nd</sup> most down-regulated gene. Ten most up-regulated and most down-regulated genes are summarized in Table 14. Because of the importance to ECM formation, it is worth to mention that *Mmp3* ranked as the 9<sup>th</sup> most up-regulated and *Eln* as the 48<sup>th</sup> most down-regulated gene following the *Lox11* siRNA-mediated knockdown. Validation of the expression changes of the most up-regulated and most down-regulated genes, including *Eln* is presented in Figure 16B.

**Table 14. List of differentially up- and down-regulated genes after a *Lox11* knockdown as assessed by microarray analysis.**

Most up-regulated genes					
n.	P <sub>(corr)</sub>	FC	Log FC	Gene Symbol	Gene name
1	0.001464	95.236550	6.573443	<b>Lcn12</b>	lipocalin 12
2	0.002228	77.167210	6.269916	<b>Lce3a</b>	late cornified envelope 3A
3	0.000605	66.348680	6.051996	<b>Akr1c18</b>	aldo-keto reductase family 1, member C18
4	0.000979	59.690400	5.899427	<b>S100a8</b>	S100 calcium binding protein A8 (calgranulin A)
5	0.000047	48.967690	5.613758	<b>Gdf10</b>	growth differentiation factor 10
6	0.007833	44.321830	5.469945	<b>Gda</b>	guanine deaminase
7	0.003628	41.499290	5.375015	<b>Bdkrb2</b>	bradykinin receptor, beta 2
8	0.000482	35.774510	5.160860	<b>Serpina3n</b>	serine (or cysteine) peptidase inhibitor, clade A, member 3N
9	0.000017	34.336160	5.101657	<b>Mmp3</b>	matrix metalloproteinase 3
10	0.012638	33.232890	5.054540	<b>Snhg11</b>	small nucleolar RNA host gene 11
Most down-regulated genes					
n.	P <sub>(corr)</sub>	FC	Log FC	Gene Symbol	Gene name
1	0.000889	-338.510000	-8.403060	<b>Ifnb1</b>	interferon beta 1
2	0.001181	-197.405000	-7.625020	<b>Cxcl9</b>	chemokine (C-X-C motif) ligand 9
3	0.014386	-118.647000	-6.890540	<b>Csf2</b>	colony stimulating factor 2 (granulocyte-macrophage)
4	0.000154	-107.855000	-6.752950	<b>Pydc3</b>	pyrin domain containing 3
5	0.000581	-103.021000	-6.686790	<b>Gbp4</b>	guanylate binding protein 4, transcript variant 1
6	0.002557	-101.103000	-6.659690	<b>Mx1</b>	myxovirus (influenza virus) resistance 1
7	0.000146	-89.209800	-6.479130	<b>Cxcl10</b>	activated spleen cDNA, RIKEN full-length enriched library
8	0.011989	-87.902900	-6.457840	<b>Cxcl2</b>	chemokine (C-X-C motif) ligand 2
9	0.001473	-80.725800	-6.334960	<b>Phf11b</b>	PHD finger protein 11B
10	0.000354	-79.342900	-6.310030	<b>Mx2</b>	myxovirus (influenza virus) resistance 2, transcript variant 1
48	0.000119	-25.523700	-4.673770	<b>Eln</b>	elastin

*n*, number; *P*<sub>(corr)</sub>, corrected *P* value; *FC*, fold change;

The knockdown of *Loxl2* expression resulted in up-regulation and down-regulation of 1,788 and 1,766 genes respectively. Among the down-regulated genes *Loxl2* itself was identified at the 621<sup>st</sup> position. A summary of the 10 most up-regulated and the 10 most down-regulated genes is listed in Table 15 and evaluation of the most up-regulated and down-regulated genes is shown in Figure 16C. Interestingly, the list of genes dysregulated after the knockdown of *Loxl2* considerably overlaps with the list of genes dysregulated after the knockdown of *Loxl1*, including the above-mentioned genes *Mmp3* and *Eln*. In summary, all three investigated lysyl oxidases: *Lox*, *Loxl1* and *Loxl2*, appear to possess gene regulatory functions, at least in primary mouse lung fibroblasts. Full microarray data sets are available through the NCBI Gene Expression Omnibus under accession number GSE89121.

**Table 15. List of differentially up- and down-regulated genes after a *Loxl2* knockdown as assessed by microarray analysis.**

Most up-regulated genes					
n.	P <sub>(corr)</sub>	FC	Log FC	Gene Symbol	Gene name
1	0.001122	88.125920	6.461494	<b>Lcn12</b>	lipocalin 12
2	0.000470	58.468300	5.869583	<b>Akr1c18</b>	aldo-keto reductase family 1, member C18
3	0.006023	52.552980	5.715701	<b>Derl3</b>	Der1-like domain family, member 3
4	0.007580	47.481460	5.569293	<b>Gda</b>	guanine deaminase
5	0.000564	43.332340	5.437372	<b>Gdf10</b>	growth differentiation factor 10
6	0.000994	42.335640	5.403801	<b>Serpina3n</b>	serine (or cysteine) peptidase inhibitor, clade A, member 3N
7	0.011145	38.967970	5.284217	<b>Snhg11</b>	small nucleolar RNA host gene 11
8	0.001575	38.265700	5.257980	<b>S100a8</b>	S100 calcium binding protein A8 (calgranulin A)
9	0.000010	34.261340	5.098510	<b>Mmp3</b>	matrix metalloproteinase 3
10	0.004006	31.428730	4.974012	<b>Bdkrb2</b>	bradykinin receptor, beta 2
Most down-regulated genes					
n.	P <sub>(corr)</sub>	FC	Log FC	Gene Symbol	Gene name
1	0.000472	-143.389000	-7.163790	<b>Ifnb1</b>	interferon beta 1, fibroblast
2	0.014314	-111.505000	-6.800960	<b>Csf2</b>	colony stimulating factor 2 (granulocyte-macrophage)
3	0.000671	-108.601000	-6.762890	<b>Cxcl9</b>	chemokine (C-X-C motif) ligand 9
4	0.016682	-88.868600	-6.473600	<b>Cxcl2</b>	chemokine (C-X-C motif) ligand 2
5	0.001389	-74.860400	-6.226130	<b>Pydc3</b>	pyrin domain containing 3
6	0.011893	-63.501600	-5.988720	<b>Traf1</b>	TNF receptor-associated factor 1
7	0.007118	-57.736200	-5.851410	<b>Cxcl1</b>	chemokine (C-X-C motif) ligand 1
8	0.003343	-50.206200	-5.649790	<b>Col10a1</b>	collagen, type X, alpha 1
9	0.002425	-46.784100	-5.547950	<b>Cxcl9</b>	chemokine (C-X-C motif) ligand 9
10	0.001405	-43.906400	-5.456360	<b>Cxcl10</b>	activated spleen cDNA, RIKEN full-length enriched library
28	0.000278	-20.349400	-4.346910	<b>Eln</b>	elastin

*n*, number; *P*<sub>(corr)</sub>, corrected *P* value; *FC*, fold change;

#### 4.8 Lentiviral overexpression of lysyl oxidase family members impacts the gene expression in murine fibroblasts

Knockdown of *Lox*, *Loxl1* and *Loxl2* in primary mouse fibroblasts resulted in changes in the expression status of numerous genes. In order to explore whether the overexpression of lysyl oxidases has a complementary effect on gene regulation as did the knockdown of lysyl oxidases, *Lox* (Figure 17A-17B), *Loxl1* (Figure 17E-17F) and *Loxl2* (Figure 17I-17J) were overexpressed in murine fibroblasts using a lentivirus transduction approach. A mouse NIH/3T3 fibroblast cell-line was used in the overexpression study due to technical difficulties concerning a lentiviral transduction in primary lung mouse fibroblasts. Following the overexpression of individual lysyl oxidases, the gene expression levels of selected potential target-genes that were suggested by microarray analysis were evaluated.

While both *Lcell* and *Mmp9* (Figure 16A; Table 13) were identified as *Lox* target-genes by microarray analysis in knockdown studies, only the expression of *Lcell* was significantly impacted upon *Lox* overexpression (Figure 17D). The gene expression of *Lcell* was up-regulated after the siRNA-mediated knockdown of *Lox*, but decreased after a lentiviral over-expression of *Lox*. In contrast, although the gene expression level of *Mmp9* was notably increased after a knockdown of *Lox* in primary mouse lung fibroblasts, no changes in *Mmp9* expression were observed after lentivirus-mediated over-expression of *Lox* in NIH/3T3 cells. It is not yet apparent if the knockdown and over-expression of *Lox* simply do not have the corresponding opposite effects on *Mmp9* gene expression or the *Lox* gene regulatory mechanisms are not fully comparable between the primary pulmonary mouse fibroblasts and mouse fibroblast cell-line.

The most dysregulated genes after *Loxl1* and *Loxl2* siRNA-mediated knockdown were largely similar (Figure 16B-16C; Tables 14-15). Interestingly, the same changes in selected potential target-genes were also observed after the lentivirus-mediated overexpression of *Loxl1* (Figure 17G-17H) and *Loxl2* (Figure 17J-17K). The mRNA levels of *Ifnb* and *Csf2* were down-regulated after a siRNA-mediated knockdown of *Loxl1* and *Loxl2* in primary mouse lung fibroblasts. Surprisingly the overexpression of *Loxl1* and *Loxl2* in the mouse NIH/3T3 fibroblast cell-line did not result in the corresponding opposite effect. Instead, the mRNA levels of both *Ifnb* (Figure 17G and 17K) and *Csf2* (Figure 17H and 17L) were again down-regulated after the lentivirus-mediated overexpression of *Loxl1* and *Loxl2*. It is possible that both increased and decreased levels of *Loxl1* and *Loxl2* lead to the same regulation of

target-genes and a precise equilibrium of *Loxl1* and *Loxl2* expression levels is required in order to maintain the native transcription status of the target-genes. Alternatively, the regulation of gene expression by *Loxl1* and *Loxl2* is not fully comparable between the primary mouse fibroblasts and mouse fibroblasts cell-line.

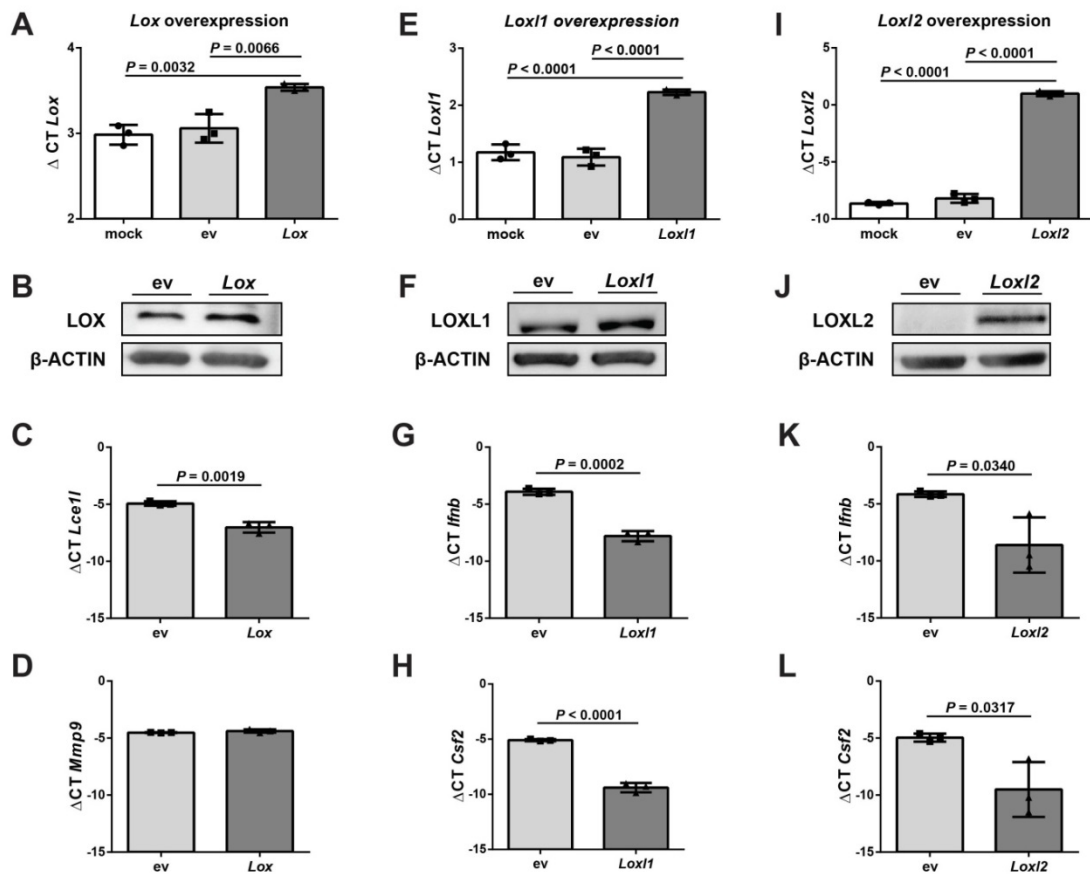


**Figure 17. Lentivirus-mediated overexpression of lysyl oxidases in the mouse NIH/3T3 fibroblast cell-line.**

The overexpression of *Lox*, *Loxl1*, and *Loxl2* in the mouse NIH/3T3 fibroblast cell-line was carried out using a lentivirus transduction system. (A-D) Lentivirus-mediated overexpression of *Lox*. The efficiency of *Lox* overexpression evaluated by real-time RT-PCR (A) and immunoblot (B). Additionally, the expression of selected candidate target-genes of *Lox*, in this case *Lce1l* (C) and *Mmp9* (D) was also evaluated by real-time RT-PCR. (E-H) Lentivirus-mediated overexpression of *Loxl1*. The efficiency of *Loxl1* overexpression evaluated by real-time RT-PCR (E) and immunoblot (F). The expression of selected candidate target-genes of *Loxl1*, in this case *Ifnb* (G) and *Csf2* (H) was also evaluated by real-time RT-PCR. (I-L) Lentivirus-mediated overexpression of *Loxl2*. The efficiency of *Loxl2* overexpression evaluated by real-time RT-PCR (I) and immunoblot (J). The expression of selected candidate target-genes of *Loxl2*, in this case *Ifnb* (K) and *Csf2* (L) was also evaluated by real-time RT-PCR. Mock-transduced and empty vector (ev)-transduced cells served as a control. Immunoblot analyses are representative of total of three experiments. Protein loading was controlled by  $\beta$ -ACTIN. Values represent mean  $\pm$  SD, ( $n = 3$  over-expression experiments, per group). The  $P$  values were determined by one-way ANOVA with Tukey's multiple comparisons test for data containing three experimental groups and by unpaired Student's  $t$ -test for data containing two experimental groups.

#### **4.9 Role of lysyl oxidase enzymatic activity in lysyl oxidase-mediated gene regulation**

In order to assess the importance of the catalytic activity of LOX, LOXL1 and LOXL2 in gene regulation, the activity of lysyl oxidases was inhibited (by approximately 50%) in primary mouse lung fibroblasts using the pan-lysyl oxidase inhibitor BAPN (Figure 18A). The inhibition of catalytic activity did not have any influence on the mRNA and protein levels of LOX (Figure 18B) and LOXL1 (Figure 18C). However a small, but significant increase in LOXL2 (Figure 17D) gene and protein expression after the BAPN treatment of the cells was observed.

Subsequently, potential gene regulatory changes caused by BAPN treatment were evaluated by microarray analysis. Full microarray data are available via the NCBI Gene Expression Omnibus under accession number GSE89119. Although the siRNA-mediated knockdown of *Lox*, *Loxl1* and *Lox2* resulted in expression changes of large groups of genes, only one significant change, in the gene expression of *Lrig2*, was detected by microarray analysis when enzymatic activity alone was blocked (Table 16). Although the microarray analysis identified the *Lrig2* gene as a potential target-gene, no changes in gene expression of *Lrig2* could be validated by real-time RT-PCR (Figure 19), indicating that enzymatic activity is not required for lysyl oxidase-mediated transcriptomic regulation in primary mouse lung fibroblasts.

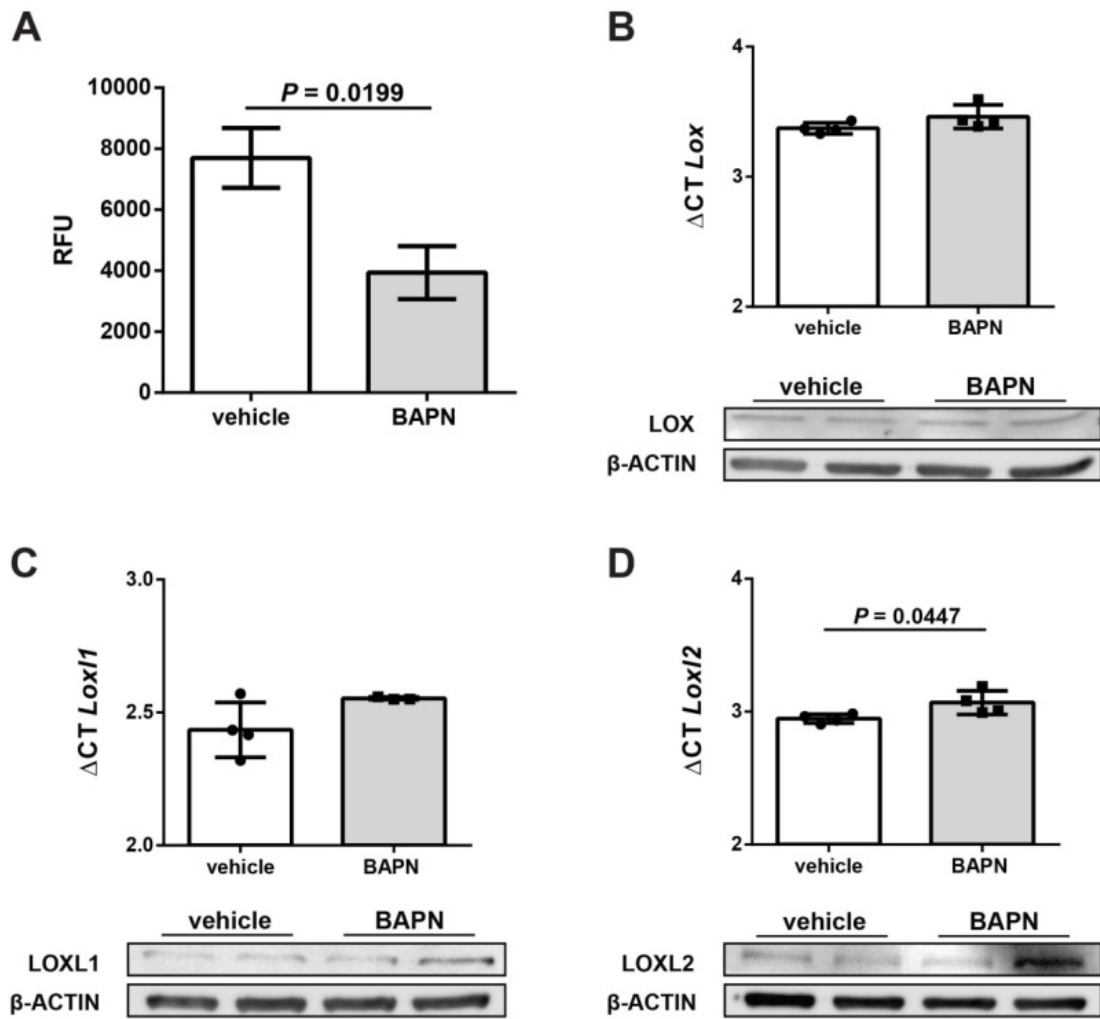


**Figure 18. Inhibition of lysyl oxidase enzymatic activity in primary mouse lung fibroblasts.**

Lysyl oxidase enzymatic activity in primary mouse lung fibroblasts was inhibited by incubation with 1 mM pan-lysyl inhibitor  $\beta$ -aminopropionitrile (BAPN) for 24 h. (A) Lysyl oxidase activity 24 h after the inhibition with BAPN. Activity is reported as the BAPN-sensitive fraction determined in the presence of 500  $\mu$ M BAPN. (B-D) Gene and protein expression of LOX (B), LOXL1 (C) and LOXL2 (D) 24 h after the inhibition with BAPN were evaluated by real-time RT-PCR and immunoblot respectively. Protein loading was controlled by  $\beta$ -ACTIN. Lysyl oxidase activity is reported as relative fluorescence units (RFU)  $\pm$  SD, ( $n = 3$ , per group). For real-time RT-PCR analysis values are represented as means  $\pm$  SD, ( $n = 4$  cell cultures, per group). The  $P$  values were determined by unpaired Student's  $t$ -test.

**Table 16. List of differentially up- and down-regulated genes after  $\beta$ -aminopropionitrile administration in primary mouse lung fibroblasts as assessed by microarray analysis.**

Most up-regulated genes					
n.	$P_{(corr)}$	FC	Log FC	Gene Symbol	Gene name
1	0.330047	4.580624	2.195544	<b>Vmn2r121</b>	vomer nasal 2, receptor 121
2	0.372661	4.273113	2.095287	<b>Cdh18</b>	cadherin 18
3	0.330047	4.221706	2.077826	<b>Oxct2b</b>	3-oxoacid CoA transferase 2B
4	0.374076	3.981276	1.993231	<b>Slc15a5</b>	solute carrier family 15, member 5
5	0.361489	3.976678	1.991564	<b>Gm13043</b>	predicted gene 13043
6	0.330047	3.974019	1.990599	<b>Defb45</b>	defensin beta 45
7	0.286779	3.967307	1.988160	<b>Speer7-ps1</b>	spermatogenesis associated glutamate (E)-rich protein 7, pseudogene 1
8	0.353551	3.959652	1.985374	<b>Gm16532</b>	predicted gene, 16532
9	0.251624	3.950184	1.981920	<b>Vmn1r181</b>	vomer nasal 1 receptor 181
10	0.357650	3.864533	1.950294	<b>Gm6507</b>	predicted gene 6507
Most down-regulated genes					
n.	$P_{(corr)}$	FC	Log FC	Gene Symbol	Gene name
1	0.021223	-2.114972	-1.080639	<b>Lrig2</b>	leucine-rich repeats and immunoglobulin-like domains 2
2	0.330047	-8.348955	-3.061596	<b>Cd8a</b>	CD8 antigen, alpha chain
3	0.334554	-7.988594	-2.997942	<b>Kcnj11</b>	potassium inwardly rectifying channel, subfamily J, member 11
4	0.376311	-6.387666	-2.675289	<b>Gsx2</b>	GS homeobox 2
5	0.339029	-6.379081	-2.673349	<b>Exph5</b>	exophilin 5
6	0.353551	-6.363410	-2.669800	<b>Ahsg</b>	alpha-2-HS-glycoprotein
7	0.267413	-6.139747	-2.618179	<b>Pnliprp1</b>	pancreatic lipase related protein 1
8	0.330047	-5.818665	-2.540688	<b>Gpa33</b>	glycoprotein A33 (transmembrane)
9	0.353559	-5.598395	-2.485013	<b>Svs5</b>	seminal vesicle secretory protein 5
10	0.339546	-5.598395	-2.485013	<b>Oaz3</b>	ornithine decarboxylase antizyme 3

*n*, number;  $P_{(corr)}$ , corrected *P* value; *FC*, fold change;

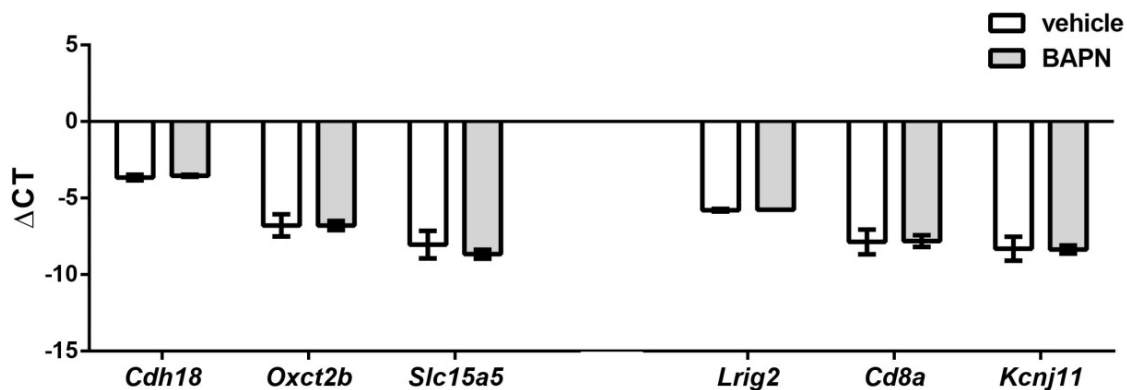


**Figure 19. Microarray analysis validation following the  $\beta$ -aminopropionitrile administration in primary mouse lung fibroblasts.**

Microarray data presented in Table 16 were validated by real-time RT-PCR. The expression of the three most up-regulated and the three most down-regulated genes following  $\beta$ -aminopropionitrile (BAPN) administration in primary mouse pulmonary fibroblasts is illustrated. Values represent mean  $\pm$  SD, ( $n = 4$ , per group). Statistical analyses were determined by unpaired Student's *t*-test. *P*-values  $> 0.05$  were regarded not significant and are not illustrated.

#### **4.10 The expression of LOX, LOXL1 and LOXL2 target-genes in a murine model of aberrant lung development**

To further evaluate the relevance of the data obtained in the *in vitro* studies in an *in vivo* setting, the expression of selected LOX, LOXL1 and LOXL2 target-genes was investigated in a hyperoxia-based mouse model of BPD. In this model, newborn mouse pups were exposed to either normal (21% O<sub>2</sub>) or hyperoxic (85% O<sub>2</sub>) environments over the first two weeks of life and the expression of selected target genes relevant to ECM formation and remodeling was assessed in total RNA pools from lung homogenates.

The mRNA levels of *Lox* (Figure 20A), *Loxl1* (Figure 21A) and *Loxl2* (figure 21B) were considerably increased in the lung homogenates from the developing mouse pups exposed to hyperoxia (85% O<sub>2</sub>) when compared with the normally-developing control mice. The hyperoxia-induced increase in the expression of lysyl oxidases was generally accompanied by the tendencies in the expression of investigated ECM-relevant lysyl oxidases target-genes. In accordance with an increased *Lox* expression, the expression of *Mmp9* was

decreased, and expression of *Rarres1* increased upon exposure of developing mice to hyperoxia. These observations *in vivo* reflect the observations made *in vitro*, where a siRNA-mediated knockdown of *Lox* in primary mouse lung fibroblasts led to an increase in *Mmp9* and decrease in *Rarres1* gene expression (Figure 15A). Similarly, the gene expression level of LOXL1 and LOXL2 target-gene *Eln* was up-regulated in the lungs of the developing mouse pups after a hyperoxia exposure when compared to normoxia-exposed control animals (Figure 21D), in an accordance with the down-regulation of *Eln* expression following the *Loxl1* and *Loxl2* knockdown in primary mouse lung fibroblasts (Figure 16B-C). Contrariwise, *Mmp3* mRNA levels, which were up-regulated in primary mouse lung fibroblasts after the siRNA-mediated knockdown of both *Loxl1* and *Loxl2*, were also increased *in vivo* in the lungs of developing mouse pups exposed to hyperoxia (85% O<sub>2</sub>) (Figure 21C).

*In vitro* studies in primary mouse lung fibroblasts suggested that enzymatic activity of lysyl oxidases was not required for lysyl oxidases-mediated gene regulation. To validate this observation *in vivo*, the catalytic activity of lysyl oxidases was neutralized in normally-developing normoxia-exposed mouse pups by pan-lysyl oxidase inhibitor BAPN. As expected, the neutralization of enzymatic activity by BAPN did not induce any changes in the lung mRNA levels of *Lox* (Figure 20D), *Loxl1* (Figure 21E) or *Loxl2* (Figure 21F). Consistent with the results of the *in vitro* experiment, no changes in gene expression of *Rarres1* (Figure 20F), *Mmp3* (Figure 21G) and *Eln* (Figure 21H) were detected following the administration of BAPN to developing mice. Interestingly, the mRNA levels of *Mmp9* were significantly decreased in the lungs of developing mouse pups treated with BAPN when compared to vehicle-treated control animals (Figure 20E), suggesting a possible lysyl oxidases-independent mechanism of *Mmp9* gene regulation in the lung.

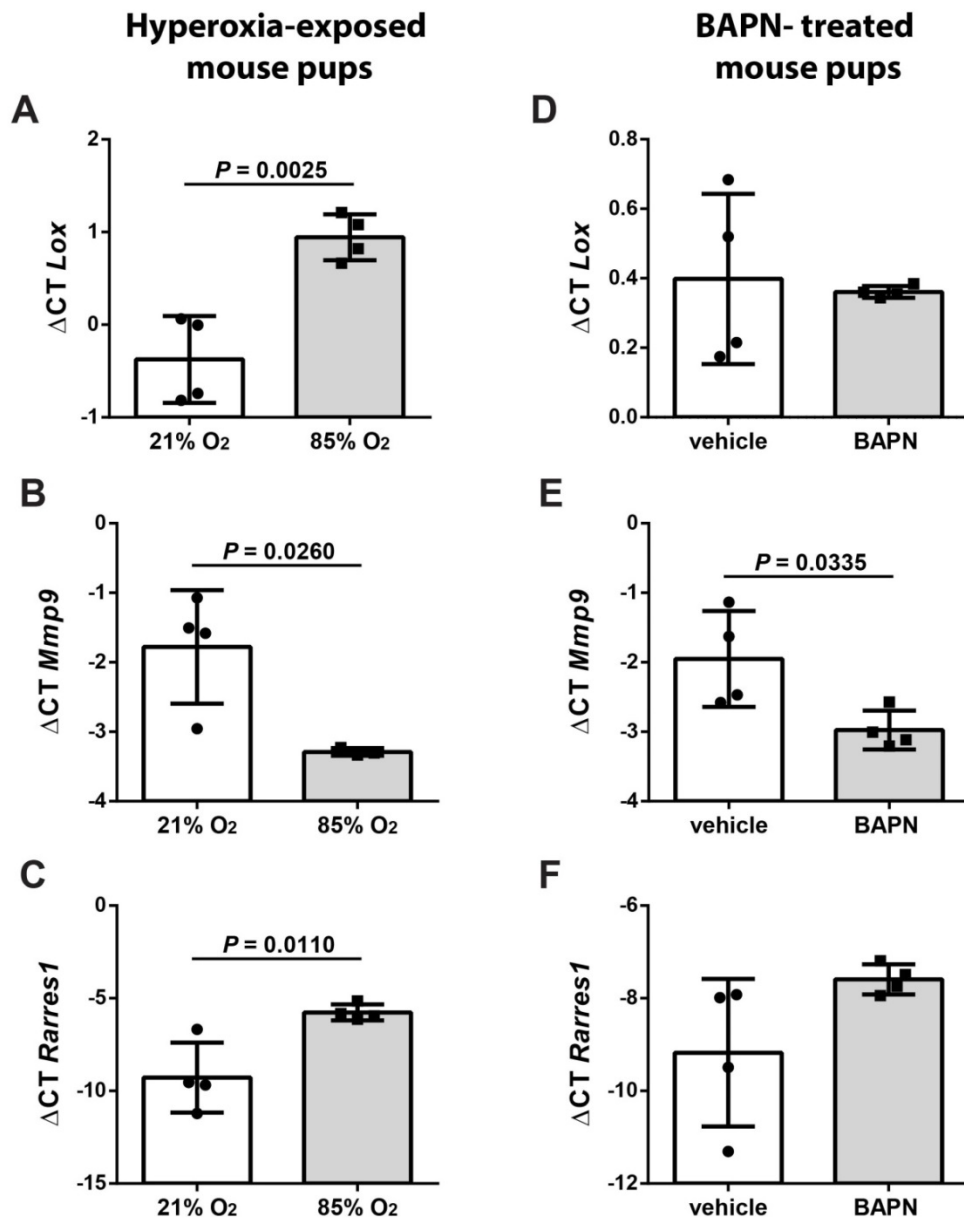


**Figure 20. Gene expression of *Lox* and selected LOX target-genes in a mouse model of an arrested lung development.**

(A-C) The expression of *Lox* (A) and selected LOX target-genes *Mmp9* (B) and *Rarres1* (C) was determined by real-time RT-PCR in hyperoxia-based mouse model of bronchopulmonary dysplasia (BPD). (D-F) The expression of *Lox* (D) and the selected LOX target-genes *Mmp9* (E) and *Rarres1* (F) was determined by real-time RT-PCR in the lungs of mice treated by  $\beta$ -aminopropionitrile (BAPN). Values represent mean  $\pm$  SD, ( $n = 4$  animals, per group). The  $P$  values were determined by unpaired Student's  $t$ -test.

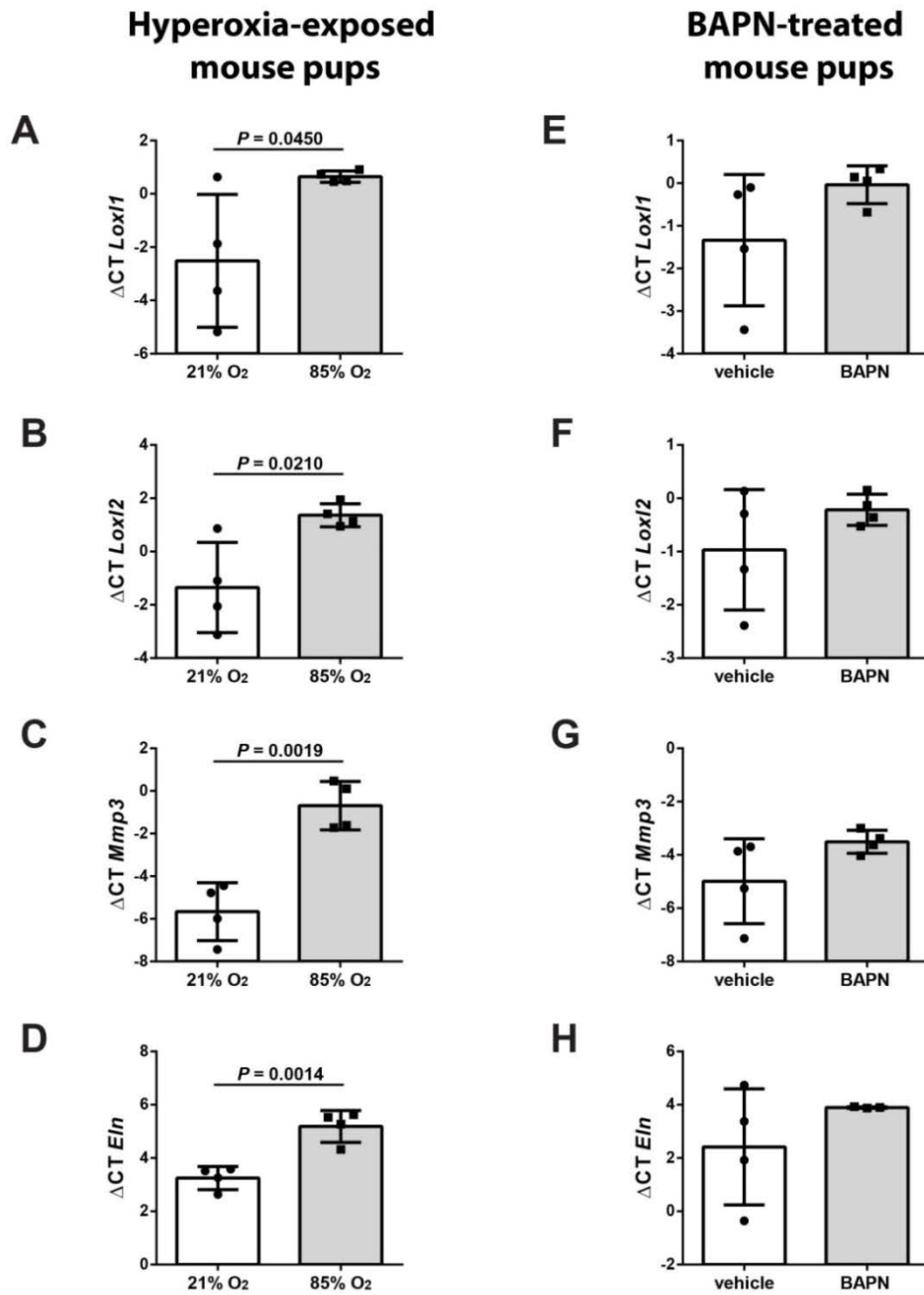


**Figure 21. Gene expression of *Loxl1* and *Loxl2*, as well as selected LOXL1 and LOXL2 target-genes in a mouse model of an arrested lung development.**

(A-D) The expression of *Loxl1* (A), *Loxl2* (B) and the selected LOXL1 and LOXL2 target-genes *Mmp3* (C) and *Eln* (D) was determined by real-time RT-PCR in well-established hyperoxia-based mouse model of bronchopulmonary dysplasia (BPD). (E-H) The expression of *Loxl1* (D), *Loxl2* (E) and LOXL1 and LOXL2 target-genes *Mmp3* (F) and *Eln* (G) was determined by real-time RT-PCR in the lungs of mice treated by  $\beta$ -aminopropionitrile (BAPN). Values represent mean  $\pm$  SD, ( $n = 4$  animals, per group). The  $P$  values were determined by unpaired Student's  $t$ -test.

## 5 DISCUSSION

### 5.1 The expression of lysyl oxidases is dysregulated in animal models of bronchopulmonary dysplasia

Bronchopulmonary dysplasia poses a substantial cause of morbidity and mortality in affected patients often with multiple long-time consequences ongoing into the adulthood [3, 27, 29, 30, 33-35]. Structurally lungs of patients deceased from BPD are generally characterized by arrest in alveolar formation, causing a severe increase in the size of alveoli accompanied by a decrease in the size of gas-exchange surface area of the lung and thickening of the alveolar septa [27, 32, 120]. Moreover, these lungs exhibit failures in the deposition of ECM structures, as well as ECM remodeling and metabolism. Among the most severely impacted ECM structures are fibrillar elastin and collagen [37, 38]. Both, elastin and collagen fibers in the lungs of patients diagnosed with BPD, as well as in the lungs obtained from various experimental animal models are described as disorganized, thickened and misshapen [37, 38, 121-123]. The importance of elastin and collagen formation during the course of normal lung development is well known and the role of ECM fibers deposition and remodeling in processes of alveolarization and secondary septation has been proposed [46, 84]. While multiple studies over the last decades have focused on the expression and production of individual structural components of ECM, only few studies so far have addressed the consecutive processes of fiber deposition and remodeling [4, 46, 96-98]. The abnormal formation and deposition of elastin and collagen fibers in the lungs of BPD patients and experimental animals has recently been accredited to dysregulation of enzymatic activity of multiple matrix-remodeling enzymes. This large family of enzymes include members of MMP, TIMP, TGM, PLOD and lysyl oxidase families [46, 70, 73, 76-78, 97, 98].

Lysyl oxidases form a family of five copper-dependent amine oxidases facilitating the oxidative deamination of lysyl and hydroxylysine residues. This process leads to formation of reactive semialdehydes and subsequent formation of intramolecular, as well as intermolecular covalent cross-links in elastin and collagen molecules [100, 101]. Although increases in the abundance and catalytic activity of lysyl oxidases have been reported in both clinical BPD [46], and various experimental animal models of BPD [46, 84, 109], no study so far has demonstrated a causal relationship between the expression of lysyl oxidases and disturbances

in ECM cross-linking and deposition in the context of arrest in alveolar formation associated with BPD.

Arrest in alveolarization and secondary septation in the study presented here was introduced by an exposure of newborn mice to hyperoxia (85% O<sub>2</sub>). Exposure of newborn mouse pups to hyperoxia resulted in an increase in the abundance of the first three members of the family, *Lox*, *Loxl1* and *Loxl2* and elevated lysyl oxidase enzymatic activity in the developing lungs, indicating the responsiveness of the lysyl oxidase family members to hyperoxia. As expected, exposure of newborn mice to increased concentration of oxygen led to an arrest in alveolar formation and considerable thickening of the alveolar walls. This structural changes were accompanied by perturbations to collagen and elastin deposition and cross-linking, and elastin foci formation.

## 5.2 Lysyl oxidase activity is essential for early postnatal development

In order to examine the causal role of lysyl oxidases in the context of ECM metabolism and alveolar and septal formation, the catalytic activity of lysyl oxidases was inhibited *in vivo* using a well-described pan-lysyl oxidase inhibitor BAPN. Foremost, the pilot study was performed to determine the appropriate dosage. The results of the dosage study stressed the importance of lysyl oxidases during the period of early postnatal development. Daily administration of BAPN at a dose of 150 mg·kg<sup>-1</sup> had a negative impact on mouse viability and mobility. Furthermore, both body mass and milk intake of BAPN-treated mice were seriously impacted by P5.5 when compared to normally developing, vehicle (1×PBS)-injected mice. This observation is in conflict with study, where BAPN applied at the same dose was well tolerated in adult mice of the same strain [106]. In the said investigation, using a murine model of pulmonary hypertension, BAPN administered was not only well tolerated, but led to an improvement in right ventricular systolic pressure and matrix architecture in lung vasculature of hypoxia-exposed mice. The results obtained in the pilot study are however in agreement with observations made in studies of *Lox*<sup>-/-</sup> and *Loxl1*<sup>-/-</sup> mice. While *Lox*<sup>-/-</sup> mice die shortly after birth from cardiorespiratory failure [58, 104], *Loxl1*<sup>-/-</sup> mice were shown to suffer from aortic aneurism and diaphragmatic hernia, [105]. A ten-times lower dose of BAPN, 15 mg·kg<sup>-1</sup>·day<sup>-1</sup>, was used in the subsequent studies. This dose was found to be efficient enough to preserve the normal levels of lysyl

oxidase activity in the lung homogenates of hyperoxia-exposed developing mouse pups without causing any negative side-effects regarding the growth, mobility or survival of the experimental animals.

### **5.3 Normalization of lysyl oxidase activity improves the formation of elastin and collagen cross-links and elastin foci structure in mouse model of bronchopulmonary dysplasia**

Exposure to elevated concentration of oxygen (85% O<sub>2</sub>) significantly increased the quantity of insoluble collagen in the lungs of developing mouse pups. Increase was noted also in the DHLNL/HLNL cross-links ratio, a marker of fibrotic status of the tissue [119, 124]. On contrary, the level of insoluble elastin was decreased by over 30% in the lungs of hyperoxia-exposed developing mouse pups when compared to normoxia-exposed control animals. This opposing changes in collagen and elastin abundance resulted in a substantial three-fold increase in the collagen-to-elastin ratio. Along with total elastin, the abundance of both elastin cross-links, desmosine and isodesmosine was similarly decreased in the developing lungs following the hyperoxia-exposure. In addition, the formation of elastin foci in the lungs of these animals appeared insufficient and the elastic fibers were disorganized and misshapen. A substantial shift in collagen-to-elastin ratio and perturbances in fibers structural integrity might suggest the formation of less elastic and therefore stiffer ECM network, possibly affecting the lung compliance. Decrease in lung compliance could have a negative influence on the role of breathing motions in alveolar formation, possibly leading to an arrest in alveolarization and formation of secondary crests in the developing lung [73, 84].

A decrease in the abundance of lysyl oxidases-generated elastin cross-links in the lungs of hyperoxia-exposed animals seems unusual considering the increase of lysyl oxidases expression and catalytic activity. Although seemingly contradictory, two possible explanations of this phenomenon exist. As lysyl oxidases are active on more than one substrate, a dramatic change in collagen-to-elastin ratio may lead to a shift in lysyl oxidases substrate homeostasis, recruiting lysyl oxidases primarily to collagen substrate. Such a change of substrate preference would make lysyl oxidases less available for elastin cross-linking. Additionally, some members of lysyl oxidase family were recently accredited with gene regulatory functions, including among others, the regulation of the *Eln* and *Col3a1*

promoters [113, 114]. It is, thus possible that lysyl oxidases regulate larger number of genes, including genes encoding other ECM remodeling elements.

Further supporting this possibility are the observations made in both normoxia-exposed and hyperoxia-exposed animals treated with BAPN, where inhibition of lysyl oxidase activity increased the abundance of elastin cross-links. Daily administration of BAPN partially normalized levels of desmosine and isodesmosine in the lungs of hyperoxia-exposed developing mice. However, no improvement in total abundance of insoluble elastin could be detected. Furthermore, levels of lung insoluble collagen were partially restored and DHLNL/HLNL cross-link ratio was normalized. Changes in the abundance of insoluble collagen following the BAPN administration also resulted in notable, although not significant decrease in collagen-to-elastin ratio, possibly affecting the lung elastic properties. Daily administration of BAPN during the period of first 19 days of life has also improved the structure and abundance of elastic foci in the lung parenchyma of the hyperoxia-exposed animals. It can be speculated that restoration in collagen-to-elastin ratio and DHLNL/HLNL ratio, together with improvements in desmosine and isodesmosine abundance in the lungs after BAPN administration resulted in improved lung compliance and reduced lung stiffness enabling a better formation of elastin fiber network and foci structure.

#### **5.4 Normalization of lysyl oxidase activity does not improve alveolarization and septal formation in mouse model of bronchopulmonary dysplasia**

Administration of BAPN to developing hyperoxia-exposed mouse pups positively impacted the collagen and elastin cross-linking and elastin foci formation. In regard to these findings, the potential beneficial effects of the lysyl oxidase inhibition on the lung architecture of hyperoxia-exposed animals were further investigated.

As expected, lungs structure of the mouse pups exposed to increased oxygen levels (85%O<sub>2</sub>) from the day of birth, for nine days was characterized by thickening of septal walls and an arrest in alveolarization associated with a decrease in gas-exchange surface area. Appearance of lung structure of hyperoxia-exposed mice daily treated with BAPN was more complex by visual inspection when compared to vehicle-treated hyperoxia-exposed animals and general trends towards an improvement in septal thickness, surface area, MLI and alveoli number were observed when assessed by stereological analysis. However, because none of the tendencies observed reached a statistical significance, study was prolonged for an

additional ten days. Nevertheless, no further improvements in lung architecture were observed in hyperoxia-exposed developing mouse pups after 19 days of BAPN administration when compared with vehicle-treated hyperoxia-exposed control animals of the same age.

Interestingly, a small, but significant increase in number of alveoli was observed in the lungs of BAPN-treated normoxia-exposed mouse pups when compared to vehicle-treated animals, which seems to be in conflict with the observations made in developing rat pups, where high doses of BAPN (500 mg·kg<sup>-1</sup> every second day) have negatively impacted the lung alveolarization [50, 125]. This phenomenon, together with observations regarding the septal wall thickness and collagen and elastin cross-linking suggested the existence of a fragile equilibrium of expression and enzymatic activity of lysyl oxidases necessary to sustain the normal processes of lung alveolarization and ECM formation during early postnatal lung development. However, although BAPN administration resulted in the partial normalization of collagen abundance and collagen and elastin crosslinking, as well as improved elastin foci formation, the data presented here do not encourage BAPN inhibition of lysyl oxidase catalytic activity as a therapeutic option.

## **5.5 Lysyl oxidase family members have gene regulatory roles in lung fibroblasts**

Although recent evidence has emerged suggesting gene regulatory roles for lysyl oxidase family members [113-115], studies addressing possible non-matrix roles of lysyl oxidases in the lung particularly, or in a context of BPD, has yet not been reported. In the present study, the possible non-matrix roles of lysyl oxidases were investigated using a microarray approach.

Three out of five lysyl oxidase family members: LOX, LOXL1 and LOXL2 were investigated. As described earlier, the expression of these three lysyl oxidases was increased in lungs of hyperoxia-exposed developing mice, implying a possible role for these members of the family in lung development and in the pathogenesis of BPD. Moreover, expression profile of *Lox*, *Loxl1* and *Loxl2* in different lung primary cell types was considerably more diverse than the expression profile of remaining two members of the family. In addition, among the cell-types screened the expression levels were highest in pulmonary fibroblasts which are largely believed to drive the process of secondary septation [126-128]. In order to

explore possible gene regulatory roles, *Lox*, *Loxl1* and *Loxl2* expression was silenced in these cells using an siRNA-mediated knockdown approach. Subsequent analyses by microarray revealed a striking gene regulatory impact of all three lysyl oxidases, causing changes in regulation of 134, 3,761 and 3,554 genes, respectively. Multiple of dysregulated genes were related to ECM either directly as a source of its structural network or as members of ECM-remodeling machinery, including elastin, several collagens and matrix proteinases. Interestingly, not only did *Loxl1* and *Loxl2* exhibited more transcriptional activity than *Lox*, but the pool of the genes regulated by *Loxl1* and *Loxl2* was largely identical between the two, while still distinct from the pool of genes regulated by *Lox*. This similarity in gene regulatory effects of *Loxl1* and *Loxl2* is extraordinary, because structurally LOXL1 is more similar to LOX than to LOXL2 [129]. However, *Loxl2* itself was among the genes regulated following the siRNA-mediated knockdown of *Loxl1* while *Loxl2* repression had no such effect on *Loxl1* expression levels. The possibility that genes identified as candidate LOXL1 targets, could be simply regulated due to the down-regulation of *Loxl2* therefore can not be excluded. On the other hand, abrogation of *Lox* also led to a small decrease in *Loxl2* expression, as assessed by real-time RT-PCR (but not by microarray), implying that similar pattern might be observed. Yet, no potential LOXL2 target-genes were affected after *Lox* knockdown. Alternatively, a certain threshold of *Loxl2* may be required in order to induce any transcriptional changes.

It was hypothesized that complementary regulation of target-genes would occur upon the over-expression of lysyl oxidases. However, the lentivirus-mediated over-expression of lysyl oxidases in NIH/3T3 cells provided mixed results. For example, while knockdown of *Lox* led to an increase in *Lcell* expression, *Lox* over-expression caused *Lcell* down-regulation, supporting the hypothesis. However no such complementary effect was observed in the case of LOXL1 and LOXL2 top target-genes *Ifnb* and *Csf2* which were down-regulated regardless of the down-regulation or over-expression of *Loxl1* and *Loxl2*. It is possible, that lysyl oxidases do not perform the same gene regulatory roles in NIH/3T3 fibroblast cell-line and in primary lung fibroblasts. Alternatively, equilibrium in the lysyl oxidases expression might be required for the expression of these genes, and both increased and decreased levels of lysyl oxidases leads to the same dysregulation effects.

Although several reports of transcriptional regulatory roles of lysyl oxidases exist, it is not yet obvious whether the catalytic activity is necessary for performing the nuclear functions of these enzymes or not. In order to determine the mode of function of lysyl

oxidases in gene regulation in pulmonary fibroblasts, the pan-lysyl oxidase enzymatic inhibitor BAPN was employed. Interestingly, no changes in gene expression were observed when lysyl oxidase catalytic activity was inhibited, suggesting that lysyl oxidases may serve rather as a scaffold in a transcription regulation complexes. This observation is further supported by other studies, where catalytically-inactive LOXL2 successfully repressed the expression of *Cdh* [111] in context of EMT. Similarly, catalytic activity was not required for LOXL2-mediated repression of *Cldn1* and *Lgl2* expression in modulation of tight junctions and cell polarity [130].

## **5.6 Gene regulatory functions for lysyl oxidases in the context of *in vivo* animal model of bronchopulmonary dysplasia**

In order to confirm the observations made *in vitro*, in the more complex situation *in vivo*, the regulation of expression of potential ECM-relevant target genes of lysyl oxidases was explored in an animal model of BPD. Hyperoxia-exposure of newborn mouse pups from the day of birth drove a considerable increase in lysyl oxidase expression and enzymatic activity. Three out of four genes investigated because of their importance to ECM metabolism, *Rarres1*, *Mmp9* and *Eln* were dysregulated after hyperoxia-exposure in line with the regulation observed *in vitro* after a siRNA-mediated knock-down of lysyl oxidases. For example *Mmp9* expression was down-regulated when *Lox* expression was silenced in primary lung fibroblasts, but up-regulated when assessed in the lungs of hyperoxia-exposed mice *in vivo*. Similarly *Eln* expression, which was down-regulated after the knockdown of both *Loxl1* and *Loxl2* *in vitro*, was increased in animals after a hyperoxia-exposure, suggesting a correlation between the *in vivo* and *in vitro* studies. Moreover, when the lysyl oxidase enzymatic inhibitor BAPN was applied to normally developing mice, no effect on gene expression was observed in three out of four investigated genes, supporting the hypothesis that catalytic activity is not always required for lysyl oxidases in order to carry out the regulatory functions.

In the light of this observation, it is interesting to note, that changes observed in the abundance of collagen and elastin, as well as the elastin and collagen crosslinks in the lungs of hyperoxia-exposed mice may be partially driven by nuclear activities of lysyl oxidases. For example, a total amount of insoluble lung collagen was significantly decreased in lungs of hyperoxia-exposed mice, when mice were also treated with BAPN, possibly suggesting a

connection between lysyl oxidase activity and collagen expression rather than collagen stability. However, no similar phenomenon was observed in the case of normoxia-exposed BAPN-treated mice, where insoluble collagen levels were not affected.

The notion of the potential catalytic activity-independent gene regulatory functions for lysyl oxidases is of great relevance in the translational sense. A large amount of genes involved in ECM deposition or metabolism was dysregulated upon a *Lox*, *Loxl1* and *Loxl2* knockdown in pulmonary fibroblasts. Selected ECM-related target-genes of LOX, LOXL1 and LOXL2 were also accordingly dysregulated in an *in vivo* hyperoxia-based mouse model of BPD. It therefore seems likely, that gene regulatory function of lysyl oxidases in major fibrogenic cells in the developing lung could contribute to the pathogenesis of BPD. Furthermore, the gene expression of the majority of the investigated target-genes was not effected by BAPN administration to the developing mouse pups. First efforts have already been made towards the use of pharmacological inhibition of lysyl oxidases in fibrosis and cancer [131], as well as pulmonary hypertension [106]. It is possible that the gene regulation by lysyl oxidases could be involved in the pathogenesis of these diseases. However, if the regulation of the gene expression would be independent of enzymatic activity, potential advantage of targeting lysyl oxidases in the context of the pathogenesis of the disease would be missed when only the catalytic activity of the protein would be neutralized.

## 6 CONCLUSIONS

Bronchopulmonary dysplasia (BPD) is a chronic lung disease of premature infancy, characterized mainly by an arrest in alveolarization and aberrant pulmonary microvascular development. The pathogenic pathways driving BPD include physical forces, inflammation, altered gene expression programs, cell-to-cell communication and extracellular matrix (ECM) deposition and remodeling. Deregulation of lysyl oxidases, a five-member family of collagen and elastin cross-linking enzymes, was reported in both BPD and experimental animal models of BPD. Although, a number of studies have suggested a role for lysyl oxidases in the pathogenesis of BPD, the causal role for lysyl oxidases in aberrant elastin and collagen formation has not yet been fully studied. In addition, nuclear, gene regulatory roles for lysyl oxidases have been recently proposed. However no study addressing the non-matrix related roles of lysyl oxidases in context of lung development or BPD exists.

The study presented here describes a successful neutralization of lysyl oxidases catalytic activity in an *in vivo* murine model of BPD. Daily administration of  $\beta$ -aminopropionitrile, an inhibitor of lysyl oxidases activity, led to the restoration of normal levels of collagen in the lungs of diseased animals. Similarly, the abundance of elastin cross-links was restored and formation of elastin foci was improved. However no improvement in lung structure was found. Furthermore, the possible non-matrix nuclear roles of three lysyl oxidase family members: *Lox*, *Loxl1* and *Loxl2* were explored in the primary mouse pulmonary fibroblasts. The present study revealed a catalytic activity-independent, lysyl oxidases-mediated gene regulation of numerous genes, including genes implicated in ECM metabolism, such as *Mmp3*, *Mmp9*, *Rarres1* or *Eln*.

In summary, data presented here support the role of lysyl oxidases in ECM stability and pathogenesis of BPD. In addition the present study describes, for the first time, a transcriptome-wide analysis of gene regulatory effects of *Lox*, *Loxl1* and *Loxl2* in primary murine lung fibroblasts, independent from their catalytic activity.

## 7 REFERENCES

1. Morrisey, E.E. and B.L. Hogan, *Preparing for the first breath: genetic and cellular mechanisms in lung development*. Dev Cell, 2010. **18**(1): p. 8-23.
2. Warburton, D., et al., *Lung organogenesis*. Curr Top Dev Biol, 2010. **90**: p. 73-158.
3. Madurga, A., et al., *Recent advances in late lung development and the pathogenesis of bronchopulmonary dysplasia*. Am J Physiol Lung Cell Mol Physiol, 2013. **305**(12): p. L893-905.
4. Silva, D.M., et al., *Recent advances in the mechanisms of lung alveolarization and the pathogenesis of bronchopulmonary dysplasia*. Am J Physiol Lung Cell Mol Physiol, 2015. **309**(11): p. L1239-72.
5. Mizikova, I. and R.E. Morty, *The Extracellular Matrix in Bronchopulmonary Dysplasia: Target and Source*. Front Med (Lausanne), 2015. **2**: p. 91.
6. Voelkel, N.F. and W. MacNee, *Chronic Obstructive Lung Diseases*. Illustrated ed. 2002: PMPH-USA. p. 428.
7. Burri, P.H., *Structural aspects of postnatal lung development - alveolar formation and growth*. Biol Neonate, 2006. **89**(4): p. 313-22.
8. Kotecha, S., *Lung growth for beginners*. Paediatr Respir Rev, 2000. **1**(4): p. 308-13.
9. Joshi, S. and S. Kotecha, *Lung growth and development*. Early Hum Dev, 2007. **83**(12): p. 789-94.
10. Herriges, M. and E.E. Morrisey, *Lung development: orchestrating the generation and regeneration of a complex organ*. Development, 2014. **141**(3): p. 502-13.
11. Rackley, C.R. and B.R. Stripp, *Building and maintaining the epithelium of the lung*. J Clin Invest, 2012. **122**(8): p. 2724-30.
12. Shi, W., S. Bellusci, and D. Warburton, *Lung development and adult lung diseases*. Chest, 2007. **132**(2): p. 651-6.
13. Ahlfeld, S.K. and S.J. Conway, *Aberrant signaling pathways of the lung mesenchyme and their contributions to the pathogenesis of bronchopulmonary dysplasia*. Birth Defects Res A Clin Mol Teratol, 2012. **94**(1): p. 3-15.
14. Rawlins, E.L., *The building blocks of mammalian lung development*. Dev Dyn, 2011. **240**(3): p. 463-76.
15. Laughon, M., et al., *Patterns of respiratory disease during the first 2 postnatal weeks in extremely premature infants*. Pediatrics, 2009. **123**(4): p. 1124-31.
16. West, J.B., *Marcello Malpighi and the discovery of the pulmonary capillaries and alveoli*. Am J Physiol Lung Cell Mol Physiol, 2013. **304**(6): p. L383-90.
17. Thurlbeck, W.M., *Postnatal growth and development of the lung*. Am Rev Respir Dis, 1975. **111**(6): p. 803-44.
18. Langston, C., et al., *Human lung growth in late gestation and in the neonate*. Am Rev Respir Dis, 1984. **129**(4): p. 607-13.
19. Emery, J.L. and A. Mithal, *The number of alveoli in the terminal respiratory unit of man during late intrauterine life and childhood*. Arch Dis Child, 1960. **35**: p. 544-7.
20. Zeltner, T.B. and P.H. Burri, *The postnatal development and growth of the human lung. II. Morphology*. Respir Physiol, 1987. **67**(3): p. 269-82.
21. Ochs, M., et al., *The number of alveoli in the human lung*. Am J Respir Crit Care Med, 2004. **169**(1): p. 120-4.
22. Galambos, C. and D.E. Demello, *Regulation of alveologenesis: clinical implications of impaired growth*. Pathology, 2008. **40**(2): p. 124-40.
23. Volckaert, T. and S.P. De Langhe, *Wnt and FGF mediated epithelial-mesenchymal crosstalk during lung development*. Dev Dyn, 2015. **244**(3): p. 342-66.

24. Mino0, P. and C. Li, *Cross-talk between transforming growth factor-beta and Wntless/Int pathways in lung development and disease*. Int J Biochem Cell Biol, 2010. **42**(6): p. 809-12.
25. McCulley, D., M. Wienhold, and X. Sun, *The pulmonary mesenchyme directs lung development*. Curr Opin Genet Dev, 2015. **32**: p. 98-105.
26. Morrissey, E.E., et al., *Molecular determinants of lung development*. Ann Am Thorac Soc, 2013. **10**(2): p. S12-6.
27. Jobe, A.H., *The new bronchopulmonary dysplasia*. Curr Opin Pediatr, 2011. **23**(2): p. 167-72.
28. Northway, W.H., Jr., R.C. Rosan, and D.Y. Porter, *Pulmonary disease following respirator therapy of hyaline-membrane disease. Bronchopulmonary dysplasia*. N Engl J Med, 1967. **276**(7): p. 357-68.
29. Jobe, A.H. and M. Ikegami, *Mechanisms initiating lung injury in the preterm*. Early Hum Dev, 1998. **53**(1): p. 81-94.
30. Northway, W.H., Jr., *Bronchopulmonary dysplasia: twenty-five years later*. Pediatrics, 1992. **89**(5 Pt 1): p. 969-73.
31. Jobe, A.H. and M. Ikegami, *Prevention of bronchopulmonary dysplasia*. Curr Opin Pediatr, 2001. **13**(2): p. 124-9.
32. Jobe, A.H., *What is BPD in 2012 and what will BPD become?* Early Hum Dev, 2012. **88 Suppl 2**: p. S27-8.
33. Baraldi, E. and M. Filippone, *Chronic lung disease after premature birth*. N Engl J Med, 2007. **357**(19): p. 1946-55.
34. Wong, P.M., et al., *Emphysema in young adult survivors of moderate-to-severe bronchopulmonary dysplasia*. Eur Respir J, 2008. **32**(2): p. 321-8.
35. Hilgendorff, A. and M.A. O'Reilly, *Bronchopulmonary dysplasia early changes leading to long-term consequences*. Front Med (Lausanne), 2015. **2**: p. 2.
36. Bruce, M.C., et al., *Altered urinary excretion of elastin cross-links in premature infants who develop bronchopulmonary dysplasia*. Am Rev Respir Dis, 1985. **131**(4): p. 568-72.
37. Thibeault, D.W., et al., *Lung elastic tissue maturation and perturbations during the evolution of chronic lung disease*. Pediatrics, 2000. **106**(6): p. 1452-9.
38. Thibeault, D.W., et al., *Collagen scaffolding during development and its deformation with chronic lung disease*. Pediatrics, 2003. **111**(4 Pt 1): p. 766-76.
39. McGowan, S.E., *Extracellular matrix and the regulation of lung development and repair*. FASEB J, 1992. **6**(11): p. 2895-904.
40. Baker, C.D. and S.H. Abman, *Impaired pulmonary vascular development in bronchopulmonary dysplasia*. Neonatology, 2015. **107**(4): p. 344-51.
41. Cutz, E. and D. Chiasson, *Chronic lung disease after premature birth*. N Engl J Med, 2008. **358**(7): p. 743-5; author reply 745-6.
42. Adamson, S.L., *Regulation of breathing at birth*. J Dev Physiol, 1991. **15**(1): p. 45-52.
43. Bourbon, J., et al., *Control mechanisms of lung alveolar development and their disorders in bronchopulmonary dysplasia*. Pediatr Res, 2005. **57**(5 Pt 2): p. 38R-46R.
44. Wessells, N.K., *Mammalian lung development: interactions in formation and morphogenesis of tracheal buds*. J Exp Zool, 1970. **175**(4): p. 455-66.
45. Powell, J.T. and P.L. Whitney, *Postnatal development of rat lung. Changes in lung lectin, elastin, acetylcholinesterase and other enzymes*. Biochem J, 1980. **188**(1): p. 1-8.
46. Kumarasamy, A., et al., *Lysyl oxidase activity is dysregulated during impaired alveolarization of mouse and human lungs*. Am J Respir Crit Care Med, 2009. **180**(12): p. 1239-52.
47. Shibahara, S.U., et al., *Modulation of tropoelastin production and elastin messenger ribonucleic acid activity in developing sheep lung*. Biochemistry, 1981. **20**(23): p. 6577-84.
48. Mariani, T.J., J.J. Reed, and S.D. Shapiro, *Expression profiling of the developing mouse lung: insights into the establishment of the extracellular matrix*. Am J Respir Cell Mol Biol, 2002. **26**(5): p. 541-8.

49. Myers, B., et al., *Elastin synthesis during perinatal lung development in the rat*. Biochim Biophys Acta, 1983. **761**(1): p. 17-22.
50. Kida, K. and W.M. Thurlbeck, *The effects of beta-aminopropionitrile on the growing rat lung*. Am J Pathol, 1980. **101**(3): p. 693-710.
51. Das, R.M., *The effect of beta-aminopropionitrile on lung development in the rat*. Am J Pathol, 1980. **101**(3): p. 711-22.
52. Nakamura, Y., S. Fukuda, and T. Hashimoto, *Pulmonary elastic fibers in normal human development and in pathological conditions*. Pediatr Pathol, 1990. **10**(5): p. 689-706.
53. Margraf, L.R., et al., *Morphometric analysis of the lung in bronchopulmonary dysplasia*. Am Rev Respir Dis, 1991. **143**(2): p. 391-400.
54. Wakafuji, S., *Pathological and histometrical studies on alveolar ducts and respiratory bronchioli*. Kobe J Med Sci, 1985. **31**(5): p. 203-20.
55. Thibeault, D.W., W.E. Truog, and Ekekezie, II, *Acinar arterial changes with chronic lung disease of prematurity in the surfactant era*. Pediatr Pulmonol, 2003. **36**(6): p. 482-9.
56. Ozbek, S., et al., *The evolution of extracellular matrix*. Mol Biol Cell, 2010. **21**(24): p. 4300-5.
57. Lang, M.R., et al., *Collagen content of alveolar wall tissue in emphysematous and non-emphysematous lungs*. Thorax, 1994. **49**(4): p. 319-26.
58. Maki, J.M., et al., *Lysyl oxidase is essential for normal development and function of the respiratory system and for the integrity of elastic and collagen fibers in various tissues*. Am J Pathol, 2005. **167**(4): p. 927-36.
59. Trask, T.M., et al., *Interaction of tropoelastin with the amino-terminal domains of fibrillin-1 and fibrillin-2 suggests a role for the fibrillins in elastic fiber assembly*. J Biol Chem, 2000. **275**(32): p. 24400-6.
60. Nakamura, T., et al., *Fibulin-5/DANCE is essential for elastogenesis in vivo*. Nature, 2002. **415**(6868): p. 171-5.
61. Benjamin, J.T., et al., *The role of integrin alpha8beta1 in fetal lung morphogenesis and injury*. Dev Biol, 2009. **335**(2): p. 407-17.
62. Nakamura, T., et al., *Mechanical strain and dexamethasone selectively increase surfactant protein C and tropoelastin gene expression*. Am J Physiol Lung Cell Mol Physiol, 2000. **278**(5): p. L974-80.
63. Olsen, K.C., et al., *Transglutaminase 2 and its role in pulmonary fibrosis*. Am J Respir Crit Care Med, 2011. **184**(6): p. 699-707.
64. Han, W., et al., *Aberrant elastin remodeling in the lungs of O(2)-exposed newborn mice; primarily results from perturbed interaction between integrins and elastin*. Cell Tissue Res, 2015. **359**(2): p. 589-603.
65. Kaarteenaho-Wiik, R., et al., *Type I and III collagen protein precursors and mRNA in the developing human lung*. J Pathol, 2004. **203**(1): p. 567-74.
66. Bradley, K.H., S.D. McConnell, and R.G. Crystal, *Lung collagen composition and synthesis. Characterization and changes with age*. J Biol Chem, 1974. **249**(9): p. 2674-83.
67. Frantz, C., K.M. Stewart, and V.M. Weaver, *The extracellular matrix at a glance*. J Cell Sci, 2010. **123**(Pt 24): p. 4195-200.
68. Kononov, S., et al., *Roles of mechanical forces and collagen failure in the development of elastase-induced emphysema*. Am J Respir Crit Care Med, 2001. **164**(10 Pt 1): p. 1920-6.
69. Shoemaker, C.T., et al., *Elevated ratios of type I/III collagen in the lungs of chronically ventilated neonates with respiratory distress*. Pediatr Res, 1984. **18**(11): p. 1176-80.
70. Alejandre-Alcazar, M.A., et al., *Hyperoxia modulates TGF-beta/BMP signaling in a mouse model of bronchopulmonary dysplasia*. Am J Physiol Lung Cell Mol Physiol, 2007. **292**(2): p. L537-49.
71. McNulty, R.J., et al., *The effect of transforming growth factor beta on rates of procollagen synthesis and degradation in vitro*. Biochim Biophys Acta, 1991. **1091**(2): p. 231-5.

72. Kotecha, S., et al., *Increase in the concentration of transforming growth factor beta-1 in bronchoalveolar lavage fluid before development of chronic lung disease of prematurity*. J Pediatr, 1996. **128**(4): p. 464-9.
73. Mammoto, T., et al., *Extracellular matrix structure and tissue stiffness control postnatal lung development through the lipoprotein receptor-related protein 5/Tie2 signaling system*. Am J Respir Cell Mol Biol, 2013. **49**(6): p. 1009-18.
74. Nakanishi, H., et al., *TGF-beta-neutralizing antibodies improve pulmonary alveologenesis and vasculogenesis in the injured newborn lung*. Am J Physiol Lung Cell Mol Physiol, 2007. **293**(1): p. L151-61.
75. Tarantal, A.F., et al., *Overexpression of transforming growth factor-beta1 in fetal monkey lung results in prenatal pulmonary fibrosis*. Eur Respir J, 2010. **36**(4): p. 907-14.
76. McGowan, S.E., *Paracrine cellular and extracellular matrix interactions with mesenchymal progenitors during pulmonary alveolar septation*. Birth Defects Res A Clin Mol Teratol, 2014. **100**(3): p. 227-39.
77. Dai, J., et al., *Overexpression of transforming growth factor-beta1 stabilizes already-formed aortic aneurysms: a first approach to induction of functional healing by endovascular gene therapy*. Circulation, 2005. **112**(7): p. 1008-15.
78. Akool el, S., et al., *Nitric oxide induces TIMP-1 expression by activating the transforming growth factor beta-Smad signaling pathway*. J Biol Chem, 2005. **280**(47): p. 39403-16.
79. Quondamatteo, F., et al., *Fibrillin-1 and fibrillin-2 in human embryonic and early fetal development*. Matrix Biol, 2002. **21**(8): p. 637-46.
80. Noguchi, A., et al., *Smooth muscle isoactin and elastin in fetal bovine lung*. Exp Lung Res, 1989. **15**(4): p. 537-52.
81. Pierce, R.A., T.J. Mariani, and R.M. Senior, *Elastin in lung development and disease*. Ciba Found Symp, 1995. **192**: p. 199-212; discussion 212-4.
82. Bruce, M.C., et al., *Risk factors for the degradation of lung elastic fibers in the ventilated neonate. Implications for impaired lung development in bronchopulmonary dysplasia*. Am Rev Respir Dis, 1992. **146**(1): p. 204-12.
83. Wendel, D.P., et al., *Impaired distal airway development in mice lacking elastin*. Am J Respir Cell Mol Biol, 2000. **23**(3): p. 320-6.
84. Hilgendorff, A., et al., *Lung matrix and vascular remodeling in mechanically ventilated elastin haploinsufficient newborn mice*. Am J Physiol Lung Cell Mol Physiol, 2015. **308**(5): p. L464-78.
85. Shifren, A., et al., *Elastin protein levels are a vital modifier affecting normal lung development and susceptibility to emphysema*. Am J Physiol Lung Cell Mol Physiol, 2007. **292**(3): p. L778-87.
86. Mascaretti, R.S., et al., *Lung morphometry, collagen and elastin content: changes after hyperoxic exposure in preterm rabbits*. Clinics (Sao Paulo), 2009. **64**(11): p. 1099-104.
87. Hilgendorff, A., et al., *Inhibiting lung elastase activity enables lung growth in mechanically ventilated newborn mice*. Am J Respir Crit Care Med, 2011. **184**(5): p. 537-46.
88. Pierce, R.A., et al., *Chronic lung injury in preterm lambs: disordered pulmonary elastin deposition*. Am J Physiol, 1997. **272**(3 Pt 1): p. L452-60.
89. McGowan, S.E. and R. McNamer, *Transforming growth factor-beta increases elastin production by neonatal rat lung fibroblasts*. Am J Respir Cell Mol Biol, 1990. **3**(4): p. 369-76.
90. McGowan, S.E., et al., *Exogenous and endogenous transforming growth factors-beta influence elastin gene expression in cultured lung fibroblasts*. Am J Respir Cell Mol Biol, 1997. **17**(1): p. 25-35.
91. Sproul, E.P. and W.S. Argraves, *A cytokine axis regulates elastin formation and degradation*. Matrix Biol, 2013. **32**(2): p. 86-94.

92. Popova, A.P., et al., *Reduced platelet-derived growth factor receptor expression is a primary feature of human bronchopulmonary dysplasia*. *Am J Physiol Lung Cell Mol Physiol*, 2014. **307**(3): p. L231-9.
93. Bland, R.D., et al., *Mechanical ventilation uncouples synthesis and assembly of elastin and increases apoptosis in lungs of newborn mice. Prelude to defective alveolar septation during lung development?* *Am J Physiol Lung Cell Mol Physiol*, 2008. **294**(1): p. L3-14.
94. Hirakawa, H., et al., *Cathepsin S deficiency confers protection from neonatal hyperoxia-induced lung injury*. *Am J Respir Crit Care Med*, 2007. **176**(8): p. 778-85.
95. Hilgendorff, A., et al., *Neonatal mice genetically modified to express the elastase inhibitor elafin are protected against the adverse effects of mechanical ventilation on lung growth*. *Am J Physiol Lung Cell Mol Physiol*, 2012. **303**(3): p. L215-27.
96. Dubick, M.A., et al., *Elastin metabolism in rodent lung*. *Biochim Biophys Acta*, 1981. **672**(3): p. 303-6.
97. Witsch, T.J., et al., *Transglutaminase 2: a new player in bronchopulmonary dysplasia?* *Eur Respir J*, 2014. **44**(1): p. 109-21.
98. Witsch, T.J., et al., *Deregulation of the lysyl hydroxylase matrix cross-linking system in experimental and clinical bronchopulmonary dysplasia*. *Am J Physiol Lung Cell Mol Physiol*, 2014. **306**(3): p. L246-59.
99. Moore, A.M., et al., *Altered expression of type I collagen, TGF-beta 1, and related genes in rat lung exposed to 85% O<sub>2</sub>*. *Am J Physiol*, 1995. **268**(1 Pt 1): p. L78-84.
100. Csiszar, K., *Lysyl oxidases: a novel multifunctional amine oxidase family*. *Prog Nucleic Acid Res Mol Biol*, 2001. **70**: p. 1-32.
101. Kagan, H.M. and W. Li, *Lysyl oxidase: properties, specificity, and biological roles inside and outside of the cell*. *J Cell Biochem*, 2003. **88**(4): p. 660-72.
102. Rodriguez, C., et al., *Regulation of lysyl oxidase in vascular cells: lysyl oxidase as a new player in cardiovascular diseases*. *Cardiovasc Res*, 2008. **79**(1): p. 7-13.
103. Maki, J.M., et al., *Inactivation of the lysyl oxidase gene *Lox* leads to aortic aneurysms, cardiovascular dysfunction, and perinatal death in mice*. *Circulation*, 2002. **106**(19): p. 2503-9.
104. Hornstra, I.K., et al., *Lysyl oxidase is required for vascular and diaphragmatic development in mice*. *J Biol Chem*, 2003. **278**(16): p. 14387-93.
105. Liu, X., et al., *Elastic fiber homeostasis requires lysyl oxidase-like 1 protein*. *Nat Genet*, 2004. **36**(2): p. 178-82.
106. Nave, A.H., et al., *Lysyl oxidases play a causal role in vascular remodeling in clinical and experimental pulmonary arterial hypertension*. *Arterioscler Thromb Vasc Biol*, 2014. **34**(7): p. 1446-58.
107. Zhan, P., et al., *Down-regulation of lysyl oxidase-like 2 (LOXL2) is associated with disease progression in lung adenocarcinomas*. *Med Oncol*, 2012. **29**(2): p. 648-55.
108. Counts, D.F., et al., *Collagen lysyl oxidase activity in the lung increases during bleomycin-induced lung fibrosis*. *J Pharmacol Exp Ther*, 1981. **219**(3): p. 675-8.
109. Bland, R.D., et al., *Dysregulation of pulmonary elastin synthesis and assembly in preterm lambs with chronic lung disease*. *Am J Physiol Lung Cell Mol Physiol*, 2007. **292**(6): p. L1370-84.
110. Li, W., et al., *Lysyl oxidase oxidizes basic fibroblast growth factor and inactivates its mitogenic potential*. *J Cell Biochem*, 2003. **88**(1): p. 152-64.
111. Peinado, H., et al., *A molecular role for lysyl oxidase-like 2 enzyme in snail regulation and tumor progression*. *EMBO J*, 2005. **24**(19): p. 3446-58.
112. Iturbide, A., A. Garcia de Herreros, and S. Peiro, *A new role for LOX and LOXL2 proteins in transcription regulation*. *FEBS J*, 2015. **282**(9): p. 1768-73.

113. Giampuzzi, M., et al., *Lysyl oxidase activates the transcription activity of human collagene III promoter. Possible involvement of Ku antigen.* J Biol Chem, 2000. **275**(46): p. 36341-9.
114. Oleggini, R., N. Gastaldo, and A. Di Donato, *Regulation of elastin promoter by lysyl oxidase and growth factors: cross control of lysyl oxidase on TGF-beta1 effects.* Matrix Biol, 2007. **26**(6): p. 494-505.
115. Herranz, N., et al., *Lysyl oxidase-like 2 (LOXL2) oxidizes trimethylated lysine 4 in histone H3.* FEBS J, 2016.
116. Hsia, C.C., et al., *An official research policy statement of the American Thoracic Society/European Respiratory Society: standards for quantitative assessment of lung structure.* Am J Respir Crit Care Med, 2010. **181**(4): p. 394-418.
117. Corti, M., A.R. Brody, and J.H. Harrison, *Isolation and primary culture of murine alveolar type II cells.* Am J Respir Cell Mol Biol, 1996. **14**(4): p. 309-15.
118. Pornprasertsuk, S., et al., *Lysyl hydroxylase-2b directs collagen cross-linking pathways in MC3T3-E1 cells.* J Bone Miner Res, 2004. **19**(8): p. 1349-55.
119. Willenborg, S., et al., *Genetic ablation of mast cells redefines the role of mast cells in skin wound healing and bleomycin-induced fibrosis.* J Invest Dermatol, 2014. **134**(7): p. 2005-15.
120. Hadchouel, A., M.L. Franco-Montoya, and C. Delacourt, *Altered lung development in bronchopulmonary dysplasia.* Birth Defects Res A Clin Mol Teratol, 2014. **100**(3): p. 158-67.
121. Bruce, M.C., R. Pawlowski, and J.F. Tomashefski, Jr., *Changes in lung elastic fiber structure and concentration associated with hyperoxic exposure in the developing rat lung.* Am Rev Respir Dis, 1989. **140**(4): p. 1067-74.
122. O'Reilly, M. and B. Thebaud, *Animal models of bronchopulmonary dysplasia. The term rat models.* Am J Physiol Lung Cell Mol Physiol, 2014. **307**(12): p. L948-58.
123. Yoder, B.A. and J.J. Coalson, *Animal models of bronchopulmonary dysplasia. The preterm baboon models.* Am J Physiol Lung Cell Mol Physiol, 2014. **307**(12): p. L970-7.
124. Gerriets, J.E., K.M. Reiser, and J.A. Last, *Lung collagen cross-links in rats with experimentally induced pulmonary fibrosis.* Biochim Biophys Acta, 1996. **1316**(2): p. 121-31.
125. Kida, K. and W.M. Thurlbeck, *Lack of recovery of lung structure and function after the administration of beta-amino-propionitrile in the postnatal period.* Am Rev Respir Dis, 1980. **122**(3): p. 467-75.
126. Ntokou, A., et al., *Characterization of the platelet-derived growth factor receptor-alpha-positive cell lineage during murine late lung development.* Am J Physiol Lung Cell Mol Physiol, 2015. **309**(9): p. L942-58.
127. Ruiz-Camp, J. and R.E. Morty, *Divergent fibroblast growth factor signaling pathways in lung fibroblast subsets: where do we go from here?* Am J Physiol Lung Cell Mol Physiol, 2015. **309**(8): p. L751-5.
128. Choi, C.W., *Lung interstitial cells during alveolarization.* Korean J Pediatr, 2010. **53**(12): p. 979-84.
129. Barker, H.E., T.R. Cox, and J.T. Erler, *The rationale for targeting the LOX family in cancer.* Nat Rev Cancer, 2012. **12**(8): p. 540-52.
130. Moreno-Bueno, G., et al., *Lysyl oxidase-like 2 (LOXL2), a new regulator of cell polarity required for metastatic dissemination of basal-like breast carcinomas.* EMBO Mol Med, 2011. **3**(9): p. 528-44.
131. Trackman, P.C., *Lysyl Oxidase Isoforms and Potential Therapeutic Opportunities for Fibrosis and Cancer.* Expert Opin Ther Targets, 2016. **20**(8): p. 935-45.

## 8 DECLARATION

I declare that I have completed this dissertation single-handedly without the unauthorized help of a second party and only with the assistance acknowledged therein. I have appropriately acknowledged and referenced all text passages that are derived literally from or are based on the content of published or unpublished work of others, and all information that relates to verbal communications. I have abided by the principles of good scientific conduct laid down in the charter of the Justus Liebig University of Giessen in carrying out the investigations described in the dissertation.

---

Mižíková Ivana

## 9 ACKNOWLEDGEMENTS

I would like to express my gratitude to those who provided me with the possibility to perform the research presented in this dissertation and with the support necessary for completing my work.

Firstly, my thanks go to my supervisor Dr. Rory E. Morty, without whom my studies would be much less successful. Thank you for the opportunity to work as a member of your research group and as a member of MBML family. Thank you for your never ending support, encouragement and patience. There is much to learn from you and I hope I learned at least a little.

I am also grateful to Prof. Dr. Werner Seeger and the Max Planck Institute in Bad Nauheim with providing me with the opportunity to work in international, encouraging and inspiring environment for young scientists.

Furthermore, I would like to thank Prof. Dr. Med. Jürgen Brinckman and Dipl.-Ing. Heiko Steenbock from the Institute of Virology and Cell Biology of University of Lübeck for their professional assistance and remarks.

I owe a lot of gratitude to Molecular Biology and Medicine of the Lung graduate program and all its lecturers for their teaching and encouragement of critical thinking. It is a great joy to be a part of this family.

I would like to acknowledge all the present and past members of Morty's laboratory. This PhD would be much less of a fun and much more of a struggle without you. In particular I would like to thank Alicia Madurga-Hernández, Jordi Ruiz-Camp, Luciana Mazzochi, Claudio Nardiello and David Surate Solaligue, who all in their own way shaped the way I think about research.

Alessandro, *grazie che non hai mai dubitato di me.*

Lastly, I would like to thank my friends Luba and Barbara and my family, my mother and my grandparents for making me the way I am (the good and the bad). *Za všetko vd'aka.*

**Der Lebenslauf wurde aus der elektronischen  
Version der Arbeit entfernt.**

**The curriculum vitae was removed from the  
electronic version of the paper.**

## 11 APPENDIX

### PUBLICATIONS AUTHORED:

Hönig J., **Mižíková I.**, Nardiello C., Surate Solaligue D., Vadász I., Mayer K., Herold S., Seeger W., Morty RE, *Perturbations to lysyl oxidase expression broadly influence the transcriptome of lung fibroblasts*. RNA, 2017. In revision.

**Mižíková I.**, Palumbo F., Tábi T., Herold S., Vadász I., Mayer K., Seeger W., Morty RE, *Perturbations to lysyl oxidase expression broadly influence the transcriptome of lung fibroblasts*. Physiological Genomics, 2017. 49(8): p. 416-429.

Pozarska A., Rodríguez-Castillo JA., Surate Solaligue D., Ntokou A., Rath P., **Mižíková I.**, Madurga A., Mayer K., Vadász I., Herold S., Albrecht K., Seeger W., Morty RE, *Stereological monitoring of mouse lung alveolarization from the early post-natal period to adulthood*. Am J Physiol Lung Cell Mol Physiol, 2017. 12(6): p. L882-L895.

Nardiello C., **Mižíková I.**, Morty RE, *Looking ahead: where to next for animal models of bronchopulmonary dysplasia?* Cell and Tissue Res; 2017. 367(3): p. 457-468.

Nardiello C., **Mižíková I.**, Silva DM., Ruiz-Camp J., Mayer K., Vadász I., Herold S., Seeger W., Morty RE, *Modelling bronchopulmonary dysplasia in mice: how much oxygen is enough?* Dis Model Mech; 2017. 10(2): p. 185-196.

Rath P., Nardiello C., Surate Solaligue D., **Mižíková I.**, Hühn S., Mayer K., Vadász I., Herold S., Runkel F., Seeger W., Morty RE, *Caffeine administration modulates TGF- $\beta$  signaling but does not attenuate blunted alveolarization in a hyperoxia-based mouse model of bronchopulmonary dysplasia*. Pediatr Res; 2017. 81(5): p.795-805.

Madurga A., Golec A., Pozarska A., Ishii I., **Mižíková I.**, Nardiello C. Vadász I., Herold S., Mayer K., Reichenberger F., Fehrenbach H., Seeger W., Morty RE, *The H<sub>2</sub>S-generating enzymes cystathionine  $\beta$ -synthase and cystathionine  $\gamma$ -lyase play a role in vascular development during normal lung alveolarization*. Am J Physiol Lung Cell Mol Physiol, 2015. 309(7): p. L710-724.

**Mižíková I.** and R.E. Morty, *The Extracellular Matrix in Bronchopulmonary Dysplasia: Target and Source*. Front Med (Lausanne), 2015. 2: p. 91.

**Mižíková I.**, Ruiz-Camp J., Madurga A., Vadász I., Herold S., Mayer K., Seeger W., Morty RE, *Collagen and elastin cross-linking is altered during aberrant late lung development associated with hyperoxia*. Am J Physiol Lung Cell Mol Physiol, 2015. 308(11): p. L1145-1158.

Madurga A., **Mižíková I.**, Ruiz-Camp J, Vadász I., Herold S., Mayer K., Fehrenbach H., Seeger W., Morty RE, *Systemic hydrogen sulfide administration partially restores normal alveolarization in an experimental animal model of bronchopulmonary dysplasia*. Am J Physiol Lung Cell Mol Physiol, 2014. 306(7): p. L684-697.

Nave, A.H., **Mižíková, I.**, Niess G., Steenbock H., Reichenberger F., Talavera ML., Veit F., Herold S., Mayer K., Vadász I., Weissmann N., Seeger W., Brinckmann J., Morty RE, *Lysyl oxidases play a causal role in vascular remodeling in clinical and experimental pulmonary arterial hypertension*. Arterioscler Thromb Vasc Biol, 2014. 34(7): p. 1446-58.

Madurga, A., **Mižíková, I.**, Ruiz-Camp J., Morty RE., *Recent advances in late lung development and the pathogenesis of bronchopulmonary dysplasia*. Am J Physiol Lung Cell Mol Physiol, 2013. 305(12): p. L893-905.

Due to space limitations only abstract including first pages of all publications are enclosed.

# Transmission of microRNA antagomiRs to mouse offspring via the maternal-placental-fetal unit

Jonas Hönig<sup>1,2</sup>, Ivana Mižíková<sup>1,2</sup>, Claudio Nardiello<sup>1,2</sup>, David E. Surate Solaligue<sup>1,2</sup>, István Vadász<sup>2</sup>, Konstantin Mayer<sup>2</sup>, Susanne Herold<sup>2</sup>, Werner Seeger<sup>1,2</sup>, Rory E. Morty<sup>1,2,\*</sup>

<sup>1</sup>Department of Lung Development and Remodelling, Max Planck Institute for Heart and Lung Research, Bad Nauheim, Germany; <sup>2</sup>Department of Internal Medicine (Pulmonology), University of Giessen and Marburg Lung Center (UGMLC), member of the German Center for Lung Research (DZL), Giessen, Germany

**Correspondence to:**

Rory E. Morty  
Department of Lung Development and Remodelling  
Max Planck Institute for Heart and Lung Research  
Parkstrasse 1  
D-61231 Bad Nauheim  
Germany  
Tel: +49 6032 705 271  
Fax: +49 6032 705 360  
e-mail: rory.morty@mpi-bn.mpg.de

**Running head:**

Maternal transmission of microRNA antagomiRs

**Table of Contents section:**

Methods

**Keywords:**

microRNA, antagomiR, development, organogenesis,  
maternal transmission

## **ABSTRACT**

The emergence of microRNA as regulators of organogenesis and tissue differentiation has stimulated interest in the ablation of microRNA expression and function during discrete periods of development. To this end, inducible, conditional modulation of microRNA expression with doxycycline-based tetracycline-controlled transactivator and tamoxifen-based estrogen receptor systems has found widespread use. However, the induction agents and components of genome recombination systems negatively impact pregnancy, parturition, and post-natal development; thereby limiting the use of these technologies between late gestation and the early post-natal period. An alternative means of regulating microRNA expression and function is described here: the maternal-placental-fetal transmission of microRNA antagomiRs, which, when administered to pregnant dams results in a pronounced and persistent reduction in steady-state microRNA levels in the heart, kidney, liver and lungs, and to a very limited extent, the brain. This effect was comparable to direct injection of newborn mouse pups with antagomiRs. Furthermore, depletion of steady-state microRNA levels via the maternal route resulted in concomitant increases in steady-state levels of microRNA targets. This novel methodology permits the temporal regulation of microRNA function during late gestation and in neonates, without recourse to conventional approaches that rely on doxycycline and tamoxifen, which may confound studies on developmental processes.

**Abstract word-count:** 198 (limit 250)

## RESEARCH ARTICLE | *Physiological Genomics of Cell States and Their Regulation and Single Cell Genomics*

# Perturbations to lysyl oxidase expression broadly influence the transcriptome of lung fibroblasts

Ivana Mižíková,<sup>1,2</sup> Francesco Palumbo,<sup>1,2</sup> Tamás Tábi,<sup>3</sup> Susanne Herold,<sup>2</sup> István Vadász,<sup>2</sup> Konstantin Mayer,<sup>2</sup> Werner Seeger,<sup>1,2</sup> and Rory E. Morty<sup>1,2</sup>

<sup>1</sup>Department of Lung Development and Remodelling, Max Planck Institute for Heart and Lung Research, Bad Nauheim, Germany; <sup>2</sup>Department of Internal Medicine (Pulmonology), University of Giessen and Marburg Lung Center (UGMLC), member of the German Center for Lung Research (DZL), Giessen, Germany; and <sup>3</sup>Department of Pharmacodynamics, Semmelweis University, Budapest, Hungary

Submitted 3 April 2017; accepted in final form 29 June 2017

**Mižíková I, Palumbo F, Tábi T, Herold S, Vadász I, Mayer K, Seeger W, Morty RE.** Perturbations to lysyl oxidase expression broadly influence the transcriptome of lung fibroblasts. *Physiol Genomics* 49: 416–429, 2017. First published July 10, 2017; doi: 10.1152/physiolgenomics.00026.2017.—Lysyl oxidases are credited with pathogenic roles in lung diseases, including cancer, fibrosis, pulmonary hypertension, congenital diaphragmatic hernia, and bronchopulmonary dysplasia (BPD). Lysyl oxidases facilitate the covalent intra- and intermolecular cross-linking of collagen and elastin fibers, thereby imparting tensile strength to the extracellular matrix (ECM). Alternative ECM-independent roles have recently been proposed for lysyl oxidases, including regulation of growth factor signaling, chromatin remodeling, and transcriptional regulation, all of which impact cell phenotype. We demonstrate here that three of the five lysyl oxidase family members, *Lox*, *Loxl1*, and *Loxl2*, are highly expressed in primary mouse lung fibroblasts compared with other constituent cell types of the lung. Microarray analyses revealed that small interfering RNA knockdown of *Lox*, *Loxl1*, and *Loxl2* was associated with apparent changes in the expression of 134, 3,761, and 3,554 genes, respectively, in primary mouse lung fibroblasts. The impact of lysyl oxidase expression on steady-state *Mmp3*, *Mmp9*, *Eln*, *Rarres1*, *Gdf10*, *Ifnb1*, *Csf2*, and *Cxcl9* mRNA levels was validated, which is interesting, since the corresponding gene products are relevant to lung development and BPD, where lysyl oxidases play a functional role. In vivo, the expression of these genes broadly correlated with *Lox*, *Loxl1*, and *Loxl2* expression in a mouse model of BPD. Furthermore,  $\beta$ -aminopropionitrile (BAPN), a selective lysyl oxidase inhibitor, did not affect the steady-state mRNA levels of lysyl oxidase target genes, in vitro in lung fibroblasts or in vivo in BAPN-treated mice. This study is the first to report that lysyl oxidases broadly influence the cell transcriptome.

bronchopulmonary dysplasia; fibroblast; lung; lysyl oxidase; transcriptome

LYSYL OXIDASES ARE a family of copper-dependent amine oxidases with acknowledged roles in the cross-linking of the extracellular matrix (ECM) (20). These activities are undertaken by five different family members, namely LOX, the first

described member of the family, as well as the LOX-like enzymes, LOXL1, LOXL2, LOXL3, and LOXL4 (11, 28). All five lysyl oxidases have a common COOH-terminal catalytic domain that undertakes the oxidative deamination of the  $\epsilon$ -amino groups of lysine and hydroxylysine residues in collagen and elastin, which facilitate intra- and intermolecular cross-linking, and thus imparts tensile strength to the ECM (32, 47). The five lysyl oxidases exhibit substantial structural heterogeneity in the NH<sub>2</sub>-terminal regions, which is thought to confer functional specificity to each members of the family (11, 28).

Lysyl oxidases are important mediators of both organogenesis and tissue remodeling during disease and have emerged as key mediators of lung development and pathophysiology in particular. Of the five family members, LOX (5, 17, 29, 30), LOXL1 (24), and LOXL3 (49) all play a functional role in the development of the respiratory tract, in early and late phases of lung development. Regarding lung pathophysiology, lysyl oxidases are implicated in adult lung diseases including lung fibrosis (4), pulmonary hypertension (37, 51), and lung cancer (40), leading to lysyl oxidases being considered candidate therapeutic targets for a spectrum of lung and other diseases (41, 45). Given the pivotal roles played by lysyl oxidases in lung development, deregulation of lysyl oxidase activity disturbs lung maturation, and consequently, lysyl oxidases have been implicated in congenital diaphragmatic hernia (46), as well as in clinical (21) and experimental (6–8, 16, 21, 33, 34) bronchopulmonary dysplasia (BPD), a common complication of preterm birth where the late phases of lung development are stunted. In general, physiological and pathological roles for lysyl oxidases in the lung have been related to ECM assembly, maturation, and metabolism.

Apart from lysyl oxidase effects on the ECM, several studies have highlighted “nonmatrix” roles for lysyl oxidases, which include the modulation of intracellular signaling and transcriptional regulation. Concerning cell signaling, by virtue of catalytic activity, lysyl oxidases can modulate growth factor activity, such as that of basic fibroblast growth factor (23) and transforming growth factor- $\beta$  (3), thereby influencing cell signaling, and cell properties such as proliferation, differentiation, and migration. Furthermore, the LOX propeptide inhibits vascular smooth muscle cell proliferation, ostensibly by inhibiting ERK1/2 phosphorylation in response to tumor necrosis factor- $\alpha$  (18).

Address for reprint requests and other correspondence: R. E. Morty, Dept. of Lung Development and Remodelling, Max Planck Inst. for Heart and Lung Research, Parkstr. 1, D-61231 Bad Nauheim, Germany (e-mail: rory.morty@mpi-bn.mpg.de).

## RESEARCH ARTICLE

# Stereological monitoring of mouse lung alveolarization from the early postnatal period to adulthood

Agnieszka Pozarska,<sup>1,2</sup> José Alberto Rodríguez-Castillo,<sup>1,2</sup> David E. Surate Solaligue,<sup>1,2</sup> Aglaia Ntokou,<sup>1,2</sup> Philipp Rath,<sup>1</sup> Ivana Mižíková,<sup>1,2</sup> Alicia Madurga,<sup>1,2</sup> Konstantin Mayer,<sup>2</sup> István Vadász,<sup>2</sup> Susanne Herold,<sup>2</sup> Katrin Ahlbrecht,<sup>1,2</sup> Werner Seeger,<sup>1,2</sup> and Rory E. Morty<sup>1,2</sup>

<sup>1</sup>Department of Lung Development and Remodelling, Max Planck Institute for Heart and Lung Research, Bad Nauheim, Germany; and <sup>2</sup>Department of Internal Medicine (Pulmonology), University of Giessen and Marburg Lung Center, member of the German Center for Lung Research, Giessen, Germany

Submitted 1 November 2016; accepted in final form 8 March 2017

**Pozarska A, Rodríguez-Castillo JA, Surate Solaligue DE, Ntokou A, Rath P, Mižíková I, Madurga A, Mayer K, Vadász I, Herold S, Ahlbrecht K, Seeger W, Morty RE.** Stereological monitoring of mouse lung alveolarization from the early postnatal period to adulthood. *Am J Physiol Lung Cell Mol Physiol* 312: L882–L895, 2017. First published March 17, 2017; doi:10.1152/ajplung.00492.2016.—Postnatal lung maturation generates a large number of small alveoli, with concomitant thinning of alveolar septal walls, generating a large gas exchange surface area but minimizing the distance traversed by the gases. This demand for a large and thin gas exchange surface area is not met in disorders of lung development, such as bronchopulmonary dysplasia (BPD) histopathologically characterized by fewer, larger alveoli and thickened alveolar septal walls. Diseases such as BPD are often modeled in the laboratory mouse to better understand disease pathogenesis or to develop new interventional approaches. To date, there have been no stereology-based longitudinal studies on postnatal mouse lung development that report dynamic changes in alveoli number or alveolar septal wall thickness during lung maturation. To this end, changes in lung structure were quantified over the first 22 mo of postnatal life of C57BL/6J mice. Alveolar density peaked at postnatal day (P)39 and remained unchanged at 9 mo (P274) but was reduced by 22 mo (P669). Alveoli continued to be generated, initially at an accelerated rate between P5 and P14, and at a slower rate thereafter. Between P274 and P669, loss of alveoli was noted, without any reduction in lung volume. A progressive thinning of the alveolar septal wall was noted between P5 and P28. Pronounced sex differences were observed in alveoli number in adult (but not juvenile) mice, when comparing male and female mouse lungs. This sex difference was attributed exclusively to the larger volume of male mouse lungs.

THE ALVEOLUS is the primary gas exchange unit of the lung, first described by Marcello Malpighi in 1661 (29, 30). The formation and maturation of alveoli occur during the final phase of lung development, where the process of secondary septation generates alveolar septa that subdivide the primitive sacculi and generate the walls of the mature alveoli (5, 49). This process generates a large number of small alveoli, thus imparting a large gas exchange surface area to the lung and occurs concomitantly with the thinning of the alveolar walls, to minimize the distance traversed by gases during gas exchange.

Address for reprint requests and other correspondence: R. E. Morty, Dept. of Lung Development and Remodelling, Max Planck Institute for Heart and Lung Research, Parkstrasse 1, D-61231 Bad Nauheim, Germany (e-mail: rory.morty@mpi-bn.mpg.de).

Despite much consideration over the past 100 years, how lung alveoli develop remains poorly understood. As early as 1881, Albert von Kölliker at the University of Würzburg (Würzburg, Germany) suggested that the structure of the adult lung was already present in newborn infants, and growth proceeded exclusively by expansion (23). This view was countered by the German anatomist Robert Heiss in 1919 (12) and by the Swedish anatomist Ivar Broman in 1923 (4), who both suggested that in mammals, the number of alveoli in the lung continued to increase after birth. The latter idea was validated by Herbert Willson in 1928 (64), who demonstrated that infant mouse and human lungs had both fewer and larger alveoli and more connective tissue “between the airspaces” (i.e., thicker septa) than did corresponding adult lungs of both species. Thus Willson captured the concept of late lung development and the process of alveolarization, namely, the generation of a large gas exchange surface area and thinning of the alveolar septal walls. The exponential growth of alveoli in human lungs in utero was subsequently documented in the 1960s, when a quantitative increase in alveolar density in lungs from 28 wk to 40 wk gestation in humans was demonstrated (8), as was the fact that preterm birth leads to fewer alveoli in the infant lung (32). Building on these studies, Dunnill (7) demonstrated a 10-fold increase in the number of alveoli in the human lung between birth and adult life, occurring primarily over the first 8 years of life (7). Later, researchers estimated that the adult human lung harbored ~300 million alveoli (57), a number later revised to 480 million (45). Subsequent studies demonstrated the exponential generation of alveoli in humans over the first two years of life, after which alveoli continue to be generated—at a reduced rate—into adolescence (13). Alveolar growth has also been studied in mice and rats (2, 5, 6); the rat lung also demonstrated a biphasic growth pattern, with a period of bulk alveolarization in the early postnatal period (*day 4 to day 21* in rats), followed by a period of late or “continued” alveolarization up to *day 60* (59), with the number of acini remaining constant (3).

Variance in the experimental methodologies applied—including tissue processing, sampling, and analyses—have led to a broad range in the total number of alveoli in the lung being reported in humans, as well as in rodent models. In response to this, concomitant with advances in our knowledge of lung development, the past decade has seen tremendous advances in

# Looking ahead: where to next for animal models of bronchopulmonary dysplasia?

Claudio Nardiello<sup>1,2</sup> · Ivana Mižiková<sup>1,2</sup> · Rory E. Morty<sup>1,2</sup>

Received: 15 August 2016 / Accepted: 1 November 2016 / Published online: 5 December 2016  
© The Author(s) 2017. This article is published with open access at Springerlink.com

**Abstract** Bronchopulmonary dysplasia (BPD) is the most common complication of preterm birth, with appreciable morbidity and mortality in a neonatal intensive care setting. Much interest has been shown in the identification of pathogenic pathways that are amenable to pharmacological manipulation (1) to facilitate the development of novel therapeutic and medical management strategies and (2) to identify the basic mechanisms of late lung development, which remains poorly understood. A number of animal models have therefore been developed and continue to be refined with the aim of recapitulating pathological pulmonary hallmarks noted in lungs from neonates with BPD. These animal models rely on several injurious stimuli, such as mechanical ventilation or oxygen toxicity and infection and sterile inflammation, as applied in mice, rats, rabbits, pigs, lambs and nonhuman primates. This review addresses recent developments in modeling BPD in experimental animals and highlights important neglected areas that demand attention. Additionally, recent progress in the quantitative microscopic analysis of pathology tissue is described, together with new *in vitro* approaches of value for the study of normal and aberrant alveolarization. The need to examine long-term sequelae of damage to the developing neonatal lung is also considered, as is the need to move beyond the study of the lungs alone in experimental animal models of BPD.

**Keywords** Bronchopulmonary dysplasia · Animal model · Hyperoxia · Ventilation · Mouse

## Introduction

The lung is the key organ of gas exchange in mammals; it undertakes the transport of oxygen from inspired air into the bloodstream and, concomitantly, the transport of carbon dioxide out of the circulating blood, which is subsequently exhaled and thus removed from the body. This gas exchange is facilitated by the highly organized structure of the alveolus, the gas-exchange unit of the lung, where the inspired air is brought into close proximity to the circulating blood (Hsia et al. 2016). The close proximity of air and blood is facilitated by the delicate alveolo-capillary barrier, a double-layered barrier consisting of alveolar epithelial cells that line the alveolar units containing the inspired air and that are intimately associated with the endothelial cells that form the capillaries of the pulmonary circulation carrying deoxygenated blood through the lung (Hsia et al. 2016). The blood-air barrier is very thin, namely 200 nm–2 µm and is permeable to many gases including oxygen and carbon dioxide, thus facilitating gas exchange. Gas exchange occurs by Fick's Law (Fick 1855) and is a passive process that is directly determined by (1) the surface area available over which the gases can diffuse, (2) the distance across which the gas molecules must diffuse and (3) the concentration gradient. The broader objective of lung development is to generate a gas-exchange structure that satisfies these three conditions. The structure should have a large surface area and a thin diffusion barrier and should facilitate the establishment of a steep concentration gradient for gas diffusion in the correct direction. To this end, lung development is initiated with the emergence of the respiratory diverticulum, which is a ventral outgrowth of the foregut endoderm, very

✉ Rory E. Morty  
rory.morty@mpi-bn.mpg.de

<sup>1</sup> Department of Lung Development and Remodelling, Max Planck Institute for Heart and Lung Research, Parkstrasse 1, 61231 Bad Nauheim, Germany

<sup>2</sup> Department of Internal Medicine (Pulmonology), University of Giessen and Marburg Lung Center (UGMLC), Giessen, Germany

## RESOURCE ARTICLE

# Standardisation of oxygen exposure in the development of mouse models for bronchopulmonary dysplasia

Claudio Nardiello<sup>1,2</sup>, Ivana Mižiková<sup>1,2</sup>, Diogo M. Silva<sup>1,2</sup>, Jordi Ruiz-Camp<sup>1,2</sup>, Konstantin Mayer<sup>2</sup>, István Vadász<sup>2</sup>, Susanne Herold<sup>2</sup>, Werner Seeger<sup>1,2</sup> and Rory E. Morty<sup>1,2,\*</sup>

## ABSTRACT

Progress in developing new therapies for bronchopulmonary dysplasia (BPD) is sometimes complicated by the lack of a standardised animal model. Our objective was to develop a robust hyperoxia-based mouse model of BPD that recapitulated the pathological perturbations to lung structure noted in infants with BPD. Newborn mouse pups were exposed to a varying fraction of oxygen in the inspired air (FiO<sub>2</sub>) and a varying window of hyperoxia exposure, after which lung structure was assessed by design-based stereology with systemic uniform random sampling. The efficacy of a candidate therapeutic intervention using parenteral nutrition was evaluated to demonstrate the utility of the standardised BPD model for drug discovery. An FiO<sub>2</sub> of 0.85 for the first 14 days of life decreased total alveoli number and concomitantly increased alveolar septal wall thickness, which are two key histopathological characteristics of BPD. A reduction in FiO<sub>2</sub> to 0.60 or 0.40 also caused a decrease in the total alveoli number, but the septal wall thickness was not impacted. Neither a decreasing oxygen gradient (from FiO<sub>2</sub> 0.85 to 0.21 over the first 14 days of life) nor an oscillation in FiO<sub>2</sub> (between 0.85 and 0.40 on a 24 h:24 h cycle) had an appreciable impact on lung development. The risk of missing beneficial effects of therapeutic interventions at FiO<sub>2</sub> 0.85, using parenteral nutrition as an intervention in the model, was also noted, highlighting the utility of lower FiO<sub>2</sub> in selected studies, and underscoring the need to tailor the model employed to the experimental intervention. Thus, a state-of-the-art BPD animal model that recapitulates the two histopathological hallmark perturbations to lung architecture associated with BPD is described. The model presented here, where injurious stimuli have been systematically evaluated, provides a most promising approach for the development of new strategies to drive postnatal lung maturation in affected infants.

**KEY WORDS:** BPD, Hyperoxia, Alveolarisation, Structure, Animal model

## INTRODUCTION

Precise modelling of human disease using animal models is a major challenge in translating bench science to the bedside, as (1) animal models must accurately recapitulate disease processes to facilitate

the identification of pathogenic pathways, and (2) animal models represent the limiting step in assessing which therapeutic interventions hold promise for subsequent study. This is particularly evident in animal models of human diseases that are characterised by perturbations to the architecture of an organ. Modelling disease pathogenesis in experimental animals is problematic from multiple perspectives. Amongst these, the injurious insult employed in the experimental model might not recapitulate key elements of disease, thereby limiting the ability to evaluate the efficacy of candidate therapeutic agents. Furthermore, the precision of the readout that is employed might be inadequate to detect small changes in anatomical structures that are targeted by both the injurious insult and candidate therapeutic intervention. A further confounding variable is the use of experimental animals in medical research, as emphasis must be placed on ‘reduction, refinement and replacement’ (the 3R concept) (Curzer et al., 2016), where the number of experimental animals employed and the level of stress to which the animal is subjected must be maintained at the minimum level possible, while still retaining the translational viability of the animal model.

Modelling bronchopulmonary dysplasia (BPD) in experimental animals is a textbook illustration of these concerns. BPD is the most common complication of preterm birth and represents significant morbidity and mortality in the neonatal intensive care unit (Jobe, 2011; Jobe and Tibboel, 2014). BPD is caused by a combination of the toxic effects of oxygen supplementation used to manage respiratory failure in preterm infants, baro- and volu-trauma from mechanical ventilation (Greenough et al., 2008), as well as other disease-modifying variables such as infection and inflammation (Balany and Bhandari, 2015). BPD results in long-term complications in respiratory function that persist into adulthood (Hilgendorff and O’Reilly, 2015). The pathology of BPD has changed over time; where ‘old’ BPD, which is particularly characterised by fibrosis, thickened septa and some alveolar simplification, results from aggressive mechanical ventilation with high oxygen levels. In contrast, ‘new’ BPD, which is the prevalent form today, is largely characterised by alveolar simplification, where preterm infants are less aggressively ventilated, with lower oxygen levels (Jobe, 2011). As a result of improvements in the medical management of BPD, the incidence of BPD is increasing because preterm infants delivered earlier have increasingly improved survival (Stoll et al., 2015). This underscores a pressing need to develop new medical management strategies. However, these efforts might be hampered by the lack of appropriate animal models of BPD. In affected individuals, two key elements of the lung structure are impacted: the oxygen supplementation arrests lung development, which causes fewer alveoli of a larger size to be generated. Concomitantly, the thickness of the delicate barrier between the alveolar airspaces in the lung and the capillary network of the lung is thickened, which compromises gas exchange, and is

<sup>1</sup>Department of Lung Development and Remodelling, Max Planck Institute for Heart and Lung Research, 61231 Bad Nauheim, Germany. <sup>2</sup>Department of Internal Medicine (Pulmonology), University of Giessen and Marburg Lung Center (UGMLC), member of the German Center for Lung Research (DZL), 35392 Giessen, Germany.

\*Author for correspondence (rory.morty@mpi-bn.mpg.de)

 R.E.M., 0000-0003-0833-9749

This is an Open Access article distributed under the terms of the Creative Commons Attribution License (<http://creativecommons.org/licenses/by/3.0>), which permits unrestricted use, distribution and reproduction in any medium provided that the original work is properly attributed.

# Caffeine administration modulates TGF- $\beta$ signaling but does not attenuate blunted alveolarization in a hyperoxia-based mouse model of bronchopulmonary dysplasia

Philipp Rath<sup>1,2</sup>, Claudio Nardiello<sup>1,3</sup>, David E. Surate Solaligue<sup>1,3</sup>, Ronald Agius<sup>4</sup>, Ivana Mižíková<sup>1,3</sup>, Sebastian Hühn<sup>2</sup>, Konstantin Mayer<sup>3</sup>, István Vadász<sup>3</sup>, Susanne Herold<sup>3</sup>, Frank Runkel<sup>2,5</sup>, Werner Seeger<sup>1,3</sup> and Rory E. Morty<sup>1,3</sup>

**BACKGROUND:** Caffeine is widely used to manage apnea of prematurity, and reduces the incidence of bronchopulmonary dysplasia (BPD). Deregulated transforming growth factor (TGF)- $\beta$  signaling underlies arrested postnatal lung maturation in BPD. It is unclear whether caffeine impacts TGF- $\beta$  signaling or postnatal lung development in affected lungs.

**METHODS:** The impact of caffeine on TGF- $\beta$  signaling in primary mouse lung fibroblasts and alveolar epithelial type II cells was assessed *in vitro*. The effects of caffeine administration (25 mg/kg/d for the first 14 d of postnatal life) on aberrant lung development and TGF- $\beta$  signaling *in vivo* was assessed in a hyperoxia (85% O<sub>2</sub>)-based model of BPD in C57BL/6 mice.

**RESULTS:** Caffeine downregulated expression of type I and type III TGF- $\beta$  receptors, and Smad2; and potentiated TGF- $\beta$  signaling *in vitro*. *In vivo*, caffeine administration normalized body mass under hyperoxic conditions, and normalized Smad2 phosphorylation detected in lung homogenates; however, caffeine administration neither improved nor worsened lung structure in hyperoxia-exposed mice, in which postnatal lung maturation was blunted.

**CONCLUSION:** Caffeine modulated TGF- $\beta$  signaling *in vitro* and *in vivo*. Caffeine administration was well-tolerated by newborn mice, but did not influence the course of blunted postnatal lung maturation in a hyperoxia-based experimental mouse model of BPD.

Caffeine is a member of the methylxanthine class of central nervous system stimulants, which along with aminophylline and theophylline are nonspecific antagonists of the adenosine receptor (at low concentrations) and inhibitors of phosphodiesterases (at higher concentrations). Aminophylline was proposed for the treatment of Cheyne-Stokes respiration by the Austrian physician Alfred Vogl in 1927 (1) and was first used to treat apnea of prematurity in 1973 (2), which remains the indication for caffeine administration in a neonatal intensive care setting. Since then, the utility of caffeine in preterm

infants has been the subject of intense study, due to the lower toxicity of caffeine compared with other methylxanthines (3). Aranda *et al.* (4) first administered caffeine for apnea of prematurity in 1977, and this idea culminated in the Caffeine for Apnea of Prematurity (CAP) trial, where caffeine therapy initiated during the first 10 d of life decreased the incidence of bronchopulmonary dysplasia (BPD) and decreased the duration of mechanical ventilation in infants weighing 500–1,250 g at birth (5). The major reason that caffeine reduces BPD is by reducing apnea and increasing respiratory drive, thereby reducing ventilation-induced lung injury (5). Subsequent studies have highlighted that caffeine therapy also leads to improved long-term neurodevelopmental outcome in affected patients (6), and that the timing of caffeine therapy was important, where early initiation of caffeine therapy (within the first 3 d of life) may be of more benefit than late caffeine therapy (7).

The ability of caffeine to influence the course of aberrant lung development that occurs in patients with BPD is less well understood (8). Blunted secondary septation leading to an arrest of alveolar development is a histopathological characteristic of the lungs of infants with BPD. Thus, it is of interest to know whether caffeine may impact postnatal lung maturation in general, and alveolarization in particular. It has been demonstrated *in vitro* that caffeine has concentration-dependent effect on cell-cycle progression and cell viability in MLE-12 mouse lung and A549 human lung epithelial cell-lines, in the background of hyperoxia (9). Furthermore, *in vivo*, caffeine application to newborn FVB/n mice worsened lung hypoplasia in a hyperoxia-based model of BPD, and this was accompanied by increased epithelial cell apoptosis, and loss of alveolar type II (ATII) cells (10). These two reports indicated a deleterious impact of caffeine in BPD animal models. In contrast, caffeine application to 6-d old rats blunted the inflammatory response provoked by hyperoxia, limiting proinflammatory cytokine expression and inflammatory cell infiltration into the lung (11). This study thus indicated a potential benefit of caffeine application in experimental BPD; however, lung structure was

<sup>1</sup>Department of Lung Development and Remodelling, Max Planck Institute for Heart and Lung Research, Bad Nauheim, Germany; <sup>2</sup>Institute of Bioprocess Engineering and Pharmaceutical Technology, Technische Hochschule Mittelhessen–University of Applied Sciences, Giessen, Germany; <sup>3</sup>Department of Internal Medicine (Pulmonology), University of Giessen and Marburg Lung Center (UGMLC), member of the German Center for Lung Research (DZL), Giessen, Germany; <sup>4</sup>Department of Forensic and Clinical Toxicology, Labor Krone, Bad Salzungen, Germany; <sup>5</sup>Faculty of Biology and Chemistry, Justus Liebig University, Giessen, Germany. Correspondence: Rory E. Morty (rory.morty@mpi-bn.mpg.de)

Received 15 August 2016; accepted 27 November 2016; advance online publication 29 March 2017. doi:10.1038/pr.2017.21

## The H<sub>2</sub>S-generating enzymes cystathionine β-synthase and cystathionine γ-lyase play a role in vascular development during normal lung alveolarization

Alicia Madurga,<sup>1,2</sup> Anita Golec,<sup>1,2</sup> Agnieszka Pozarska,<sup>1,2</sup> Isao Ishii,<sup>3</sup> Ivana Mižíková,<sup>1,2</sup> Claudio Nardiello,<sup>1,2</sup> István Vadász,<sup>2</sup> Susanne Herold,<sup>1</sup> Konstantin Mayer,<sup>1</sup> Frank Reichenberger,<sup>4</sup> Heinz Fehrenbach,<sup>5</sup> Werner Seeger,<sup>1,2</sup> and Rory E. Morty<sup>1,2</sup>

<sup>1</sup>Department of Internal Medicine (Pulmonology), University of Giessen and Marburg Lung Center, German Center for Lung Research, Giessen, Germany; <sup>2</sup>Department of Lung Development and Remodelling, Max Planck Institute for Heart and Lung Research, Bad Nauheim, Germany; <sup>3</sup>Keio University Graduate School of Pharmaceutical Sciences, Tokyo, Japan; <sup>4</sup>Department of Pulmonology, Asklepios Lung Centre, Munich-Gauting, Germany; and <sup>5</sup>Division of Experimental Pneumology, Priority Area Asthma and Allergy, Airway Research Center North, German Center for Lung Research, Borstel, Germany

Submitted 29 April 2015; accepted in final form 24 July 2015

**Madurga A, Golec A, Pozarska A, Ishii I, Mižíková I, Nardiello C, Vadász I, Herold S, Mayer K, Reichenberger F, Fehrenbach H, Seeger W, Morty RE.** The H<sub>2</sub>S-generating enzymes cystathionine β-synthase and cystathionine γ-lyase play a role in vascular development during normal lung alveolarization. *Am J Physiol Lung Cell Mol Physiol* 309: L710–L724, 2015. First published July 31, 2015; doi:10.1152/ajplung.00134.2015.—The gas transmitter hydrogen sulfide (H<sub>2</sub>S) is emerging as a mediator of lung physiology and disease. Recent studies revealed that H<sub>2</sub>S administration limited perturbations to lung structure in experimental animal models of bronchopulmonary dysplasia (BPD), partially restoring alveolarization, limiting pulmonary hypertension, limiting inflammation, and promoting epithelial repair. No studies have addressed roles for endogenous H<sub>2</sub>S in lung development. H<sub>2</sub>S is endogenously generated by cystathionine β-synthase (Cbs) and cystathionine γ-lyase (Cth). We demonstrate here that the expression of Cbs and Cth in mouse lungs is dynamically regulated during lung alveolarization and that alveolarization is blunted in Cbs<sup>-/-</sup> and Cth<sup>-/-</sup> mouse pups, where a 50% reduction in the total number of alveoli was observed, without any impact on septal thickness. Laser-capture microdissection and immunofluorescence staining indicated that Cbs and Cth were expressed in the airway epithelium and lung vessels. Loss of Cbs and Cth led to a 100–500% increase in the muscularization of small- and medium-sized lung vessels, which was accompanied by increased vessel wall thickness, and an apparent decrease in lung vascular supply. Ablation of Cbs expression using small interfering RNA or pharmacological inhibition of Cth using propargylglycine in lung endothelial cells limited angiogenic capacity, causing a 30–40% decrease in tube length and a 50% decrease in number of tubes formed. In contrast, exogenous administration of H<sub>2</sub>S with GYY4137 promoted endothelial tube formation. These data confirm a key role for the H<sub>2</sub>S-generating enzymes Cbs and Cth in pulmonary vascular development and homeostasis and in lung alveolarization.

lung development; gas transmitter; hydrogen sulfide; H<sub>2</sub>S; alveolarization

THE FORMATION OF THE ALVEOLAR gas exchange units occurs during late lung development and results in the generation of a thin alveolo-capillary barrier with a large surface area, representing an optimal interface for gas exchange (11, 22). The processes that drive the formation of alveoli remain poorly

understood and are believed to involve the concerted action of transcription factors, growth factors, the lung extracellular matrix, and physical forces such as breathing motions (42). There is currently much interest in better understanding what factors regulate formation of alveoli and how these factors act (17). In addition to providing a better understanding of the complex process of alveolarization, this might reveal pathways that can be targeted in an effort to drive alveolar formation in pathologies such as bronchopulmonary dysplasia (BPD), where alveolarization is blocked, or emphysema (49), where driving neoalveolarization in diseased lungs would be desirable (16, 34).

One novel group of candidate mediators of lung development and homeostasis is the endogenous gas transmitters, which comprises hydrogen sulfide (H<sub>2</sub>S), nitric oxide (NO), and carbon monoxide (CO) (41). Both CO and H<sub>2</sub>S have recently been implicated in lung alveolarization. CO and the CO-generating enzyme hemeoxygenase-1 (Hmox1) are vasculoprotective (10) in a popular rodent model of BPD (5, 25). Two recent reports have also indicated that H<sub>2</sub>S may play an important role in late lung development. Both of these studies have relied on the exogenous application of chemical donors of H<sub>2</sub>S in the same hyperoxia-based rodent models of BPD. The Thébaud group (40) first documented that exogenous H<sub>2</sub>S administration protected rat pups against the injurious effects of hyperoxia exposure, namely, alveolar growth was improved and pulmonary hypertension was limited. Building on those studies, our group subsequently demonstrated that exogenous H<sub>2</sub>S administration partially restored alveolar growth in hyperoxia-exposed mouse pups, stimulated epithelial wound repair, and dramatically limited macrophage, neutrophil, and eosinophil recruitment to the lungs, possibly through the normalization of interleukin (IL)-10 levels (18). Particularly intriguing was the observation that H<sub>2</sub>S administration to healthy, normally developing lungs also increased the total number of alveoli in the lung. H<sub>2</sub>S is also known to modulate alveolar ion and fluid transport (9), which is disturbed in BPD patients; however, this aspect has not yet been explored in experimental BPD. Together, these data document that exogenous H<sub>2</sub>S can improve alveolarization.

All of the aforementioned reports have examined exogenous H<sub>2</sub>S application, largely in diseased lungs. However, mammalian lungs do have the capacity to generate H<sub>2</sub>S endogenously, primarily via two enzymatic systems: cytosolic cystathionine

Address for reprint requests and other correspondence: R. E. Morty, Dept. of Lung Development and Remodelling, Max Planck Institute for Heart and Lung Research, Parkstrasse 1, D-61231 Bad Nauheim, Germany (e-mail: rory.morty@mpi-bn.mpg.de).



# The Extracellular Matrix in Bronchopulmonary Dysplasia: Target and Source

Ivana Mižiková<sup>1,2</sup> and Rory E. Morty<sup>1,2\*</sup>

<sup>1</sup> Department of Lung Development and Remodelling, Max Planck Institute for Heart and Lung Research, Bad Nauheim, Germany, <sup>2</sup> Pulmonology, Department of Internal Medicine, University of Giessen and Marburg Lung Center, Giessen, Germany

## OPEN ACCESS

### Edited by:

Anne Hilgendorff,  
Helmholtz Zentrum München,  
Germany

### Reviewed by:

Michael Adam O'Reilly,  
The University of Rochester, USA  
Eleni Papakonstantinou,  
Aristotle University of Thessaloniki,  
Greece

### \*Correspondence:

Rory E. Morty  
rory.morty@mpi-bn.mpg.de

### Specialty section:

This article was submitted to  
Pulmonary Medicine,  
a section of the journal  
Frontiers in Medicine

**Received:** 21 August 2015

**Accepted:** 08 December 2015

**Published:** 23 December 2015

### Citation:

Mižiková I and Morty RE (2015) The  
Extracellular Matrix in  
Bronchopulmonary Dysplasia:  
Target and Source.  
*Front. Med.* 2:91.  
doi: 10.3389/fmed.2015.00091

Bronchopulmonary dysplasia (BPD) is a common complication of preterm birth that contributes significantly to morbidity and mortality in neonatal intensive care units. BPD results from life-saving interventions, such as mechanical ventilation and oxygen supplementation used to manage preterm infants with acute respiratory failure, which may be complicated by pulmonary infection. The pathogenic pathways driving BPD are not well-delineated but include disturbances to the coordinated action of gene expression, cell–cell communication, physical forces, and cell interactions with the extracellular matrix (ECM), which together guide normal lung development. Efforts to further delineate these pathways have been assisted by the use of animal models of BPD, which rely on infection, injurious mechanical ventilation, or oxygen supplementation, where histopathological features of BPD can be mimicked. Notable among these are perturbations to ECM structures, namely, the organization of the elastin and collagen networks in the developing lung. Dysregulated collagen deposition and disturbed elastin fiber organization are pathological hallmarks of clinical and experimental BPD. Strides have been made in understanding the disturbances to ECM production in the developing lung, but much still remains to be discovered about how ECM maturation and turnover are dysregulated in aberrantly developing lungs. This review aims to inform the reader about the state-of-the-art concerning the ECM in BPD, to highlight the gaps in our knowledge and current controversies, and to suggest directions for future work in this exciting and complex area of lung development (patho)biology.

**Keywords:** bronchopulmonary dysplasia, extracellular matrix, hyperoxia, mechanical ventilation, collagen, elastin, lung development

## BRONCHOPULMONARY DYSPLASIA IN CONTEXT

The lung is the key organ of gas exchange in air-breathing mammals. This gas exchange structure is derived from the primitive foregut and proceeds through a phase of early (embryonic) development (1–3), when the conducting airways and conducting vessels are generated and organized (4). Early lung development initiates with the embryonic stage that occurs 4–7 weeks post-conception in humans [embryonic day (E)9–E12 in the mouse]. The embryonic stage is followed by the pseudoglandular stage, which occurs at 5–17 weeks post-conception in humans (E12–E17 in mice). The final stage of *early lung development* is the canalicular stage, occurring at 16–26 weeks post-conception

## Collagen and elastin cross-linking is altered during aberrant late lung development associated with hyperoxia

Ivana Mižíková,<sup>1</sup> Jordi Ruiz-Camp,<sup>1</sup> Heiko Steenbock,<sup>3</sup> Alicia Madurga,<sup>1,2</sup> István Vadász,<sup>2</sup> Susanne Herold,<sup>2</sup> Konstantin Mayer,<sup>2</sup> Werner Seeger,<sup>1,2</sup> Jürgen Brinckmann,<sup>3,4</sup> and Rory E. Morty<sup>1,2</sup>

<sup>1</sup>Department of Lung Development and Remodelling, Max Planck Institute for Heart and Lung Research, Bad Nauheim, Germany; <sup>2</sup>Department of Internal Medicine (Pulmonology), University of Giessen and Marburg Lung Center, German Center for Lung Research, Giessen, Germany; <sup>3</sup>Institute of Virology and Cell Biology, University of Lübeck, Lübeck, Germany; and <sup>4</sup>Department of Dermatology, University of Lübeck, Lübeck, Germany

Submitted 30 January 2015; accepted in final form 3 April 2015

**Mižíková I, Ruiz-Camp J, Steenbock H, Madurga A, Vadász I, Herold S, Mayer K, Seeger W, Brinckmann J, Morty RE.** Collagen and elastin cross-linking is altered during aberrant late lung development associated with hyperoxia. *Am J Physiol Lung Cell Mol Physiol* 308: L1145–L1158, 2015. First published April 3, 2015; doi:10.1152/ajplung.00039.2015.—Maturation of the lung extracellular matrix (ECM) plays an important role in the formation of alveolar gas exchange units. A key step in ECM maturation is cross-linking of collagen and elastin, which imparts stability and functionality to the ECM. During aberrant late lung development in bronchopulmonary dysplasia (BPD) patients and animal models of BPD, alveolarization is blocked, and the function of ECM cross-linking enzymes is deregulated, suggesting that perturbed ECM cross-linking may impact alveolarization. In a hyperoxia (85% O<sub>2</sub>)-based mouse model of BPD, blunted alveolarization was accompanied by alterations to lung collagen and elastin levels and cross-linking. Total collagen levels were increased (by 63%). The abundance of dihydroxylysino-norleucine collagen cross-links and the dihydroxylysino-norleucine-to-hydroxylysino-norleucine ratio were increased by 11 and 18%, respectively, suggestive of a profibrotic state. In contrast, insoluble elastin levels and the abundance of the elastin cross-links desmosine and isodesmosine in insoluble elastin were decreased by 35, 30, and 21%, respectively. The lung collagen-to-elastin ratio was threefold increased. Treatment of hyperoxia-exposed newborn mice with the lysyl oxidase inhibitor  $\beta$ -aminopropionitrile partially restored normal collagen levels, normalized the dihydroxylysino-norleucine-to-hydroxylysino-norleucine ratio, partially normalized desmosine and isodesmosine cross-links in insoluble elastin, and partially restored elastin foci structure in the developing septa. However,  $\beta$ -aminopropionitrile administration concomitant with hyperoxia exposure did not improve alveolarization, evident from unchanged alveolar surface area and alveoli number, and worsened septal thickening (increased by 12%). These data demonstrate that collagen and elastin cross-linking are perturbed during the arrested alveolarization of developing mouse lungs exposed to hyperoxia.

lung development; elastin; collagen; lysyl oxidase; alveolarization

POSTNATAL LUNG DEVELOPMENT in mice is characterized by a period of intensive growth and remodeling of the lung parenchyma, which rapidly (over a period of days) generates a large number of small alveoli and thus maximizes the alveolar surface area over which gas exchange can take place. Secondary septation, the generation of new septa from preexisting septa, which then divide the air spaces, peaks in mice between

4 and 7 days after birth and is largely complete 21 days after birth. In humans, secondary septation is already well underway during late stages of pregnancy, and thus occurs in utero, and continues several years into postnatal life. Disturbances to the formation of secondary septa, such as the arrested secondary septation associated with bronchopulmonary dysplasia (BPD) in humans, leads to malformed lungs with fewer and larger alveoli. This common complication of premature birth is associated with significant morbidity and mortality.

The molecular mechanisms underlying the generation of secondary septa remain poorly understood, but most likely rely on the coordinated action of transcription factors, growth factor signaling, extracellular matrix (ECM) deposition and remodeling, and physical forces, such as breathing motions (41, 42). The generation and shaping of the lung ECM has received much attention in the context of normal and aberrant lung alveolarization (20, 38, 45). Infants with BPD exhibit increased collagen abundance in the lung (14), and collagen fibers and the lung collagen scaffold are malformed (60). There is also evidence of altered elastin turnover, as assessed by urinary excretion of the desmosine elastin cross-link, in infants with BPD (12). These data point to disturbances to ECM production and processing in BPD, which may be mimicked in animal models, employing either hyperoxia, caloric restriction, mechanical ventilation, or preterm delivery as an injurious stimulus in rats, mice, lambs, and baboons (6, 13, 49, 66). The lung histopathology that results is reminiscent of that of BPD in humans, with evident air space enlargement, septal wall thickening, and a reduced number of alveoli, as well as perturbations to ECM structures. Increased collagen levels have been reported in the lungs of hyperoxia-exposed adult rats (44). Elastin has received more attention, since normal elastin production and deposition are critical for proper development of alveoli (43, 57, 58). In hyperoxia-exposed or calorie-restricted mice, late lung development is impeded, and elastic fibers are described to be “irregularly distributed, tortuous, and abruptly terminating” (11). Similarly, in mechanically ventilated preterm lambs, late lung development is also impeded, and excessive production of elastin and accumulation of short, brush-like elastin fibers in the developing lung has been noted (2, 52).

To date, the underlying reasons for these perturbations to ECM structures have remained elusive. Excessive elastase activity has been considered as a mediator of pathological elastin degradation, which might underlie the paucity of elastin and bizarre elastin fiber patterns seen in affected lungs (21–23, 36). Additionally, the altered expression of proteins required for proper elastin fiber assembly has also been suggested to

Address for reprint requests and other correspondence: R. E. Morty, Dept. of Lung Development and Remodelling, Max Planck Institute for Heart and Lung Research, Parkstrasse 1, D-61231 Bad Nauheim, Germany (e-mail: rory.morty@mpi-bn.mpg.de).

## Systemic hydrogen sulfide administration partially restores normal alveolarization in an experimental animal model of bronchopulmonary dysplasia

Alicia Madurga,<sup>1,2</sup> Ivana Mižíková,<sup>2</sup> Jordi Ruiz-Camp,<sup>2</sup> István Vadász,<sup>1</sup> Susanne Herold,<sup>1</sup> Konstantin Mayer,<sup>1</sup> Heinz Fehrenbach,<sup>3</sup> Werner Seeger,<sup>1,2</sup> and Rory E. Morty<sup>1,2</sup>

<sup>1</sup>Department of Internal Medicine (Pulmonology), University of Giessen and Marburg Lung Center (UGMLC), German Center for Lung Research (DZL), Giessen, Germany; <sup>2</sup>Department of Lung Development and Remodelling, Max Planck Institute for Heart and Lung Research, Bad Nauheim, Germany; and <sup>3</sup>Division of Experimental Pneumology, Priority Area Asthma and Allergy, Airway Research Center North (ARCN), German Center for Lung Research (DZL), Borstel, Germany

Submitted 10 December 2013; accepted in final form 4 February 2014

**Madurga A, Mižíková I, Ruiz-Camp J, Vadász I, Herold S, Mayer K, Fehrenbach H, Seeger W, Morty RE.** Systemic hydrogen sulfide administration partially restores normal alveolarization in an experimental animal model of bronchopulmonary dysplasia. *Am J Physiol Lung Cell Mol Physiol* 306: L684–L697, 2014. First published February 7, 2014; doi:10.1152/ajplung.00361.2013.—Arrested alveolarization is the pathological hallmark of bronchopulmonary dysplasia (BPD), a complication of premature birth. Here, the impact of systemic application of hydrogen sulfide (H<sub>2</sub>S) on postnatal alveolarization was assessed in a mouse BPD model. Exposure of newborn mice to 85% O<sub>2</sub> for 10 days reduced the total lung alveoli number by 56% and increased alveolar septal wall thickness by 29%, as assessed by state-of-the-art stereological analysis. Systemic application of H<sub>2</sub>S via the slow-release H<sub>2</sub>S donor GYY4137 for 10 days resulted in pronounced improvement in lung alveolarization in pups breathing 85% O<sub>2</sub>, compared with vehicle-treated littermates. Although without impact on lung oxidative status, systemic H<sub>2</sub>S blunted leukocyte infiltration into alveolar air spaces provoked by hyperoxia, and restored normal lung interleukin 10 levels that were otherwise depressed by 85% O<sub>2</sub>. Treatment of primary mouse alveolar type II (ATII) cells with the rapid-release H<sub>2</sub>S donor NaHS had no impact on cell viability; however, NaHS promoted ATII cell migration. Although exposure of ATII cells to 85% O<sub>2</sub> caused dramatic changes in mRNA expression, exposure to either GYY4137 or NaHS had no impact on ATII cell mRNA expression, as assessed by microarray, suggesting that the effects observed were independent of changes in gene expression. The impact of NaHS on ATII cell migration was attenuated by glibenclamide, implicating ion channels, and was accompanied by activation of Akt, hinting at two possible mechanisms of H<sub>2</sub>S action. These data support further investigation of H<sub>2</sub>S as a candidate interventional strategy to limit the arrested alveolarization associated with BPD.

lung development; gasotransmitter; inflammation; alveolar type II cell

BRONCHOPULMONARY DYSPLASIA (BPD) is a chronic lung disorder encountered in prematurely born infants, particularly in very low birth weight infants, and infants that receive oxygen therapy. Currently, the clinical diagnosis of BPD is based on a need for oxygen supplementation at a defined postmenstrual age, which does not reflect the pathological characteristics of BPD (6). Since the first description of BPD in 1967 (57), these pathological characteristics have changed, in response to the

medical management of infants at risk for BPD, such as surfactant replacement therapy. Today, BPD is characterized largely by an arrest of alveolarization and the development of a dysmorphic pulmonary circulation (34–36, 52, 54). The pathogenic mechanisms that underlie the development of BPD are not well defined (29); however, candidates include oxidative stress and oxygen toxicity (10, 64), barotrauma (28), volutrauma (13, 14, 18), perinatal infection (33, 39), and inflammation (16, 45, 71, 72, 80, 86). BPD also has a vascular component, which may be both a contributor to and a consequence of perturbed alveolarization (15, 74–76).

The endogenous gasotransmitters hydrogen sulfide (H<sub>2</sub>S), nitric oxide (NO), and carbon monoxide (CO) (84) are emerging as potentially interesting contributors to pulmonary physiology and pathology. Additionally, because of the ease of local delivery of gas directly to lung via the trachea, there is much interest in the exploitation of these gases in therapeutic or management strategies for lung diseases. The gases are credited with anti-inflammatory, antioxidant, antibacterial, and vasodilatory properties. Given that infection, inflammation, oxidative stress, and vasoconstriction form the basis of many lung diseases, including BPD, these gases have potentially exciting applications in the management of lung disease, provided they can be employed at doses that are not toxic.

Inhaled NO (iNO) has found widespread clinical use (5, 7, 62, 63), although the use iNO in preterm infants with respiratory failure remains controversial (69). Additionally, overexpression of Hmox1 (which can generate CO) in the alveolar epithelium may offer protection against perturbed lung and pulmonary vascular development associated with hyperoxia (25).

To date, systemic H<sub>2</sub>S administration has not been evaluated in an experimental animal model of BPD. H<sub>2</sub>S is currently under evaluation as a therapeutic modality in a spectrum of other lung diseases. Inhaled H<sub>2</sub>S has been evaluated in experimental mouse models of acute lung injury (21, 23), and in an experimental model of ventilator-induced acute lung injury (22) a protective effect was observed (at 80 ppm) and attributed to the anti-inflammatory properties of H<sub>2</sub>S, although another study employing 70 ppm inhaled H<sub>2</sub>S (but more injurious mechanical ventilation) reported deleterious effects of H<sub>2</sub>S inhalation (26). Additionally, parenteral administration of the H<sub>2</sub>S donor NaHS attenuated acute lung injury in adult mice, ostensibly through the antioxidant properties of H<sub>2</sub>S (22). Systemic administration of H<sub>2</sub>S with NaHS also attenuates

Address for reprint requests and other correspondence: R. E. Morty, Dept. of Lung Development and Remodelling, Max Planck Institute for Heart and Lung Research, Parkstrasse 1, D-61231 Bad Nauheim, Germany (e-mail: rory.morty@mpi-bn.mpg.de).

# Lysyl Oxidases Play a Causal Role in Vascular Remodeling in Clinical and Experimental Pulmonary Arterial Hypertension

Alexander H. Nave, Ivana Mižíková, Gero Niess, Heiko Steenbock, Frank Reichenberger, María L. Talavera, Florian Veit, Susanne Herold, Konstantin Mayer, István Vadász, Norbert Weissmann, Werner Seeger, Jürgen Brinckmann, Rory E. Morty

**Objective**—Pulmonary vascular remodeling, the pathological hallmark of pulmonary arterial hypertension, is attributed to proliferation, apoptosis resistance, and migration of vascular cells. A role of dysregulated matrix cross-linking and stability as a pathogenic mechanism has received little attention. We aimed to assess whether matrix cross-linking enzymes played a causal role in experimental pulmonary hypertension (PH).

**Approach and Results**—All 5 lysyl oxidases were detected in concentric and plexiform vascular lesions of patients with idiopathic pulmonary arterial hypertension. Lox, LoxL1, LoxL2, and LoxL4 expression was elevated in lungs of patients with idiopathic pulmonary arterial hypertension, whereas LoxL2 and LoxL3 expression was elevated in laser-capture microdissected vascular lesions. Lox expression was hypoxia-responsive in pulmonary artery smooth muscle cells and adventitial fibroblasts, whereas LoxL1 and LoxL2 expression was hypoxia-responsive in adventitial fibroblasts. Lox expression was increased in lungs from hypoxia-exposed mice and in lungs and pulmonary artery smooth muscle cells of monocrotaline-treated rats, which developed PH. Pulmonary hypertensive mice exhibited increased muscularization and perturbed matrix structures in vessel walls of small pulmonary arteries. Hypoxia exposure led to increased collagen cross-linking, by dihydroxylysinoxidation and hydroxylysinoxidation cross-links. Administration of the lysyl oxidase inhibitor  $\beta$ -aminopropionitrile attenuated the effect of hypoxia, limiting perturbations to right ventricular systolic pressure, right ventricular hypertrophy, and vessel muscularization and normalizing collagen cross-linking and vessel matrix architecture.

**Conclusions**—Lysyl oxidases are dysregulated in clinical and experimental PH. Lysyl oxidases play a causal role in experimental PH and represent a candidate therapeutic target. Our proof-of-principle study demonstrated that modulation of lung matrix cross-linking can affect pulmonary vascular remodeling associated with PH. (*Arterioscler Thromb Vasc Biol.* 2014;34:1446-1458.)

**Key Words:** anoxia ■ extracellular matrix ■ hypertension, pulmonary ■ muscle, smooth ■ protein-lysine 6-oxidase

Pulmonary arterial hypertension (PAH) is a life-threatening disease characterized by elevated pulmonary artery pressure caused by increased pulmonary vascular resistance, ultimately leading to right heart failure and death.<sup>1</sup> A combination of vasoconstriction, and vascular wall remodeling, which includes excessive extracellular matrix (ECM) deposition, and smooth muscle cell hyperplasia leads to occlusion of the small pulmonary arteries.<sup>2</sup> Therapeutic options for the clinical management of PAH are limited, and the disease remains essentially untreatable, underscoring the need for a better understanding of the pathogenic mechanisms at play that

give rise to increased pulmonary vascular resistance.<sup>3</sup> In this regard, 1 key area of interest is to clarify the causes and nature of the pulmonary vascular remodeling associated with PAH.

To date, most studies that have explored vascular remodeling in pulmonary hypertension (PH) have focused on increased cell proliferation and apoptosis resistance as an underlying cause of medial hypertrophy and neointimal formation. Regulation of pulmonary artery smooth muscle cell (PASMC) proliferation, apoptosis, and contraction has received much attention, with potassium and calcium channels, growth factors (including transforming growth factor- $\beta$ ,

Received on: August 15, 2012; final version accepted on: April 29, 2014.

From the Division of Pulmonology, Department of Internal Medicine, University of Giessen and Marburg Lung Center (UGMLC), Giessen, Germany (A.H.N., I.M., G.N., F.R., M.L.T., F.V., S.H., K.M., I.V., N.W., W.S., R.E.M.); Department of Lung Development and Remodelling, Max Planck Institute for Heart and Lung Research, Bad Nauheim, Germany (A.H.N., I.M., G.N., W.S., R.E.M.); and the Department of Dermatology (J.B.) and Institute of Virology and Cell Biology (J.B., H.S.), University of Lübeck, Lübeck, Germany.

Current address for A.H.N.: Department of Neurology, Center for Stroke Research, Charité Universitätsmedizin, Charitéplatz 1, 10117 Berlin, Germany.

Current address for F.R.: Department of Pneumology, Asklepios Lung Center, Robert-Koch-Allee 2, 82131 Munich-Gauting, Germany.

Current address for M.L.T.: University Hospital Favalaro Foundation, Belgrano AV, 1782, C1093AAS Buenos Aires City, Argentina.

**The online-only Data Supplement is available with this article at <http://atvb.ahajournals.org/lookup/suppl/doi:10.1161/ATVBAHA.114.303534/-DC1>.** Correspondence to Rory E. Morty, PhD, Department of Lung Development and Remodelling, Max Planck Institute for Heart and Lung Research, Parkstrasse 1, D-61231 Bad Nauheim, Germany. E-mail rory.morty@mpi-bn.mpg.de

© 2014 American Heart Association, Inc.

*Arterioscler Thromb Vasc Biol* is available at <http://atvb.ahajournals.org>

DOI: 10.1161/ATVBAHA.114.303534

## Recent advances in late lung development and the pathogenesis of bronchopulmonary dysplasia

Alicia Madurga,<sup>1,2</sup> Ivana Mižíková,<sup>1</sup> Jordi Ruiz-Camp,<sup>1</sup> and Rory E. Morty<sup>1,2</sup>

<sup>1</sup>Department of Lung Development and Remodelling, Max Planck Institute for Heart and Lung Research, Bad Nauheim, Germany; and <sup>2</sup>Department of Internal Medicine (Pulmonology), University of Giessen and Marburg Lung Center (UGMLC), member of the German Center for Lung Research (DZL), Giessen, Germany

Submitted 23 September 2013; accepted in final form 1 November 2013

**Madurga A, Mižíková I, Ruiz-Camp J, Morty RE.** Recent advances in late lung development and the pathogenesis of bronchopulmonary dysplasia. *Am J Physiol Lung Cell Mol Physiol* 305: L893–L905, 2013. First published November 8, 2013; doi:10.1152/ajplung.00267.2013.—In contrast to early lung development, a process exemplified by the branching of the developing airways, the later development of the immature lung remains very poorly understood. A key event in late lung development is secondary septation, in which secondary septa arise from primary septa, creating a greater number of alveoli of a smaller size, which dramatically expands the surface area over which gas exchange can take place. Secondary septation, together with architectural changes to the vascular structure of the lung that minimize the distance between the inspired air and the blood, are the objectives of late lung development. The process of late lung development is disturbed in bronchopulmonary dysplasia (BPD), a disease of prematurely born infants in which the structural development of the alveoli is blunted as a consequence of inflammation, volutrauma, and oxygen toxicity. This review aims to highlight notable recent developments in our understanding of late lung development and the pathogenesis of BPD.

BPD; lung development; alveolarization; hypoxia; growth factor; oxidative stress

THE PRIMARY FUNCTION OF THE lung is to transport oxygen from the inspired air into the blood and to clear accumulated carbon dioxide from the blood. The alveolus is the site of this gas exchange in the lung, which takes place across the alveolocapillary barrier, a double barrier that consists of the alveolar epithelium and the capillary endothelium located in close proximity to one another, and supported by the extracellular matrix (ECM). To facilitate effective gas exchange across this barrier, it is desirable that this barrier is as thin as possible to give the gas molecules a short distance to traverse, and also that the functional surface area of the barrier is as large as possible, to maximize the functional gas exchange capacity of the lung. It is the objective of late lung development, through the process of alveolarization, to deliver these two essential elements of a mature, functional lung (114).

This is achieved first by the establishment of the core lung structure, during airway branching in the embryonic (4–7 wk postconception) and pseudoglandular (5–17 wk postconception) stages of early lung development. Late lung development follows with the canalicular stage (16–24 wk postconception), which is marked by the thinning of the interstitial tissue and the “opening” of air spaces in the developing lung. This is followed by the formation of saccular units by the developing

airways in the saccular stage (24–35 wk postconception), after which secondary septa divide the saccular units during the alveolar stage (36 wk postconception to several years postnatal), increasing the number and reducing the size of the alveoli. Alveolar septal formation, the key event in alveolarization, proceeds from ~34 wk postconception. This process remains very poorly understood and is thought to be regulated by the concerted action of gene expression programs, growth factor signaling, ECM production and maturation, and physical forces, such as those generated by breathing motions (112, 113, 178).

When late lung development is disturbed, the lung architecture is malformed. Depending on the severity of the architectural malformation, there may be serious consequences in terms of respiratory function, as well as long-term consequences in later life. This is exemplified by diseases such as bronchopulmonary dysplasia (BPD) (124), a common complication of preterm birth, which is characterized by perturbations to lung structure that include reduced alveolar number, thickened septa, and a malformed pulmonary circulation. These structural abnormalities lead to respiratory complications during infancy, which may persist into adulthood (14, 188, 189). Improved medical management of BPD has dramatically increased the survival of BPD patients and has changed the pathophysiological picture of BPD today. BPD is now characterized less by fibroproliferative airway damage and parenchymal fibrosis and more by alveolar hypoplasia and a dysmorphic pulmonary circulation, making BPD today largely a disease of arrested lung development (84, 85). This has underscored an urgent need to better understand the molecular basis of late lung development. Additionally, improved perinatal care has increased the survival of very premature infants (61), which has also led to an increase in the incidence of BPD, highlighting the need for a better understanding of the pathogenic mechanisms at play, which might be targeted in the medical management and treatment of BPD. This review, which complements a recent Update article in the *American Journal of Respiratory and Critical Care Medicine* (105), aims to provide a perspective on very recent advances in our understanding of late lung development and BPD.

### *Hyperoxia and Oxidative Stress*

Adult patients with compromised respiratory function are often ventilated with high oxygen concentrations for life support. Similarly, prematurely born infants have lungs that are insufficiently developed to allow for proper gas exchange, and oxygen supplementation thus also represents a life-saving intervention in the neonatal intensive care unit. However, high oxygen levels are also very toxic and damage the lung, either

Address for reprint requests and other correspondence: R. E. Morty, Dept. of Lung Development and Remodelling, Max Planck Institute for Heart and Lung Research, Parkstrasse 1, D-61231 Bad Nauheim, Germany (e-mail: rory.morty@mpi-bn.mpg.de).